AN ABSTRACT OF THE THESIS OF

Farid Abooameri for the degree of Masters of Science in Chemical Engineering presented on September 28, 1994. Title: Evaluation of Cathodic Protection in Reinforced Concrete Bridges

Redacted for Privacy

Abstract approved: __

Milo D. Koretsky

Steel corrosion in reinforced concrete is a major concern to transportation agencies nationwide because of the expenses incurred for repair and ultimate shortening of bridge life. Cathodic protection (CP), as a remedy, has been applied to reinforced bridges in the US since 1974. However, application of this technique is largely empirical, lacking fundamental understanding. In order to optimize the performance of a CP system, it is important to monitor the rebar potential with respect to a reliable reference electrode. Moreover, because of potential variation in the concrete, reference cell placement is fundamental to ensure effective protection.

The work plan was divided into two parts: laboratory scale experimentation and computer simulation. In the experimentation section, the response of graphite probes was compared to that of an Orion silver-silver chloride electrode. Graphite probes behaved as well as the standard electrode. Furthermore, the home-made graphite probes behaved the same as the commercial ones. This will allow much greater experimental latitude since the home-made probes are much more economical than the commercial ones.

A finite difference code was developed to assess the performance of cathodic protection. The potential distribution in a two dimensional geometry of a concrete block with a sprayed zinc anode at one boundary and an iron cathode at the other side was calculated under cathodic protection. The equations were solved by means of a Gauss-Seidel iterative method with the help of an overrelaxation factor. An interval halving method was used to solve for nonlinear boundary condition at the iron.

The effects of concrete pore saturation, concrete cover, and applied potential were studied to determine the degree of protection and proper placement of the reference electrode in concrete. Furthermore, a sensitivity analysis was performed versus input parameters: concrete conductivity, oxygen mass transfer coefficient, and oxygen reduction polarization parameters. The results of the simulation showed that the center of the rebar is less protected than the other locations. Therefore, the reference electrode should be located as close to the center as possible.

Evaluation of Cathodic Protection in Reinforced Concrete Bridges

by

Farid Abooameri

A THESIS

submitted to

Oregon State University

in partial fulfillment of
the requirements for the
degree of

Master of Science

Completed September 28, 1994
Commencement June 1995

Master of Science thesis of <u>Farid Abooameri</u> presented on <u>September 28, 1994</u>

APPROVED:

Redacted for Privacy

_____

Major Professor, representing Chemical Engineering

Redacted for Privacy

_____

Chair of Department of Chemical Engineering

Redacted for Privacy

_____

Dean of Graduate School

I understand that my thesis will become part of the permanent collection of Oregon State University libraries. My signature below authorizes release of my thesis to any reader upon request.

Redacted for Privacy

_____

Farid Abooameri, Author

ACKNOWLEDGMENT

I would like to take this opportunity to express my gratitude and appreciation to those who have made major contributions to this research.

- To my major Professor, Dr. Milo Koretsky for his advice, guidance, encouragement, and financial support throughout my stay in the department.

- To Professor John Westall whose tremendous contribution to all aspects of this study is indeed invaluable.

- To Dr. Heidi Pattee for all the help and precious discussions which enabled me to complete the simulation section.

- To Eric Webb who enthusiastically made the effort of providing the raw data for the simulation section.

- Finally and most importantly, to my parents without whom the journey would have been impossible.

TABLE OF CONTENTS

TABLE OF CONTENTS (Continued)

LIST OF FIGURES

LIST OF FIGURES (Continued)

LIST OF FIGURES (Continued)

LIST OF FIGURES (Continued)

LIST OF TABLES

NOMENCLATURE

a_m	activity of species m
b	inverse of the Tafel slope (V/decade)
C_m	concentration of species m (mol/m^3)
D_m	diffusion coefficient of species m (m^2/s)
E	half cell potential (V)
E^{eq}	half cell equilibrium potential (V)
E^o	standard half cell potential (V)
E_{corr}	corrosion potential of iron (V)
E_{appl}	applied potential (V)
E_{ohm}	potential drop in bulk of concrete (V)
F	Faraday constant (96,485 C/mol)
H	Henry's law constant
i	current (A)
I	current density (A/m^2)
I^o	exchange current density (A/m^2)
I_{corr}	corrosion current density (A/m^2)
I_i	component of current density in i direction (A/m^2)
I_L	limiting current density (A/m^2)
J_m	molar flux of species m (mol/m^2 s)
K_{O_2}	mass transfer coefficient of oxygen (m/s)
n	number of electrons
n	unit vector perpendicular to insulating surface
P_{O_2}	equivalent partial pressure of oxygen adjacent to rebar (atm)
PS	pore saturation
R	gas constant (8.314 J/mol K)

NOMENCLATURE (Continued)

R_B	bulk resistance (ohm)
$R_{Fe,mt}$	mass transfer resistance at iron electrode (ohm)
$R_{Fe,ct}$	charge transfer resistance at iron electrode (ohm)
R_u	uncompensated resistance (ohm)
T	temperature (K)
V	bulk velocity of fluid (m/s)
X	length of sprayed zinc (m)
Y	distance between iron and zinc (m)
z_m	integer charge of ion m
δ	thickness of water layer at iron electrode (m)
Δx	dimension of control volume in x direction (m)
Δy	dimension of control volume in y direction (m)
Δz	dimension of control volume in z direction (m)
ϕ	electric potential in concrete (V)
κ	conductivity of concrete (ohm^{-1} m^{-1})
μ_m	chemical potential (J/mol)
$\bar{\mu}_m$	electrochemical potential (J/mol)
μ_m°	standard chemical potential (J/mol)
ρ	resistivity of concrete (ohm m)
∇	gradient operator
	Subscript
Fe,center	center of rebar
Fe,edge	edge of rebar
Fe/Fe^{2+}	iron oxidation reaction

NOMENCLATURE (Continued)

O_2/OH^- oxygen reduction reaction

Zn/Zn^{2+} zinc oxidation reaction

Superscript

liq,y=L   liquid phase at iron surface

Evaluation of Cathodic Protection in Reinforced Concrete Bridges

1. INTRODUCTION

1.1 Corrosion of Steel in Reinforced Coastal Bridges

Steel corrosion in reinforced concrete is a major concern to transportation agencies nationwide because of the expenses incurred for repair and ultimate shortening of bridge life. The estimated value to repair all the deficient bridges in the United States is about $90 billion[1]. One cause of this deficiency is corrosion of reinforcing bars in concrete. Cathodic protection (CP), as a remedy, has been applied to reinforced bridges since 1974[2]. In Oregon, an estimated savings of $250 million within 10 years will be realized by applying CP systems on 35 coastal bridges[3]. While the principle of cathodic protection is well established, engineering issues on how to optimize these systems remain unresolved. This project evaluates the performance of graphite reference cells in monitoring the effectiveness of cathodic protection systems. Moreover, cell placement strategy is examined through numerical modeling.

Corrosion is a natural electrochemical process whereby metals return to a lower energy oxidized state in the presence of an oxidant. A schematic of the corrosion process for the reinforced steel (reinforcing bar or rebar) in coastal bridges is shown in Figure 1.1.

In the alkaline concrete, iron forms a chemically resistant oxide (γ-Fe_2O_3) surface layer which isolates the underlying steel from any possible oxidant[4]. Consequently, the iron does not oxidize and retains its metallic form. In the marine environment, however, chloride ions (Cl^-) from salt diffuse to the rebar and attack the protective surface layer. In this case, the surface of the exposed metal can act as a mixed electrode upon which coupled anodic and cathodic reactions take place.

The anodic (oxidation) reaction leads to dissolution of iron

$$Fe \rightarrow Fe^{2+} + 2e^- \hspace{5cm} (1\text{-}1)$$

Since both oxygen and water are present in the marine environment, the most likely cathodic reaction is the reduction of oxygen

$$\tfrac{1}{2}O_2 + H_2O + 2e^- \rightarrow 2OH^- \qquad\qquad (1\text{-}2)$$

Fe

Concrete

Cl^-

$Fe \rightarrow Fe^{2+} + 2e^-$

e^-

$H_2O + \dfrac{1}{2}O_2 + 2e^- \rightarrow 2OH^-$
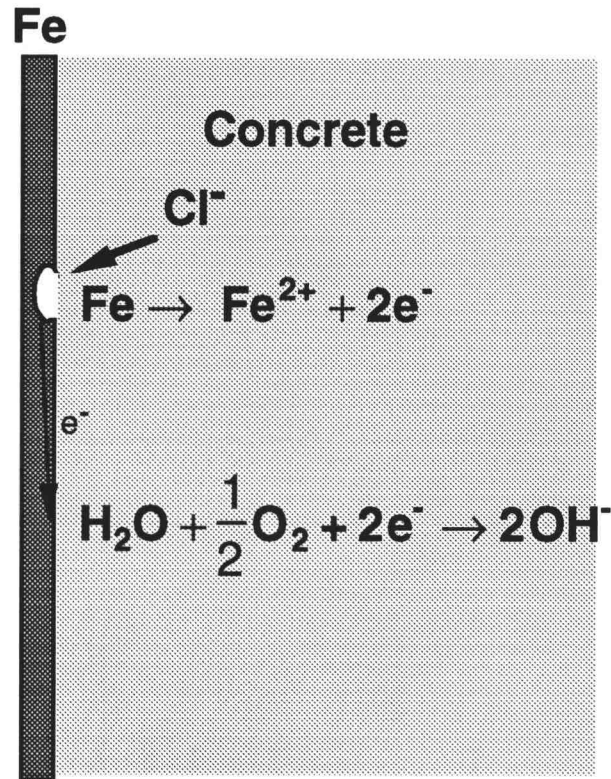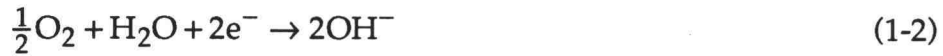
Figure 1.1 Corrosion in reinforced concrete

The electrons produced by the anodic reaction flow through the iron to the cathodic site. If the oxidation and reduction reactions occur at approximately the same site, the process is termed microcorrosion. In macrocorrosion the electrons flow to a different location. In this case, the porous concrete serves as an electrolyte to close the circuit and maintain electroneutrality.

Corrosion is controlled by the thermodynamics and kinetics of the oxidation /reduction pair. Figure 1.2 plots the potential, E, vs. the log of the current density, I (A/m^2), for the reactions (1-1) and (1-2).
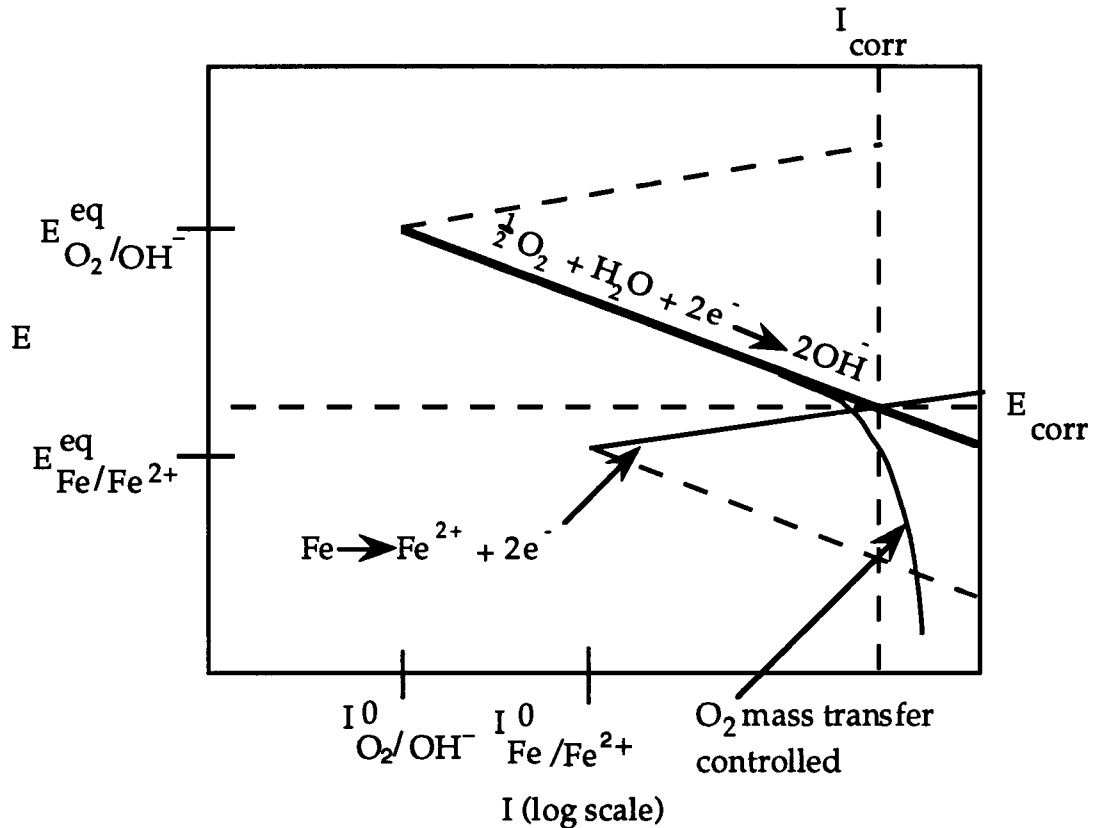
Figure 1.2 Schematic Evans diagram of corrosion of reinforced steel

The equilibrium potential, E^{eq}, is a measure of the energy of each half reaction in the absence of a net current. These values can be calculated using the Nernst equation. For example, the equilibrium potential of the iron half cell is given by

$$E^{eq}_{Fe/Fe^{2+}} = E^{o}_{Fe/Fe^{2+}} + \frac{RT}{nF} \ln a_{Fe^{2+}}$$

(1-3)

where $E^o_{Fe/Fe^{2+}}$ is the standard half cell potential (V with respect to the standard hydrogen electrode), $a_{Fe^{2+}}$ is the activity of ferrous ions adjacent to the electrode, n is the number of electrons, in this case 2, R is the gas constant (8.314 J/mol K), T the temperature (K) and F is the Faraday constant (96, 485 C/mol). Similarly the equilibrium potential of oxygen can be calculated according to

$$E^{eq}_{O_2/OH^-} = E^o_{O_2/OH^-} + \frac{RT}{nF}\ln\left[\frac{p_{O_2}}{a_{OH^-}}\right] \tag{1-4}$$

where p_{O_2} is the equivalent partial pressure of oxygen adjacent to the rebar (atm). Note the equilibrium potential changes with both oxygen concentration and pH. Hence it is very sensitive to the chemical environment adjacent to the rebar. The larger the difference in equilibrium potentials between the anodic and cathodic half cells is, the larger the difference in energy and the greater the driving force for corrosion.

At the equilibrium potential, the current of the cathodic half reaction, e.g.,

$$\tfrac{1}{2}O_2 + H_2O + 2e^- \rightarrow 2OH^- \tag{1-5}$$

is equal and opposite of its corresponding anodic half reaction

$$2OH^- \rightarrow \tfrac{1}{2}O_2 + H_2O + 2e^- \tag{1-6}$$

resulting in no net reaction and no net current. The absolute value of the current density of each half reaction at equilibrium is termed the exchange current

density, I^o (amp/m^2). The exchange current densities for reactions (1-1) and (1-2) are shown in Figure 1.2.

As Figure 1.2 shows, when a corrosion current begins to flow, the electrodes depart from their equilibrium potentials; the cathodic half cell becomes more negative and the anodic more positive. This phenomenon is termed polarization. In the case of a single activated process, the change in potential with respect to the log of the current gives a straight line at large current densities, with a slope (the inverse of the "Tafel" slope) proportional to the activation energy. In microcorrosion, the corrosion current will increase until the potential of both half cells are identical. This defines the corrosion potential of the iron, E_{corr}; the rate of corrosion is proportional to the corrosion current density, I_{corr}. If one of the reactant species becomes depleted, for example, oxygen, then the corrosion rate becomes limited by its availability. This is termed mass transfer control and is also illustrated in Figure 1.2.

For corrosion to proceed, chloride ions must be present to expose the underlying steel. Additionally both oxygen and water must be available to participate in the reduction reaction. In the absence of any of these chemical species, corrosion may not occur.

1.2 Cathodic Protection

Reinforcement coating and cathodic protection (CP) are two major means of preventing for corrosion. Cathodic protection is especially useful for the already constructed bridges where coating is not possible. In 1989, more than 275 bridges in the United States and Canada were being protected in this manner[5].

The principle of cathodic protection is to provide an alternative anodic reaction to that of iron oxidation. Consequently, some of the electrons needed to drive the oxygen reduction half-reaction, equation (1-2), are supplied by an externally applied anode instead of the reinforced steel, and the steel does not corrode as fast. In the limiting case, the applied anode supplies enough electrons to reduce all of the oxygen present at the rebar and the iron corrodes at a negligible rate.

The behavior of a cathodic protection system depends on the electrochemical process occurring at the applied electrode as well as the properties of the porous concrete electrolyte. Cathodic protection anodes include conductive graphite paint, catalyzed titanium, conductive polymeric wire, and sprayed zinc[5]. This research focuses on sprayed zinc anodes.

A schematic of the processes occurring in a sprayed zinc cathodic protection system is shown in Figure 1.3.
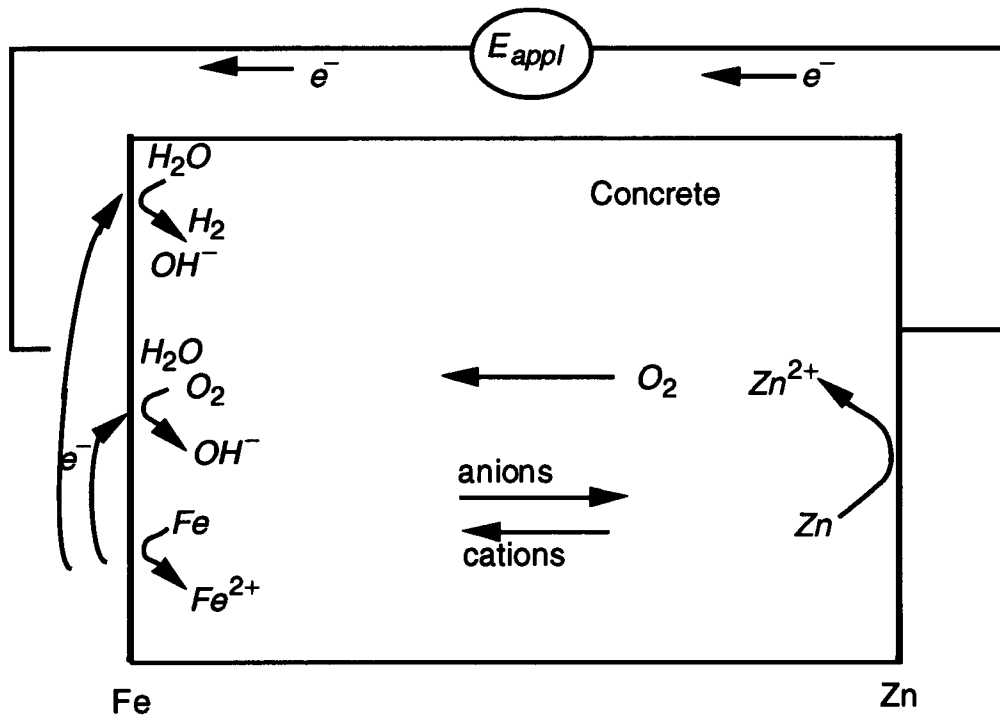
Figure 1.3 One-dimensional schematic of processes occurring in cathodic protection using sprayed zinc

A zinc anode is sprayed onto the outer surface of the corroding structure and electrically connected to the rebar through a voltage source. The zinc oxidation reaction,

$$Zn \rightarrow Zn^{2+} + 2e^- \qquad (1\text{-}7)$$

"competes" with the oxidation of iron, Equation (1-1), in supplying electrons to reduce oxygen. Since zinc is not as noble as iron and has very fast reaction kinetics, it can effectively supply electrons. However, its effectiveness is limited by the highly resistive concrete electrolyte through which the negative charge must return to the zinc (in the form of OH^- or other charged species).

Consider this system in the <u>absence</u> of an applied voltage (but with the zinc connected in a short circuit). In this configuration, which is termed galvanic protection, the total cathodic current increases relative to the open circuit system current. An increase in the oxygen reduction rate corresponds to a more negative electrical potential of iron compared to E_{corr} (see Figure 1.2). Therefore the amount of current associated with the iron half-cell decreases and corrosion is retarded. The lower the potential relative to E_{corr}, the lower the corrosion rate.

A schematic of the currents associated with the possible electrochemical reactions as a function of applied potential, E_{appl}, is shown in Figure 1.4. In the case of a short circuit ($E_{appl}=0$, the case discussed above), the cathodic current is much greater than the corrosion current. The additional anodic current comes from the oxidation of zinc.

The applied potential at which the cathodic current equals the corrosion current is labeled E_{corr}. In this case, the cathodic current equals the anodic current and no electrons flow in the external circuit. This is equivalent, in principle, to free corrosion where there is no CP system in place.

In order to decrease the rate of corrosion even further, a (negative) potential must be applied between the zinc and the rebar. In this case, this configuration is called impressed current cathodic protection, even more electrons will be supplied by the zinc to the reduction of oxygen. Again the total cathodic current will increase. Similarly the potential of iron will be more negative with respect to E_{corr}, and the oxidation of iron will be further retarded. This trend will continue until the concrete adjacent to the electrode is effectively depleted of oxygen. This mass transfer controlled behavior is marked by the flat portion of the cathodic current.

As the applied potential is increased even further, other electrochemical processes occur. As Figure 1.4 illustrates, at sufficiently large potentials, hydrogen evolution commences.

$$2H_2O + 2e^- \rightarrow 2OH^- + H_2 \qquad (1\text{-}8)$$

This leads to hydrogen embrittlement of the iron and can also cause concrete cracking. Thus there is an optimum applied potential. If the applied potential is too low, the iron is underprotected and corrosion still occurs at an appreciable rate. Too large an applied potential leads to overprotection with the deleterious reduction of water to form hydrogen gas.
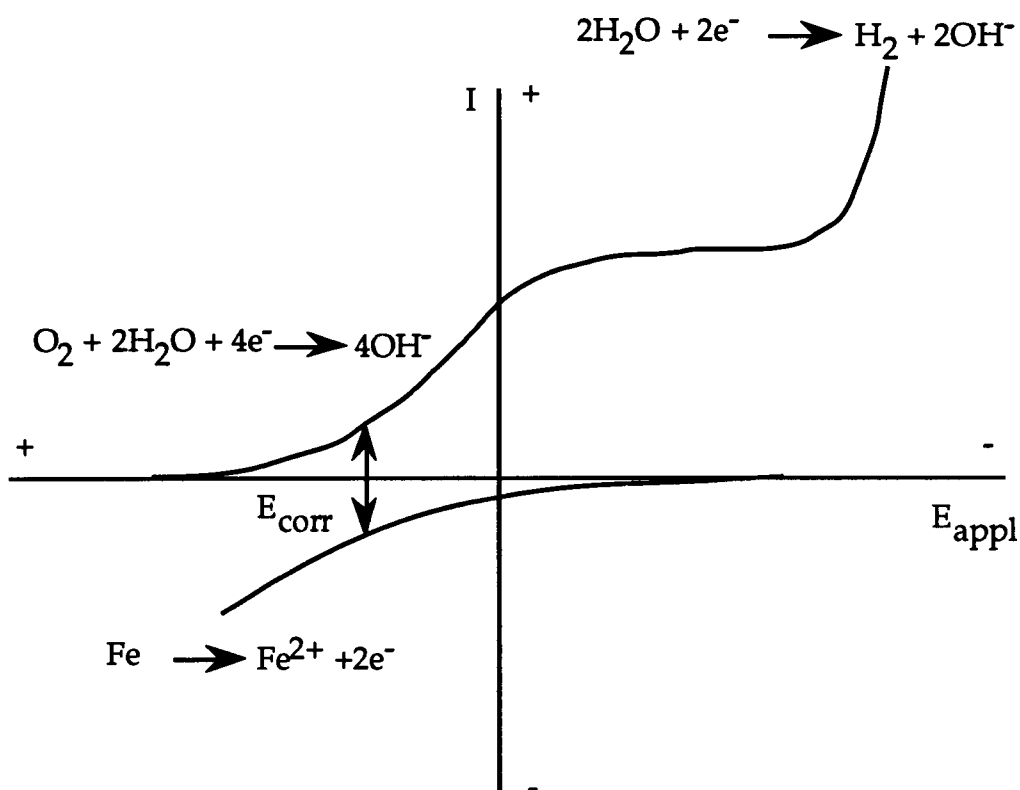
Figure 1.4 Schematic of polarization behavior at rebar/concrete interface

In order to optimize the performance of a CP system, it is important to apply the appropriate potential. This applied potential reduces the potential of iron with respect to E_{corr} and lowers the corrosion rate. However, if the potential

of iron is too negative hydrogen evolution results. This suggests that a convenient monitor of the effectiveness of CP is achieved by measuring the potential of the protected iron (rebar) with respect to E_{corr}. In order to implement this strategy, the proper value of (E_{Fe}-E_{corr}) must be determined. The measurement which is often made, the polarization decay, is related to this potential difference. The decay is determined by interrupting the protection current (open circuit) and monitoring the decay of potential relative to a stable reference electrode. Some investigators have reported 100 mV is an adequate potential decay for protection while others believe the value is closer to 150 [mV][5-10]. In either case, a reliable and durable reference electrode is needed which can accurately track the iron potential.

1.3 Potential Measurement and Reference Electrodes

The rebar potential must be measured with respect to a reference electrode. Figure 1.5 shows a graphite reference electrode imbedded in the concrete near the rebar. In this Figure, R_B and R_u are the bulk and uncompensated resistances respectively. Since concrete is a highly resistive electrolyte, the reference electrode must be placed close to the rebar to minimize error in potential due to the uncompensated resistance.

The potential of the reference electrode needs to be as stable as possible. In selecting a reference electrode, a half reaction with a stable equilibrium potential and minimal polarization is desirable. Recall from the discussion of Figure 1.2, the equilibrium potential can be affected by the chemical species around the reference electrode. An effective reference electrode's equilibrium potential is independent of the chemical species (especially pH) and temperature. Furthermore the reference electrode should be rugged enough to be embedded in concrete and inexpensive.

Standard laboratory reference electrodes such as the silver-silver chloride electrode or the saturated calomel electrode have stable equilibrium potentials. In these electrodes the half-reactions are also well defined. Unfortunately these electrodes are unsuitable for embedding in concrete due to leakage of electrolyte. Solid probes like graphite are more suitable in this regard. On the other hand, a graphite electrode does not have a well defined half reaction but may be

dependent on the species present in the concrete electrolyte. Hence their potential is not as stable as a laboratory electrode.
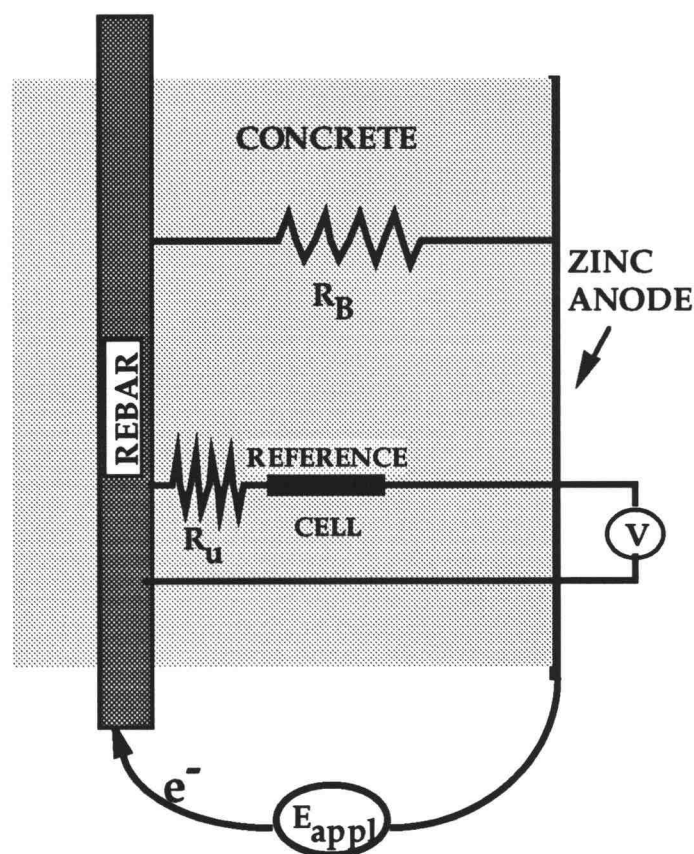
Figure 1.5 Schematic of the placement of graphite probe

1.4 Objectives

The need for a permanent reference electrode to monitor proper protection was discussed in the preceding section. In this regard, graphite probes are being used by Oregon Department of Transportation. However, the correlation between these probes and standard reference electrodes is uncertain. This research will compare graphite probes to silver-silver chloride (Ag/AgCl) electrodes.

This research will also examine the proper placement of reference cells for control of cathodic protection rectifiers. If proper cell placement is not achieved, areas of the bridge may be underprotected and continue to corrode.

In summary, two major research objectives were
1. Determine graphite probe performance with respect to laboratory reference electrodes.
2. Optimize placement of reference cells to ensure effective protection of reinforcing bars.

1.5 Outline of the Thesis

The organization of the thesis is as follows: Chapter two discusses the laboratory tests of reference electrodes (e.g. silver-silver chloride and graphites). Chapter three covers modeling of cathodic protection. In this chapter the input parameters used in the simulation are quantified. Simulation in two dimensions is presented in Chapter 4. Finally, Chapter 5 presents the conclusions and recommendations for future work.

2. LABORATORY TESTS OF REFERENCE ELECTRODES

2.1 Introduction

The long-range goal of this part of the study is to test reference electrodes for their suitability in circuits with which cathodic protection systems are controlled. The current standard for control of cathodic protection systems is the 100-mV depolarization criterion; thus, the immediate objective of this study is the suitability of reference electrodes in the 100-mV depolarization test. Furthermore, cathodic protection can be applied in one of three modes: (a) control potential applied between zinc and iron; (b) control current applied between zinc and iron; and (c) control, as nearly as possible, through a three-electrode cell with or without feedback compensation, the potential at the Fe/concrete interface -- then the value that is controlled is $E_{Fe} + IR_u$, where R_u is an "uncompensated resistance". The three electrode cell mode provides the best control of cathodic protection if the reference electrode continuously operates properly. Thus, a secondary objective is the suitability of reference electrodes for continuous monitoring of the cathodic protection in a 3-electrode potentiostatic mode.

Two characteristics that are important for the reference electrode are ruggedness and reproducibility. These two characteristics are difficult to attain in the same electrode. For example, the silver/silver chloride reference cell is extremely reproducible when it is used under controlled laboratory conditions and the liquid junction is carefully maintained. Furthermore, its potential can be understood from first principles; thus, the effects of various environmental factors (such as pH, O_2, etc.) on electrode response can be predicted. However, careful maintenance of the liquid junction is virtually impossible under field conditions. In contrast, the graphite reference electrode requires virtually no maintenance, but it is not recognized as a particularly reproducible electrode, its response is not easily understood from first principles, and thus one cannot be sure how it will be affected by various environmental factors (e.g., pH, O_2 temperature, water activity, etc.).

This study is broken down into two steps:

1.   Characterization of a system in which reference electrodes can be tested.

The goal is to create a well characterized environment within which electrodes can be tested. A rectangular concrete block is cast. One face is covered with a 1 M KCl soaked sponge to which an Fe plate is affixed The opposite face is covered with a 1 M KCl soaked sponge to which a Zn plate is affixed. The purpose of the sponges is to reduce the charge transfer resistance at the metal plates to the point that it is negligible compared to the ohmic resistance of the concrete. Then, if the concrete block is homogeneous in electrical conductivity, the performance of reference electrodes can be tested by two methods: (a) if a constant potential is maintained between Fe and Zn, the potential between the reference electrode and the Fe plate should vary linearly with distance from the Fe plate; (b) if the reference electrode is maintained at a fixed location in or on the concrete, the potential difference between the reference electrode and the Fe plate should vary linearly with potential difference between Fe and Zn plates.

Thus the first step of the procedure is to use the Ag/AgCl electrode as a "best case scenario" to establish if these linear relations exist initially and if they change over the course of time as a result of the test procedure.

2.   Comparison of the behavior of the graphite electrodes to Ag/AgCl electrodes.

The second step of the procedure is to evaluate how graphite electrodes respond in comparison to Ag/AgCl electrodes. Furthermore, the reproducibility of the graphite electrodes to that of the Ag/AgCl electrodes is to be evaluated. These tests are to be carried out under standard laboratory conditions.

Two additional steps would be useful to complete the characterization of reference electrodes used in cathodic protection:

3.   Effect of environmental variables (temperature, relative humidity) on electrode response.

In this step of the procedure the performance of the electrode would be evaluated under controlled variations in environmental conditions (e.g., temperature 0-40 C, relative humidity 40-100%). For the graphite electrode, of which the response mechanism in concrete is unknown, this step is important. Other environmental variables such as O_2 content and pH value could play a role as well.

4.   Mechanism of response of the graphite electrode.

The chemical species that poise the potential of the graphite electrode in concrete are unknown. It would be useful to determine the reactions that are responsible for poising the electrode in order to predict the sensitivity of the electrode to environmental variables. These last two steps were not completed as part of this thesis.

2.2 Materials and Methods

2.2.1 Concrete Blocks

A block of concrete (35 X 15 X 15 cm^3) in accordance with ODOT mix formulation from a 1953 bridge project was cast and cured. The composition of the concrete was (dry weights per cubic yard): 564 lb of cement, 2100 lb of 3/4 to 3/2 inch aggregate, 1115 lb sand, and 270 lb water. To this mix was added 2 lb/yd^3 sodium chloride. Sufficient air entraining agent was added to provide 3-6% air content. The block was cast in the OSU cement laboratory.

2.2.2 Electrodes

The iron electrode was a 15 cm X 15 cm X 1 cm cast steel plate purchased from Gerlinger company in Salem, OR. The zinc electrode was a 15 cm X 15 cm X 0.08 cm Zn metal plate purchased from VWR Scientific. Two types of reference electrodes were used. The Ag/AgCl reference electrodes were Orion Research

Model 90-02 double junction reference electrodes. The inner compartment was filled with Orion Model 90-00-02 filling solution, which poises the electrode at +0.242 V vs. the standard hydrogen electrode at 25 C. The outer filling solution was 1 M KCl. Commercial graphite electrodes were obtained from Electrochemical Devices, Inc. (EDI Model CG-GRA). The home-made graphite electrodes were made from graphite rods (grade 8k-05, 1.6 cm X 30 cm) purchased from McMaster-Carr Supply Company. These rods were cut into pieces 6.5 to 7 cm in length, and a piece of wire was connected to each by a stainless steel screw. The graphite electrodes were used as received or preconditioned by soaking in 0.5 M $Ca(OH)_2$ for 24 hours.

2.2.3 Instrumentation

Potential difference between the Fe and Zn electrodes was maintained with an EG&G Princeton Applied Research (PAR) Model 173 potentiostat (in a 2-electrode mode) connected to a PAR Model 175 Universal Programmer. The total charge passed was monitored with a PAR Model 179 digital coulometer. The potential difference between the reference electrodes (see description of cell below) was monitored with a Keithley Model 197 digital voltmeter (DVM) with 1 Gohm input impedance. Independent tests showed that the ground of the Keithley 197 was isolated from the ground of the potentiostat.

2.2.4 Test Cell

The Fe and Zn electrodes were mechanically attached to the concrete block through sponges as shown in Figure 2.1. The purpose of the sponges was to reduce the charge transfer resistance at the metal surface such that they would be negligible compared to the ohmic resistance of the concrete block. The sponges had been wet with 1 M KCl and squeezed to remove excess water. The Fe and Zn electrodes were connected to the PAR 173.

In all of the experiments, one Ag/AgCl reference electrode was placed in a hole in the sponge at the Fe plate. Two configurations were used for the other

reference electrode: (a) the other reference electrode was mounted in a hole bored in a sponge cube (2.5 cm X 2.5 cm X 2.5 cm, treated with 1 M KCl), and the sponge cube was placed on the surface of the concrete block, see (Figure 2.2), and (b) the reference electrode was embedded into the concrete block and sealed with a mixture of cement, concrete powder from the hole, and water. The reference electrode at the iron plate and the other reference electrode (in either configuration) were connected directly to the Keithley 197.
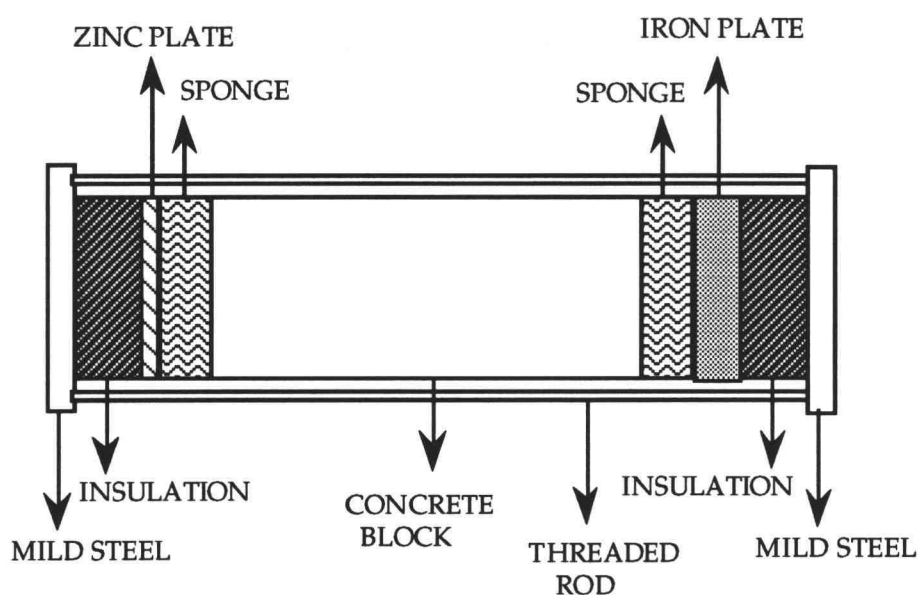
Figure 2.1 Schematic of the electrochemical cell

2.3. Results and Discussion

2.3.1 Evaluation of the Test Procedure with Ag/AgCl Electrodes

The potential difference between the two Ag/AgCl reference electrodes as a function of position and applied potential between the Zn and Fe plates is shown in Figure 2.3. The experiment was performed at -2, -1, 0, 1, and 2 V overpotentials. Overpotential is defined as the difference between the applied

potential and the open circuit potential between the Fe and Zn plates. As indicated by the straightness of the lines, the concrete is reasonably homogeneous, the potential differences at the Fe and Zn interfaces are negligible compared to the potential difference across the concrete, and the Ag/AgCl electrodes do behave as would be predicted from first principles. The resistivity of the concrete was calculated from the current and voltage data from all of the
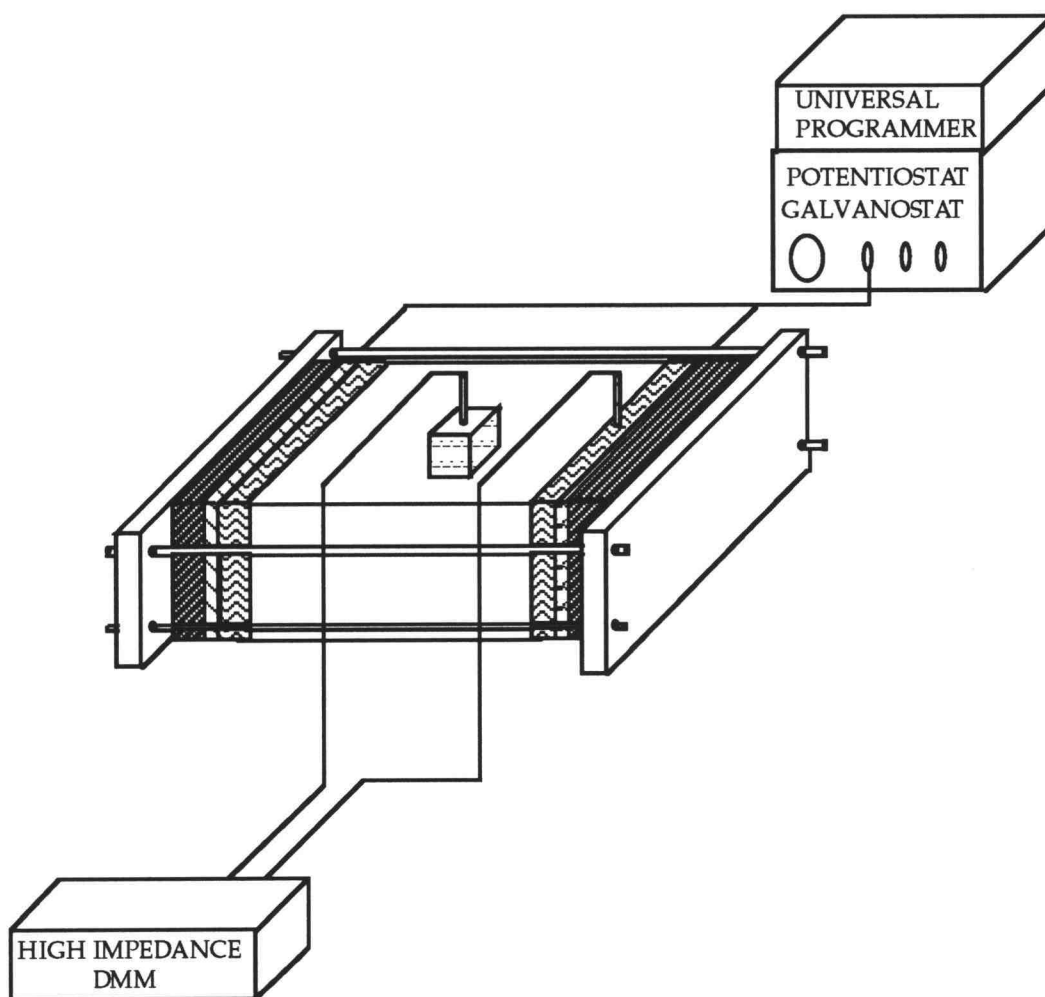
Figure 2.2 Experimental apparatus for the case where the reference electrode is placed on the surface of concrete through a sponge

experiments to be 33 kohm cm. Thus, one concludes that the test cell is indeed a satisfactory system for testing other reference electrodes. However, it should be noted, that as additional experiments were performed, there was evidence that KCl solution introduced from the sponges at both ends of the block and the reference electrode sponge reduced the resistivity of the block and led to inhomogeneities of the electric field.

Ag/AgCl vs. Ag/AgCl-Fe Potential [V]

2

1

0

-1

-2

□ overpotential=-2[V]

◆ overpotential=-1[V]

○ overpotential=0[V]

△ overpotential=+1[V]

▦ overpotential=+2[V]

0   10   20   30   40

Distance from Fe Plate [cm]
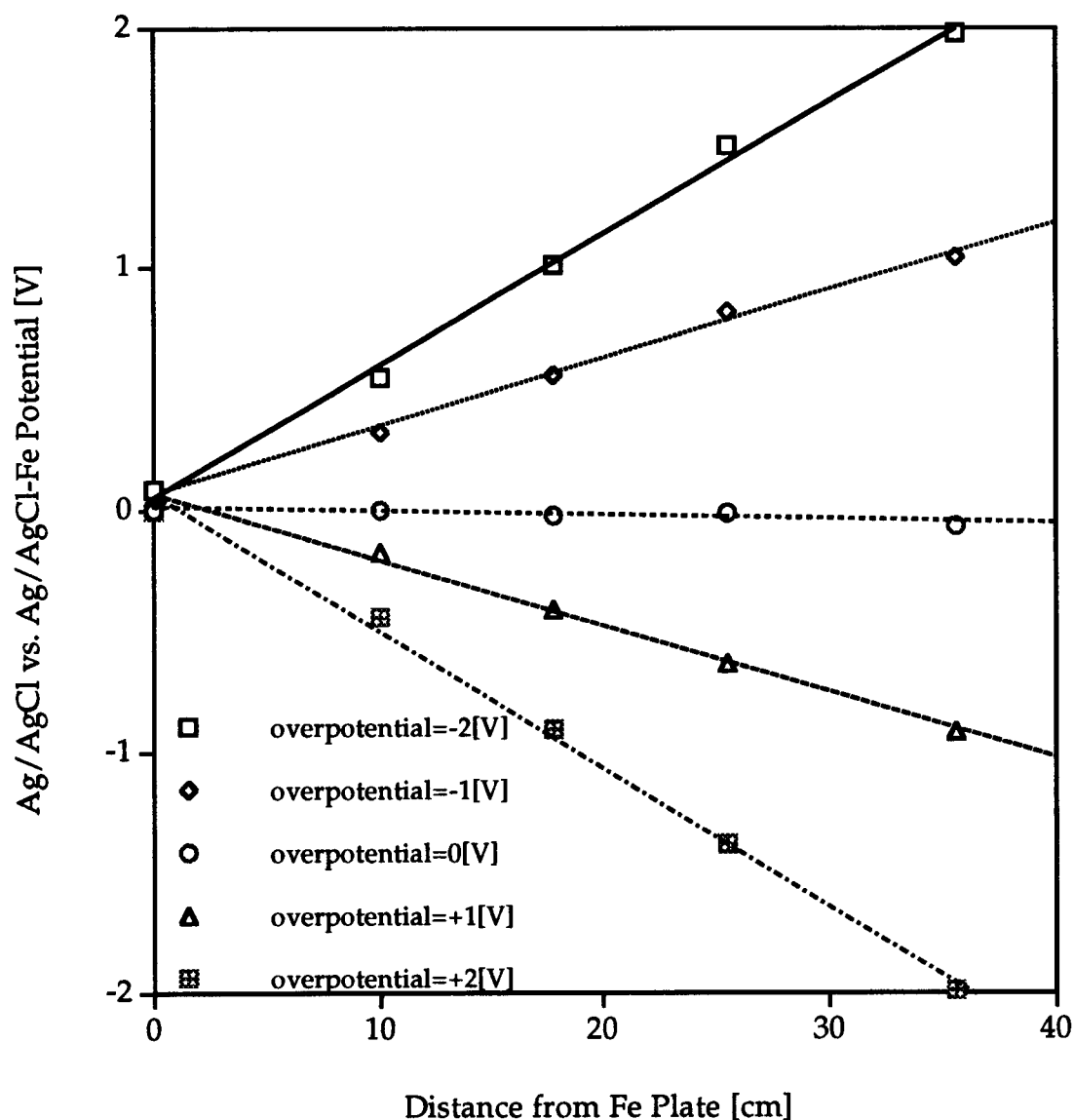
Figure 2.3 Map of electric field at different overpotentials

In order to examine the reproducibility, the entire experiment was repeated immediately after the first run. A histogram of the magnitude of the differences between the first run and the second run is presented in Figure 2.4. With the exception of a few outliers, all readings were reproducible within 25 mV, and 70% were within 10 mV. It should be pointed out that, with a potential drop of 2000 mV across 35 cm, the gradient is 6 mV/mm; thus locating the reference electrode could be a major source of error.
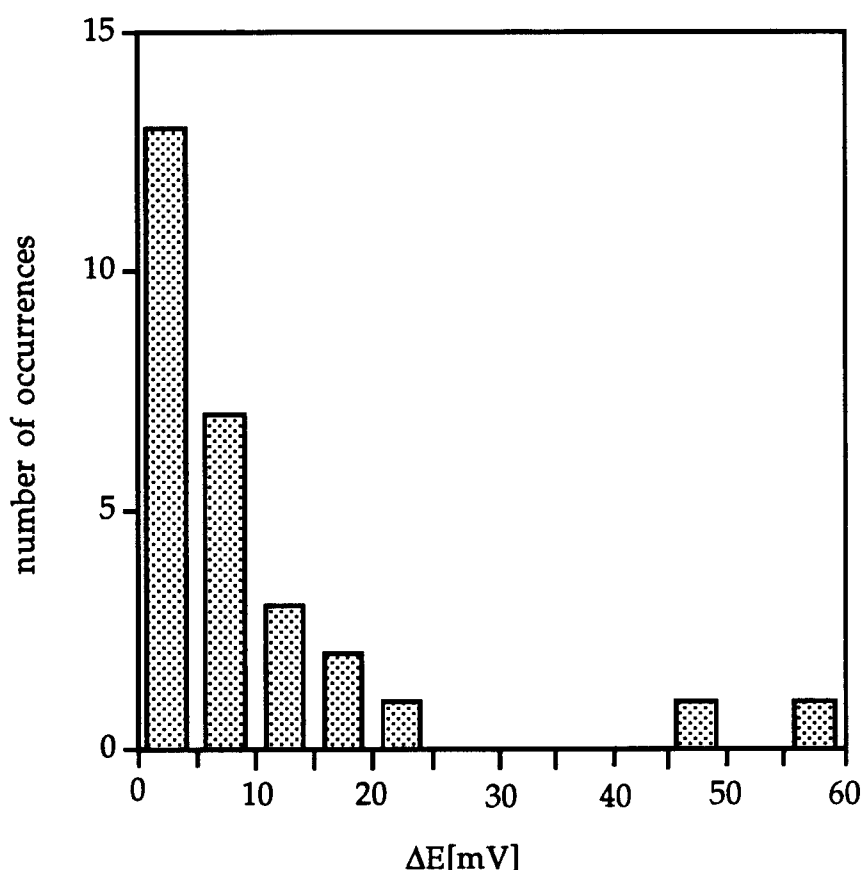
Figure 2.4 Reproducibility of Orion Ag/AgCl electrode

2.3.2 Comparison of the Ag/AgCl and Graphite Electrodes

The entire test procedure was repeated several weeks later with both an Orion Ag/AgCl and an EDI graphite electrode placed at various locations across

the top of the block. By this time, the homogeneity of the concrete had been reduced by local intrusions of KCl from the sponges. As seen in the histograms of reproducibility in Figure 2.5, the graphite electrode (in a 1 M KCl soaked sponge) performed as well as the Orion Ag/AgCl. Again the placement of the reference electrode may be a major source of error.
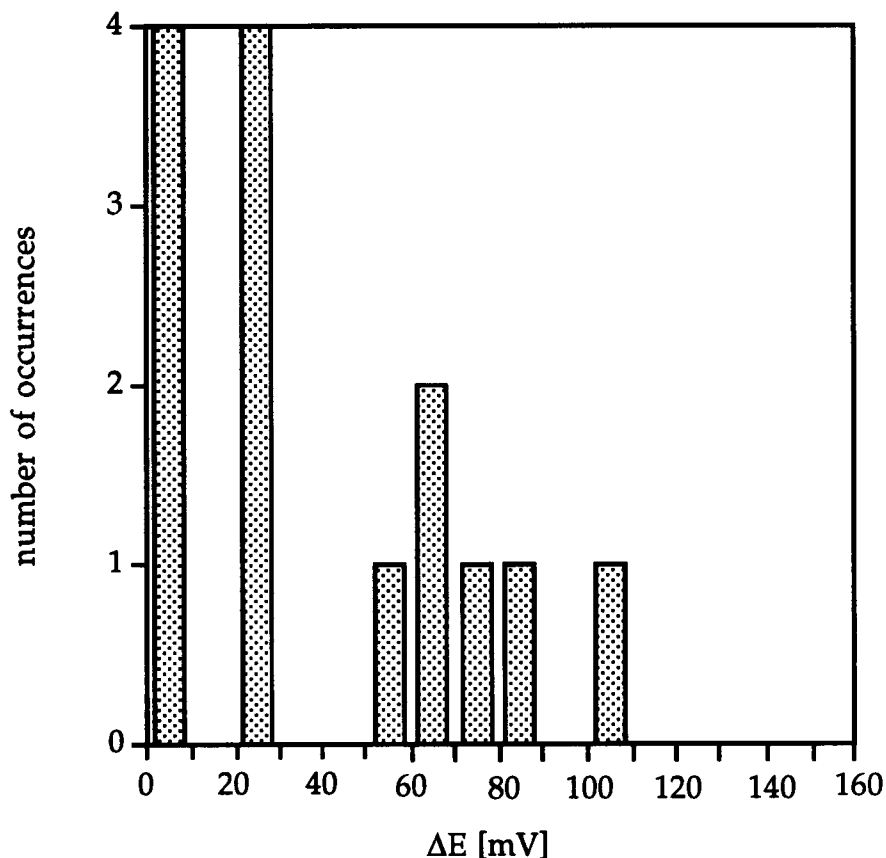
Figure 2.5a Reproducibility of Ag/AgCl electrode

2.3.3 Comparison Among Graphite Electrodes

The performances of home-made graphites were compared to those of two EDI and one Ag/AgCl electrodes. Two overpotentials of -1 and -2 V were used. Graphite electrodes were conditioned (soaked in 0.5 M Ca(OH)$_2$ for 24 hours) and the test was repeated. Table 2.1 represents the tests performed on the

commercial and home-made graphite electrodes (unconditioned and conditioned), and Orion Ag/AgCl electrode.
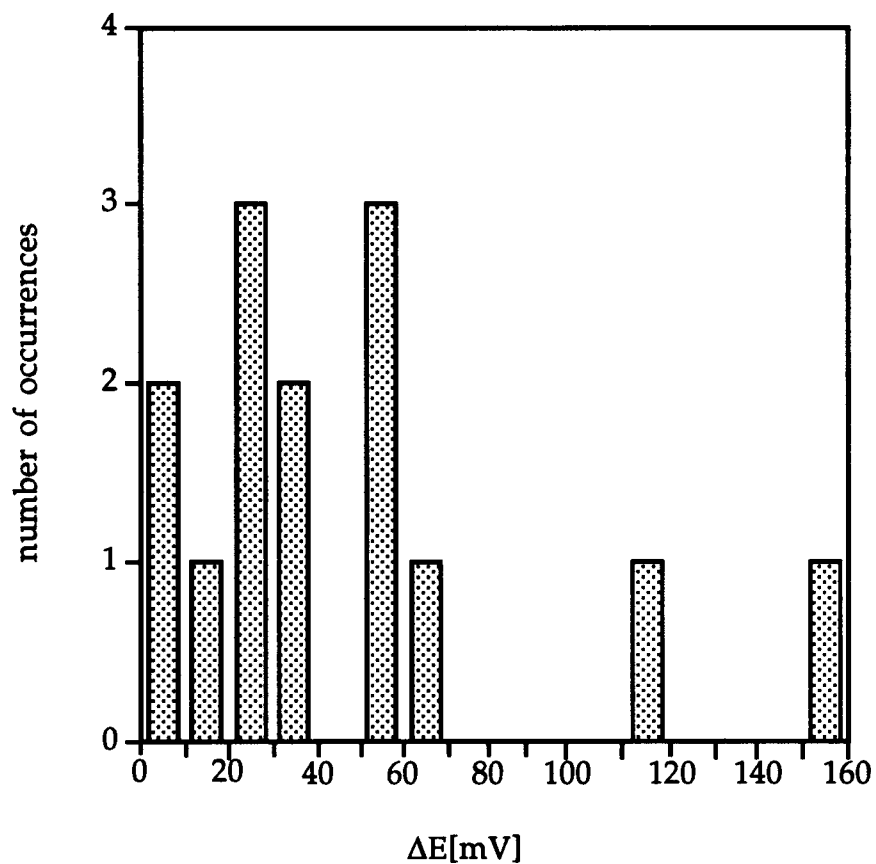
Figure 2.5b Reproducibility of graphite electrode

Table 2.1 Tests performed on graphite and Ag/AgCl electrodes

	conditioned	1st run η=-2 V	1st run η=-1 V	2nd run η=-1 V	2nd run η=-2 V
Orion Ag/AgCl		√	√	-	-
EDI # 1		√	√	-	-
EDI # 2		√	√	√	√
home-made # 1		√	√	√	√
home-made # 2		√	√	√	√
EDI #1	√	√	√	√	√
EDI #2	√	√	√	√	√
home-made # 1	√	√	√	√	√
home-made # 2	√	√	√	√	√

All of the electrodes appear to track the potential along the concrete block reasonably well, as shown in Figures 2.6 and 2.7. Moreover, home-made graphite probes behaved the same as the EDI electrodes and the Ag/AgCl reference electrode. This will allow much greater experimental latitude since the home-made probes are much more economical than the commercial ones. Furthermore, the conditioned graphite probes showed potential values closer to each other than those of the unconditioned ones, as a comparison of Figures 2.6 and 2.7 illustrates. **Conditioning causes the probes behave more uniformly.** Histograms for unconditioned and conditioned probes are shown in Figures 2.8 and 2.9, respectively. **These data show that the reproducibility of the probes increase after conditioning.**

2.3.4 Comparison of Embedded Graphite and Ag/AgCl Electrodes

In this experiment the potential of the embedded electrodes relative to the reference electrode in the sponge of the Fe plate was determined as the potential applied between the Zn and Fe electrodes was changed. As seen in Figure 2.10, both the conditioned home-made graphite electrode and the Ag/AgCl electrode track the applied potential well.
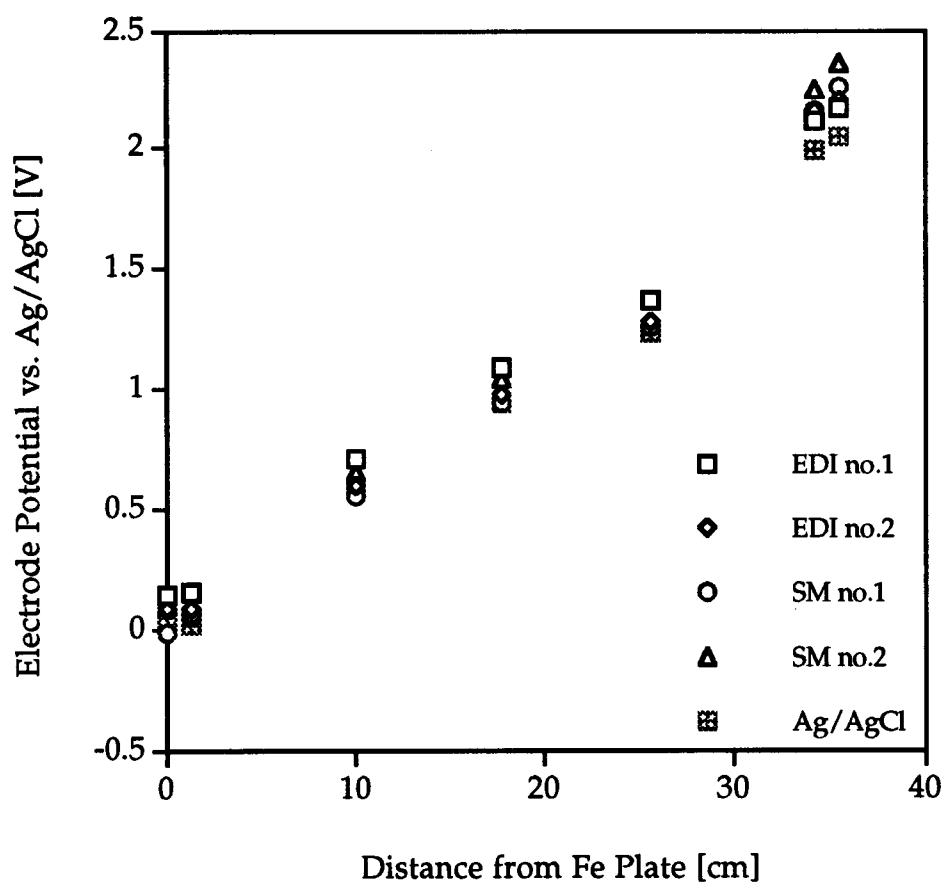
Figure 2.6 Map of electric potential using unconditioned graphite probes and Ag/AgCl, (overpotential=-2[V]).
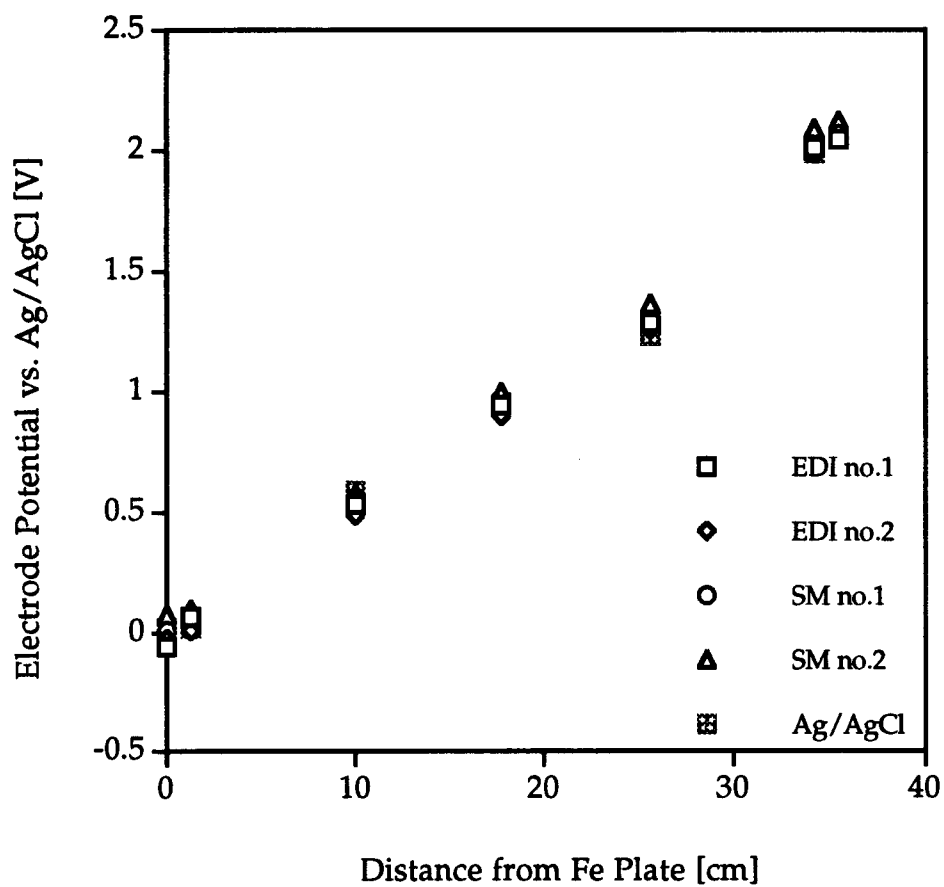
Figure 2.7 Map of electric potential using conditioned graphite probes and Ag/AgCl, (overpotential=-2[V]).
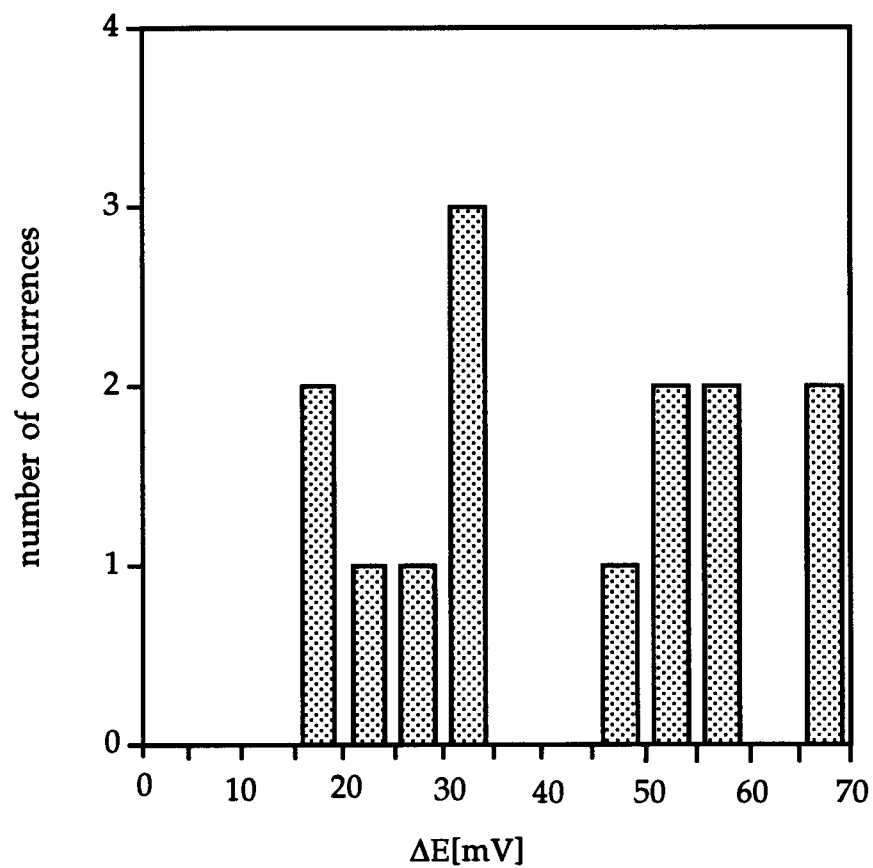
Figure 2.8 Potential reproducibility of an unconditioned commercial graphite
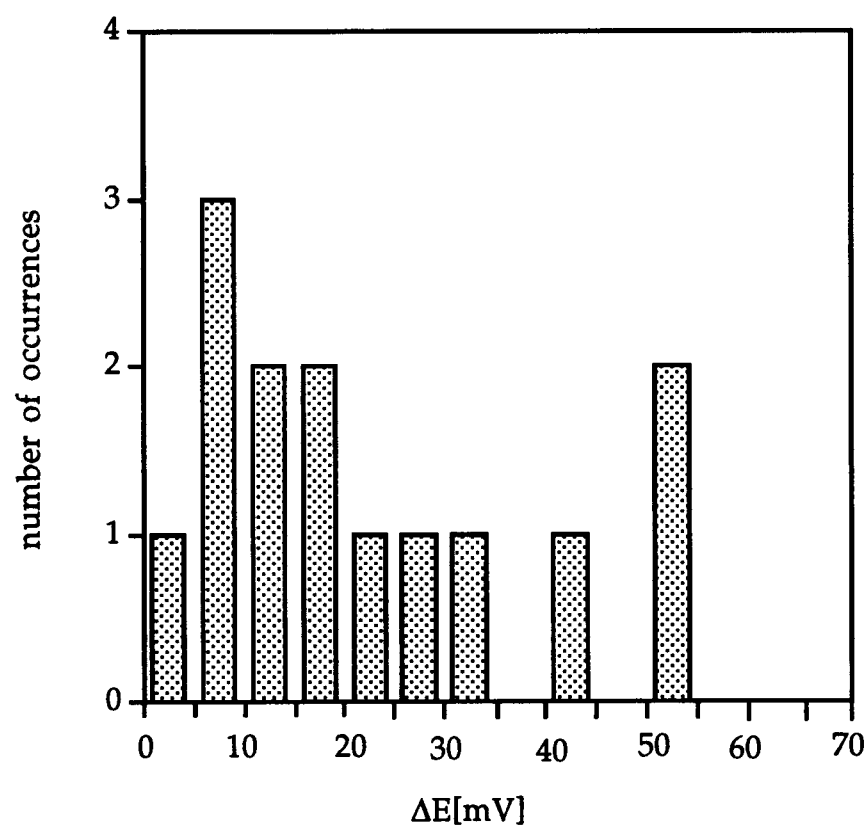
Figure 2.9 Potential reproducibility of a conditioned commercial graphite
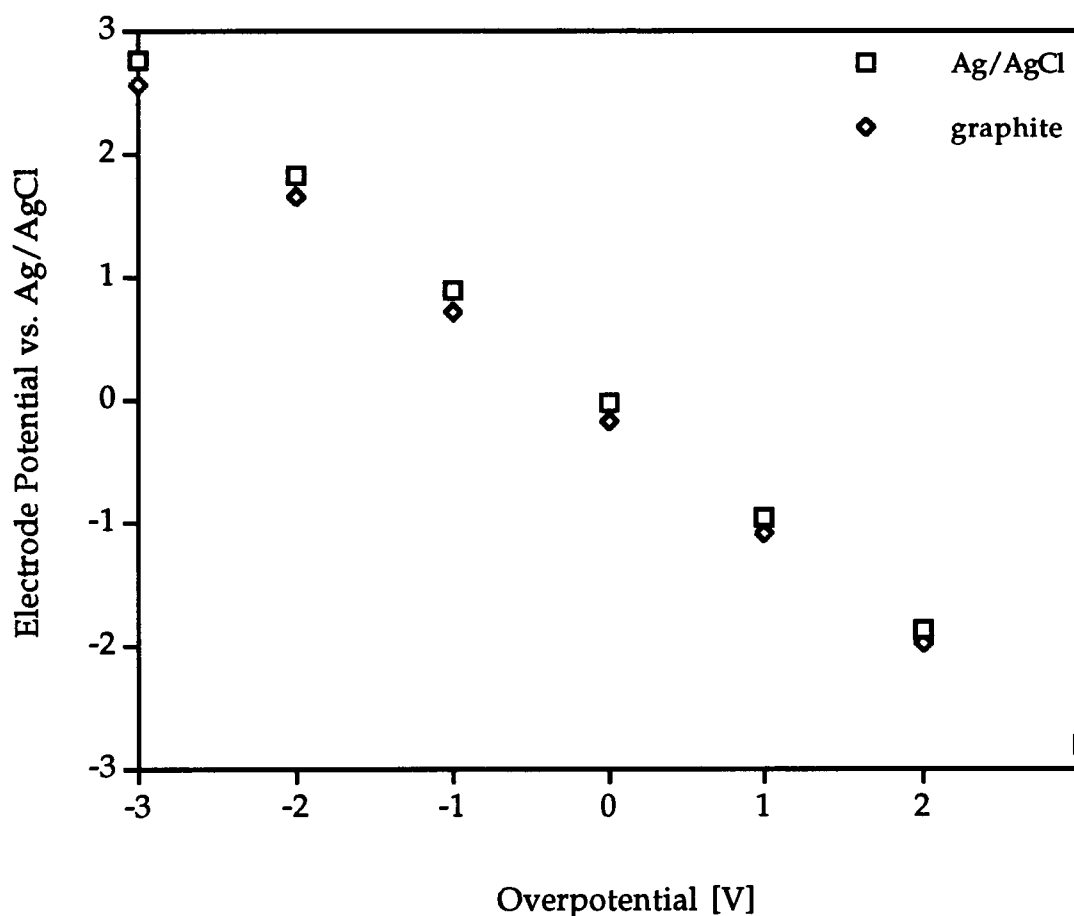
Figure 2.10 A comparison between embedded graphite and Ag/AgCl electrodes

2.4 Summary

At the level of testing performed here, there seemed to be no striking difference between the conditioned home-made and EDI graphite electrodes and the Orion Ag/AgCl electrode. The tests with the movement of the reference electrode showed higher variability than one would like to see (approximately 50 mV deviation), but part of that variability is attributed to the placement of the reference electrode. Thus, it is recommended that future tests monitor long-term stability of embedded electrodes under conditions similar to those of the 100-mV depolarization test of the 3-electrode controlled potential protection circuit.

2.5 Conclusions

1.   The concrete block was reasonably homogeneous, the potential differences at the Fe and Zn interfaces were negligible compared to the potential difference across the concrete, and the Ag/AgCl electrodes did behave as would be predicted from first principles. Thus the test cell was indeed a satisfactory system for testing other reference electrodes.

2.   Locating the reference electrode on top of the concrete block could be a major source of error.

3.   Graphite probes behaved as well as the Ag/AgCl reference electrode. Furthermore, the home-made graphite probes behaved the same as the commercial ones and the Ag/AgCl reference electrode. This will allow much greater experimental latitude since the home-made probes are much more economical than the commercial ones.

4.   The conditioned graphite probes showed potential values closer to each other than those of the unconditioned ones. Also the reproducibility of the probes increased after conditioning.

5.   Embedded graphite probe behaved similarly to the Ag/AgCl reference electrode. They both well tracked the applied potential.

3. A MATHEMATICAL MODEL AND INPUT PARAMETERS FOR CATHODIC PROTECTION

3.1 Background

In this chapter, the processes that are considered in cathodic protection of reinforced concrete are briefly described qualitatively, followed by development of the mathematical expressions which are used to quantify these processes. As with any numerical modeling, many assumptions and simplifications are introduced. While the critical assumptions are assessed, this model should be regarded as "a way of thinking about the problem" rather than "the basis for action."

The system to be considered is a block of concrete with an iron plate on one face and a zinc plate on the opposing face as was illustrated in Figure 1.3. In the absence of cathodic protection, the two plates are not connected; for cathodic protection, the iron plate and the zinc plate are connected through an adjustable constant potential power supply.

As Chapter 1 describes, the corrosion process is the oxidation of iron, which can be represented by the reaction

$$Fe \rightarrow Fe^{2+} + 2e^- \tag{3-1}$$

which is coupled to the reduction of oxygen

$$\tfrac{1}{2}O_2 + H_2O + 2e^- \rightarrow 2OH^- \tag{3-2}$$

In the absence of cathodic protection, the electrons produced by the oxidation of iron are quantitatively consumed by the reduction of oxygen and no current flows through the concrete electrolyte to the zinc plate or through the external

circuit. The reaction rates are determined by the intrinsic kinetics of each reaction as well as by the mass transport of oxygen for Reaction (3-2). This model considers actively corroding rebar.

Oxygen enters the system through the (hypothetically gas-permeable) zinc-plate boundary and moves through the pores, voids, and cracks of the concrete to the iron plate. This transport process is very complex consisting of diffusion and capillary convection involving three phases : gas, water, and solid. A thin water film is believed to cover the iron plate. The rate of oxygen transport is dependent on the percentage of pore volume that is water saturated. Oxygen diffuses much more readily in the gas phase than through water. It is also much more concentrated in the gas phase. In fact the current can be "limited" by the supply of oxygen. This limiting current increases as the amount of water decreases.

When the iron is cathodically protected, most of the electrons necessary to reduce the oxygen are supplied by the zinc plate. The electrons produced by the oxidation of zinc flow through the external circuit and support the reduction of oxygen at the iron plate. The cathodic protection circuit is completed by transport of ions through the concrete pores. The charge introduced through OH^- ions at the iron plate is exactly compensated by the charge introduced by the Zn^{2+} ions at the zinc plate, resulting in the net transfer of negative charge from the iron plate through the concrete to the zinc plate, or a net transfer of positive charge from the zinc plate through the concrete to the iron plate. The actual charge carriers are mobile ions in the concrete, for example, OH^-, Cl^-, SO_4^{2-}, Na^+, Ca^{2+}, etc. The rate of transport is dependent on the resistivity of the concrete electrolyte. Again this parameter can be related to the percentage of pore volume that is water saturated. The greater the water content the lower the resistivity.

Thus, in cathodic protection , there are five processes, the rates of which must be quantified: (a) diffusion of oxygen from the zinc plate to the iron plate; (b) electron transfer in the reduction of oxygen; (c) electron transfer in the oxidation of iron; (d) electron transfer in the oxidation of zinc; and (e) migration of ions through the concrete.

Cathodic protection could be operated in three modes (see Section 1.2): (a) constant potential, (b) constant current, and (c) constant rebar potential through a three-electrode cell. The results of the model could be presented from any of these points of view, but in this study the control E_{appl} paradigm is chosen.

3.2. The Governing Equation for the Concrete Electrolyte

In this section the governing equation for the potential distribution in concrete is developed. It is approached from first principles so that the basic assumptions are explicitly stated and evaluated.

A control volume in rectangular coordinates with Δx, Δy, and Δz dimensions (Figure 3.1) is considered. I_x, I_y, and I_z are the components of current density in the x, y, and z directions respectively. The governing equation is provided by the conservation of electric charge, as follows:

input rate of charge - output rate of charge = charge accumulation

which leads to the following equation under the condition of no charge accumulation (electroneutrality):

$$\left(I_x\big|_x - I_x\big|_{x+\Delta x}\right)\Delta y\Delta z + \left(I_y\big|_y - I_y\big|_{y+\Delta y}\right)\Delta x\Delta z + \left(I_z\big|_z - I_z\big|_{z+\Delta z}\right)\Delta x\Delta y = 0$$

(3-3)

After dividing by $\Delta x\Delta y\Delta z$ and taking the limit, one gets

$$\frac{\partial I_x}{\partial x} + \frac{\partial I_y}{\partial y} + \frac{\partial I_z}{\partial z} = 0$$

(3-4)

In other words the divergence of the current density is equal to zero

$$\nabla \cdot I = 0$$

(3-5)

where ∇ is the gradient operator and I is the current density.
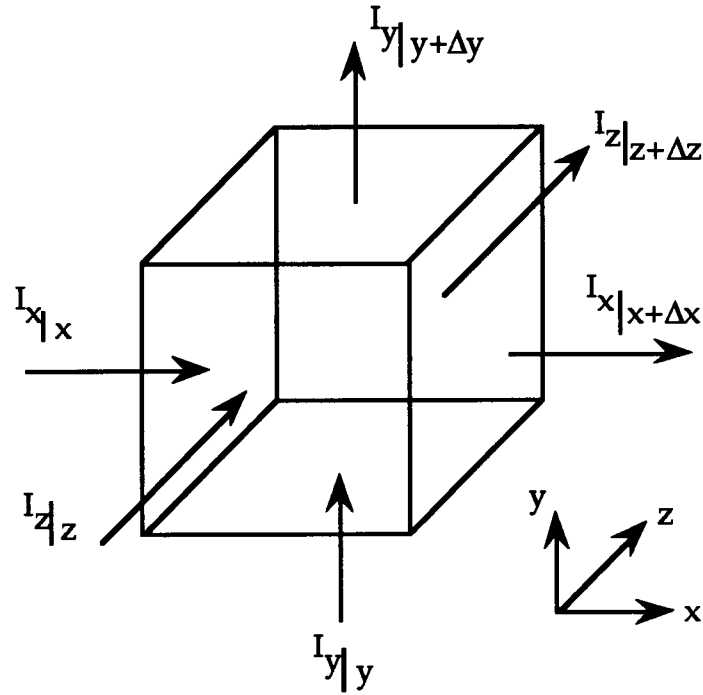
Figure 3.1 Control volume in rectangular coordinate

The molar flux of species m, J_m (mol/m^2 s), is proportional to the gradient in electrochemical potential, $\bar{\mu}_m$ (J/mol), of that species. The constant of proportionality is $\dfrac{C_m D_m}{RT}$ where C_m is concentration of species m,.D_m is diffusion coefficient of species m, R is gas constant , and T is absolute temperature of the concrete[11]. The diffusion coefficient is represented as a scalar, independent of ion concentration and direction (i.e., the concrete is isotropic for ion transportation). As a result the equation of flux is

$$J_m = -\left(\frac{C_m D_m}{RT}\right)\nabla\bar{\mu}_m \qquad (3\text{-}6)$$

In addition to the electrochemical potential gradient, capillary convection might influence the movement of ions in concrete. In such a scenario, the flux of species m is

$$J_m = -\left(\frac{C_m D_m}{RT}\right)\nabla\overline{\mu}_m + C_m V \tag{3-7}$$

where V is the bulk velocity of the fluid (m/s). Furthermore, the electrochemical potential can be divided into two terms:

$$\overline{\mu}_m = \mu_m + z_m F\phi \tag{3-8}$$

where z_m is the integer charge on ion m, F is Faraday's constant, and ϕ is electrostatic potential. The chemical potential, μ_m, is defined as follows:

$$\mu_m = \mu_m^\circ + RT\ln a_m \tag{3-9}$$

where μ_m° and a_m are the standard chemical potential and the activity of species m respectively. Combining Equations (3-7), (3-8), (3-9), and replacing the activity of species m with its concentration leads to

$$J_m = -\left(\frac{C_m D_m}{RT}\right)\left[\nabla(RT\ln C_m) + \nabla(z_m F\phi)\right] + C_m V \tag{3-10}$$

which in turn is simplified to

$$J_m = -D_m \nabla C_m - \frac{z_m F}{RT} D_m C_m \nabla \phi + C_m V \qquad (3\text{-}11)$$

Equation (3-11) is called the Nernst-Plank equation. The first term on the right hand side of this equation represents the flux of ion m due to diffusion (movement due to a concentration (chemical potential) gradient), the second term is due to migration (movement due to a (electric) potential gradient) and the third term is due to capillary convection.

The flux of each species contributes to the current density (A m^{-2}) at any point in the concrete such that

$$I = \sum_m z_m F J_m \qquad (3\text{-}12)$$

Substituting Equation (3-11) into (3-12) yields:

$$I = -\sum_m [F z_m D_m \nabla C_m] - \sum_m \left[\frac{F^2}{RT} z_m^2 D_m C_m \nabla \phi \right] + \sum_m F V z_m C_m \qquad (3\text{-}13)$$

The last term falls out due to electroneutrality:

$$\sum_m z_m C_m = 0 \qquad (3\text{-}14)$$

Combining equations (3-5) and (3-13):

$$\sum_m \left[\nabla \cdot F z_m D_m \nabla C_m \right] + \sum_m \left[\nabla \cdot \frac{F^2}{RT} z_m^2 D_m C_m \nabla \phi \right] = 0 \qquad (3\text{-}15)$$

This partial differential equation couples species transport to the potential distribution.

In order to solve Equation (3-15), two approximations are made. First, it is approximated that diffusion is negligible compared to migration. This approximation is very accurate under the following circumstances: (a) only one type of ion is mobile in concrete and responsible for virtually all the charge transport (the concentration of immobile sites is constant); (b) all the ions have equal diffusion coefficients. In reality different ionic species have different mobilities and are probably present in different concentrations. As long as data for diffusion coefficients of ions in partially saturated porous concrete are unavailable, however, this assumption is necessary.

The conductivity, κ (ohm^{-1} m^{-1}), which is the inverse of resistivity (ρ), is defined to be

$$\kappa = \frac{1}{\rho} = \frac{F^2}{RT} \sum_m z_m^2 D_m C_m \qquad (3\text{-}16)$$

In the second approximation the conductivity is constant in time and space. The use of this approximation is justified by the fact that bulk conductivity of the concrete is easy to measure while single ion diffusivities are unknown.

With these approximations Equations (3-11) and (3-12) can be combined to give

$$I = \kappa \nabla \phi \qquad\qquad (3\text{-}17)$$

which is just Ohm's Law. Moreover, with these approximations, Equation (3-15) reduces to Laplace's equation

$$\nabla^2 \phi = 0 \qquad\qquad (3\text{-}18)$$

In summary, the rigorous governing equation for the concrete system is described by the coupled partial differential Equation (3-15). However, due to the unavailability of data, this microscopic model must be abandoned for a much more macroscopic model expressed in terms of bulk conductivity. However, by considering the microscopic model from first principles, the approximations of the macroscopic model can be evaluated.

3.3 Mechanism of Oxygen Transport through Concrete

Both the corrosion half-reaction (Equation 1-1) and the cathodic protection half-reaction (Equation 1-7) are coupled to the reduction of oxygen at the rebar (Equation 1-2). Since the availability of oxygen can limit the reaction rate, it is important to have an expression to quantify the oxygen mass transfer through the porous concrete.

Concrete is a porous material with a tortuous mass transfer path. The pore structure is dependent on the hydration processes. In general there are many different size pores: gel pores (0.2 nm), small capillary pores distributed around 6-8 nm, large capillary pores distributed around 100-1000 nm, and voids >10 μm)[12,13]. The pore structure complicates the transport process as the smaller pores can completely fill with water while gas is accessible to the larger pores which only have a film of water. Oxygen moves much more readily in the gas phase; the diffusion coefficient of oxygen in the gas phase is 4 orders of magnitude higher than in the liquid, and oxygen is 35 times more concentrated in

the gas. Moreover, the pores can bottleneck containing pockets of liquid slowing the diffusion process. Oxygen could also move by capillary convection.

Again a more precise description is needed for a microscopic description of diffusion based on liquid and gas oxygen diffusivities in this complex pore structure. Consequently a macroscopic approach is adapted based on a bulk mass transfer coefficient,

$$J_{O_2} = k_{O_2} (C_{O_2}^{air} - HC_{O_2}^{liq,y=L}) \qquad (3\text{-}19)$$

where k_{O_2} is the mass transfer coefficient of oxygen through the porous concrete (m/s), $C_{O_2}^{air}$ is the concentration of oxygen in air (0.21P/RT, 8.5 mol/m^3 at 25 C), and H is Henry's law constant for oxygen between air and water. Sandler[14] gives a mole fraction of oxygen in water to be 2.2×10^{-7} (mol O_2/mol H_2O) where oxygen partial pressure is 0.21 bar. From here Henry's law constant is found to be 33 cm^3 mol^{-1} air/cm^3 mol^{-1} water. This constant accounts for the fact that the oxygen in the bulk is in the gas phase while a film of water is assumed to cover the rebar which is located at y=L. The oxygen mass transfer coefficient depends on the percentage of water in the pores (pore saturation), as well as concrete cover depth. Values for the mass transfer coefficient can be obtained from measured oxygen flux through concrete.

3.4 Values for the Concrete Resistivity and the Oxygen Mass Transfer Coefficient vs. Pore Saturation

The concrete resistivity and the oxygen mass transfer coefficient both depend on the pore saturation. In order to model the cathodic protection system over the range of conditions typical of the coastal bridges, values for these parameters were estimated from data available in the literature. Rainfall, relative humidity and temperature are some of the environmental factors influencing pore saturation but are only indirectly related to the resistivity and oxygen mass transfer coefficient. Two studies of concrete resistivity as a function of pore

saturation, PS, were found[15,16]. The data of Gjorv et al[15]. was used since their experiments were performed on concrete (w/c = 0.4) while the other data was for mortar. The fit of the data is shown in Figure 3.2. As a base case, a pore saturation of 60% was chosen. This gives a resistivity of 134 ohm m, typical for the coastal bridges.

Several groups have studied the relationship between oxygen flux and relative humidity[13,17-19], but only one group has explicitly reported oxygen flux versus pore saturation[20]. Data from several of these studies were combined (in a logical way that will not be discussed in detail here) to yield the curves of mass transfer coefficient versus pore saturation that are presented in Figure 3.2. For the base case, a concrete cover of 2.54 cm (1 inch) gave the mass transfer coefficient of 1×10^{-7} m/s.

These experimental data account for the flux through the concrete but not through the water film adjacent to the rebar. An order of magnitude calculation based on the diffusivity of oxygen in water shows the mass transfer resistance of this film is probably important which has not been considered in this research. For the same flux of oxygen through air and water adjacent to the rebar, $K_{O_2} = \dfrac{D}{\delta H}$ where K_{O_2} is oxygen mass transfer coefficient, D is oxygen diffusion coefficient through water, δ is the thickness of water layer, and H is the Henry's law constant (Table 3-1). If $K_{O_2} = 1 \times 10^{-7}$ m/s and $D = 1 \times 10^{-9}$ m^2/s, δ is 300 μm which can be a reasonable value for the water thickness.

3.5 Electrode Kinetics

Charge transfer kinetics are often described by an equation of the following form

$$I = I^{\circ} \exp\left[\frac{-2.3\left(E_{electrode} - E^{eq}\right)}{b}\right]$$

(3-20)

where the parameters I°, the exchange current density, E^{eq}, the equilibrium potential, and b, the inverse of Tafel slope were defined in discussion of Figure 1.2. In order to model the cathodic protection system, these intrinsic reaction rate parameters of Reactions (1-1), (1-2), and (1-7) must be quantified.
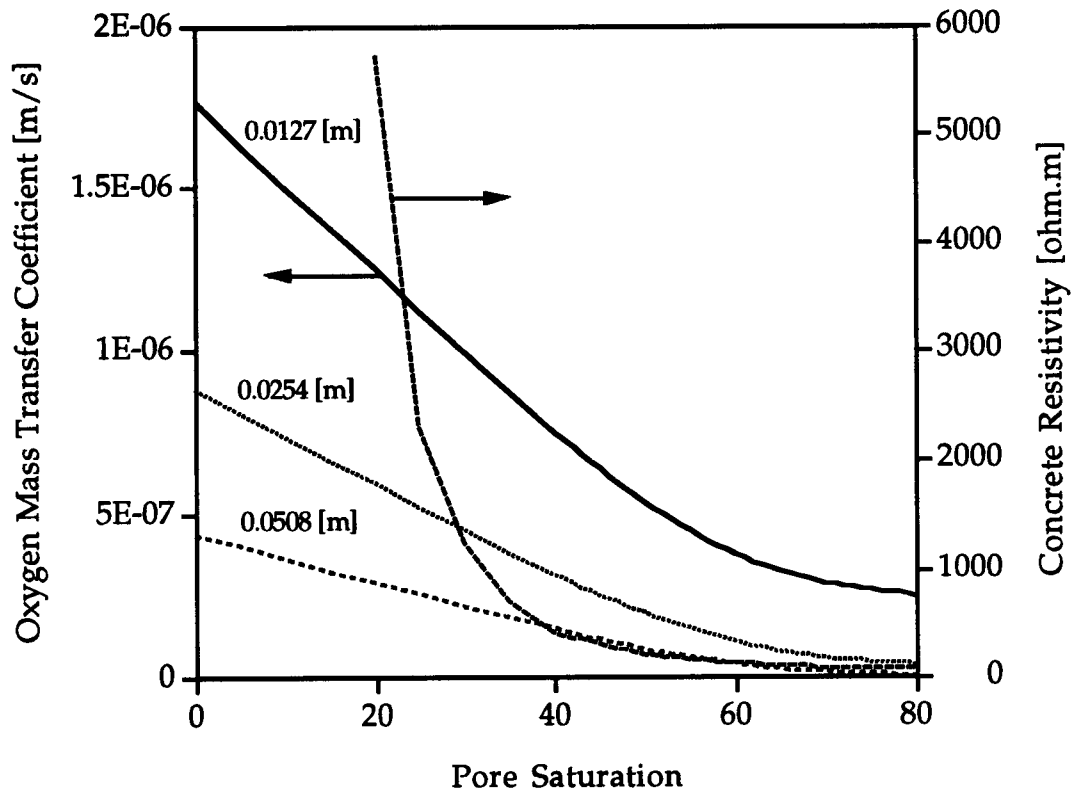

Figure 3.2 Oxygen mass transfer coefficient and concrete resistivity vs. percent pore saturation at three different cover thicknesses of concrete

3.6 Iron Electrode: Values for the Polarization Parameters and Derivation of the Boundary Condition

3.6.1 Values for the Polarization Parameters of Oxygen Reduction and Iron Oxidation

The values of the parameters $I^{\circ}_{O_2/OH^-}$, b_{O_2}, $I^{\circ}_{Fe/Fe^{2+}}$, and b_{Fe} (Equation 3-28) were determined from the data of Locke and Siman[21] through the following procedure.

First, the effective equilibrium potentials for each half reaction (Reactions 1-1 and 1-2) were calculated from the Nernst equation (Equations 1-3 and 1-4). The standard potentials were taken from Pourbaix[22]. For the O_2 reaction, the partial pressure of O_2 was set to 0.21 atm and the concentration of OH^- was set to 0.01 M, consistent with the estimated pH of the concrete, pH=12. For the Fe reaction, the standard potential was used, i.e., the concentration of Fe^{2+} was set to 1 M. These values, which are relative to a standard hydrogen electrode, were then re-expressed relative to a saturated $Cu/CuSO_4$ electrode, the potential of which relative to a standard hydrogen electrode is 0.32 V[23]. These values of the equilibrium potentials are calculated to provide a "reference potential" at which comparisons of electrode kinetic data can be made. However, the precise values of these equilibrium potentials in the final model are inconsequential, since they co-vary completely with the value of I*, as will be seen in the electrode kinetic equations, Equations (3-25) and (3-26).

To determine the values of the electrode kinetic parameters, the data of Locke and Siman[21] for concrete with 0.2% NaCl (their Figures 3 and 4) were used. Locke and Siman state that iR_B compensation was not used in their experiments, but that iR_B drops were probably significant. Thus, the electrode kinetic parameters were determined by nonlinear least squares optimization from the data of Locke and Siman and the electrode kinetic Equations (Equations 3-25 to 3-27) with and without the iR_B term. Then the values from the two methods were averaged, and the average values, which are presented in Table 3.1, were used in this study. The original data of Locke and Siman and the electrode kinetic model (Equations 3-25 to 3-27) with the parameters from Table 3.1 are presented in Figure 3.3.

The model for electrode kinetics here is simply an accurate representation of experimental data, especially for oxygen reduction where the current densities of the data reflect values typical for cathodic protection systems. The parameter values used in this study are consistent with other values reported in the literature[7,24,25]. However, in none of these cases were experimental data presented.
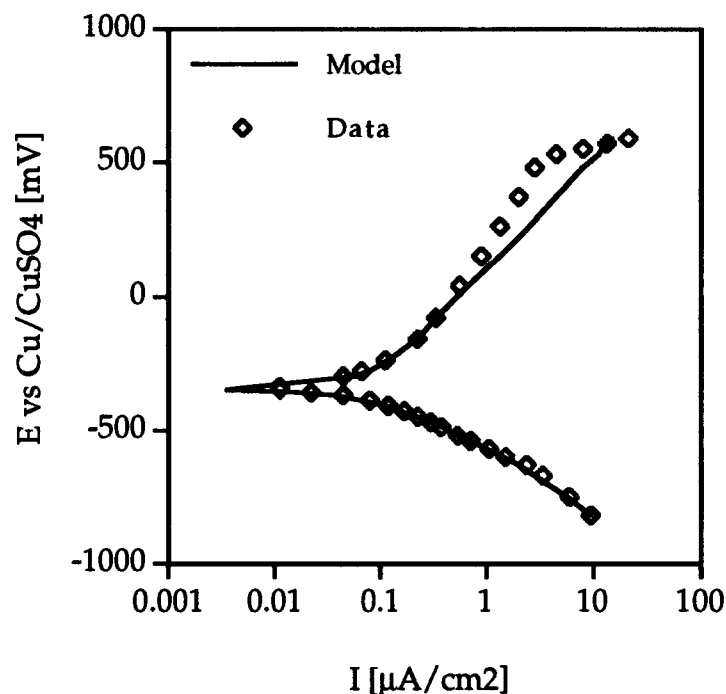
Figure 3.3 Model fit of polarization data for iron in concrete with a 0.2% NaCl concentration by weight

3.6.2 Oxygen Reduction Current Density

The combination of mass transfer resistance due to oxygen transport and charge transfer resistance's of the reduction and oxidation reactions leads to the boundary condition described in this section. Oxygen reduction current density is described by an equation of the following form:

Table 3.1 Values of input parameters for the base case of cathodic protection model.

Symbol	Units	Value	Source(s)
PS	%	60	Typical value
ρ	ohm m	134	Gonzalez et al. (1993)
k_{O_2}	m s^{-1}	1×10^{-7}	Kobayashi, K. and K. Shuttoh (1991) Tuuti (1982)
H	-	33	Sandler (1989)
$C_{O_2}^{air}$	mol m^{-3}	8.5	Ideal gas law
I_{O_2/OH^-}°	A m^{-2}	7.7×10^{-7}	Locke and Simon (1980)
E_{O_2/OH^-}^{eq}	V vs CSE	0.189	Pourbaix (1974)
b_{O_2}	V/decade	0.18	Locke and Simon (1980)
$I_{Fe/Fe^{2+}}^{\circ}$	A m^{-2}	7.1×10^{-5}	Locke and Simon (1980)
$E_{Fe/Fe^{2+}}^{eq}$	V vs CSE	-0.760	Pourbaix (1974)
b_{Fe}	V/decade	0.41	Locke and Simon (1980)
$E_{Zn/Zn^{2+}}^{eq}$	V vs CSE	-0.678	SHRP-S-670
n	-	4	Reaction stoichiometry
F	C mol^{-1}	96,485	Fundamental constant
Y	m	.0254	Typical value (ODOT)
pH		12	Typical value

$$I_{O_2} = I^{\circ}_{O_2/OH^-} \left(\frac{HC^{liq,y=L}_{O_2}}{C^{air}_{O_2}} \right) \exp\left[\frac{-2.3\left(E_{Fe} - E^{eq}_{O_2/OH^-} \right)}{b_{O_2}} \right] \quad (3\text{-}21)$$

where the parameters $I^{\circ}_{O_2/OH^-}$, the exchange current density, $E^{eq}_{O_2/OH^-}$, the equilibrium potential, and b_{O_2}, (the inverse of) the Tafel slope were defined in discussion of Figure 1.2.

Oxygen reduction (cathodic) current density and molar flux of oxygen are related by:

$$I_{O_2} = nFJ_{O_2} \quad (3\text{-}22)$$

which, in combination with Equation (3-19), leads to:

$$I_{O_2} = nFk_{O_2}(C^{air}_{O_2} - HC^{liq,y=L}_{O_2}) \quad (3\text{-}23)$$

If $C^{air}_{O_2} \gg HC^{liq,y=L}_{O_2}$, which means diffusion of oxygen is in control of cathodic current, the "limiting cathodic current density" results:

$$I_L = nFk_{O_2}C^{air}_{O_2} \quad (3\text{-}24)$$

Dividing Equation (3-23) by (3-24) and incorporating the result into Equation (3-21) results in a relation between cathodic current density and iron potential as follows:

$$I_{O_2} = \frac{I_L I^{\circ}_{O_2/OH^-} \exp\left\{\dfrac{-2.3\left(E_{Fe}-E^{eq}_{O_2/OH^-}\right)}{b_{O_2}}\right\}}{I_L + I^{\circ}_{O_2/OH^-} \exp\left\{\dfrac{-2.3\left(E_{Fe}-E^{eq}_{O_2/OH^-}\right)}{b_{O_2}}\right\}}$$

(3-25)

3.6.3 Iron Oxidation Current Density

Charge transfer kinetics of iron oxidation is described by:

$$I_{Fe} = I^{\circ}_{Fe/Fe^{2+}} \exp\left\{\dfrac{2.3\left(E_{Fe}-E^{eq}_{Fe/Fe^{2+}}\right)}{b_{Fe}}\right\}$$

(3-26)

where the parameters $I^{\circ}_{Fe/Fe^{2+}}$, the exchange current density, $E^{eq}_{Fe/Fe^{2+}}$, the equilibrium potential, and b_{Fe}, (the inverse of) the Tafel slope were defined in discussion of Figure 1.2.

3.6.4 Net Current Density and Iron Boundary Condition

The total current density is the net of the cathodic (positive) and anodic (negative) contributions,

$$I = I_{O_2} - I_{Fe}$$

(3-27)

where I is the net current density in the external circuit, which is positive for a net cathodic process at the Fe electrode and negative for a net anodic process at the Fe electrode. Hence, from Equations (3-17), (3-25), (3-26), and (3-27) the following is obtained.

$$-\kappa\nabla\phi = \frac{I_L I^{\circ}_{O_2/OH^-}\exp\left\{\dfrac{-2.3\left(E_{Fe}-E^{eq}_{O_2/OH^-}\right)}{b_{O_2}}\right\}}{I_L + I^{\circ}_{O_2/OH^-}\exp\left\{\dfrac{-2.3\left(E_{Fe}-E^{eq}_{O_2/OH^-}\right)}{b_{O_2}}\right\}} - I^{\circ}_{Fe/Fe^{2+}}\exp\left\{\dfrac{2.3\left(E_{Fe}-E^{eq}_{Fe/Fe^{2+}}\right)}{b_{Fe}}\right\}$$

$$(3\text{-}28)$$

This non-linear equation is considered as the iron boundary condition in solving for potential distribution for the cathodic protection system.

3.7 Zinc Electrode: A Boundary with Constant Potential

In the simple model discussed above, the potential difference at the concrete-zinc interface, E_{Zn}, was treated as a constant, the value of which was found experimentally to be -0.678 V vs. Cu/CuSO$_4$ (CSE) electrode[26]. An equilibrium model cannot explain the high (more positive) experimental value of the zinc potential (see Appendix A1 for details). It is currently unclear what drives the potential to this value. Perhaps this represents a mixed potential possibly mediated by a surface film. A better understanding of the processes occurring at the zinc electrode is needed.

3.8 Equivalent Circuit Representation and Sign Conventions

As stated in Section (3.6.4), the total current density is the net of the cathodic (positive) and anodic (negative) contributions:

$$I = I_{O_2} - I_{Fe} \qquad (3\text{-}29)$$

To restate the sign convention, flow of electrons from zinc to iron in the external circuit is positive current. Current density (I, amp/m^2) is distinguished from current (i, amp).

An equivalent circuit of the system, based on the approximations and assumptions stated above, is illustrated in Figure 3.4. The potential differences around the circuit include E_{appl}, the applied potential; E_{Fe} and E_{Zn}, the two metal/electrolyte interfacial potential differences; and E_{ohm}, the Ohm's law potential drop in the bulk of the concrete. Continuity requires that

$$E_{appl} = E_{Fe} - E_{ohm} - E_{Zn} \qquad (3\text{-}30)$$

where the signs are consistent with Figure 3.4 and the definition of I. While E_{Zn} is represented by a constant potential, E_{Fe} includes a mass transfer resistance due to oxygen availability, $R_{Fe,mt}$, and a charge transfer resistance to account for electrode kinetics, $R_{Fe,ct}$ (Equation 3-28).

3.9 The Boundary Value Problem

The governing equation with the potential equations for iron and zinc, form the boundary value problem to be solved. A summary of the equations follows.

Laplace's equation governs the bulk of the concrete

$$\nabla^2 \phi = 0 \qquad\qquad (3\text{-}31)$$

where ϕ is the electric potential in the concrete (V, in this study relative to a $Cu/CuSO_4$ (CSE) electrode at that point). At the zinc electrode, a constant potential boundary condition is chosen,

$$\phi = const \qquad\qquad (3\text{-}32)$$
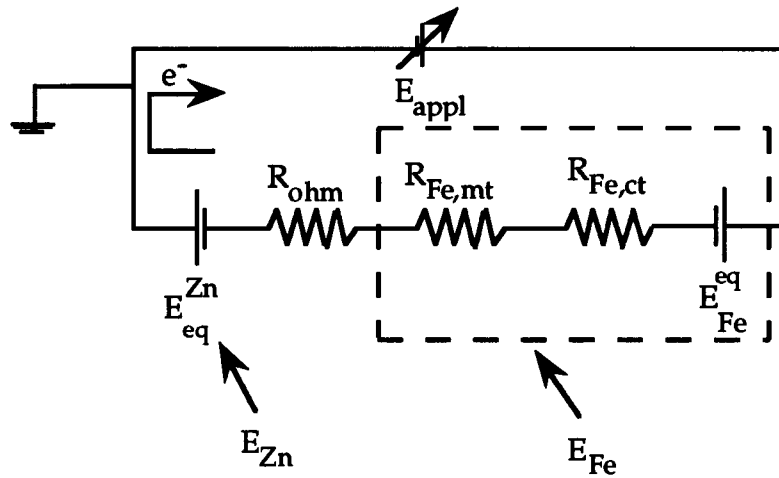
Figure 3.4 Equivalent circuit of the system

while at the iron boundary the potential is given by the boundary condition,

$$-\kappa\nabla\phi = \cfrac{I_L I^{\circ}_{O_2/OH^-} \exp\left\{\cfrac{-2.3\left(E_{Fe}-E^{eq}_{O_2/OH^-}\right)}{b_{O_2}}\right\}}{I_L + I^{\circ}_{O_2/OH^-} \exp\left\{\cfrac{-2.3\left(E_{Fe}-E^{eq}_{O_2/OH^-}\right)}{b_{O_2}}\right\}} - I^{\circ}_{Fe/Fe^{2+}} \exp\left\{\cfrac{2.3\left(E_{Fe}-E^{eq}_{Fe/Fe^{2+}}\right)}{b_{Fe}}\right\}$$

(3-33)

where E_{Fe} is the potential (V) of the iron plate with respect to the $Cu/CuSO_4$ electrode (CSE), which is equivalent to the potential of the iron plate with respect to the electrolyte immediately adjacent to the plate, b_{O_2} and b_{Fe} are the (inverse of the) Tafel Slope parameters for Reactions (3-1) and (3-2) respectively (V/decade), and κ is the conductivity of the concrete electrolyte (ohm m)$^{-1}$. The limiting current density, I_L, is given by

$$I_L = nFk_{O_2}C^{air}_{O_2}$$

(3-34)

The values for the input parameters used in the base case of this model are shown in Table 3-1.

4. SIMULATION IN TWO DIMENSIONS

4.1 Methodology

In order to optimize the placement of reference electrodes in cathodic protection, mathematical modeling was performed in two dimensions, where the effects of non-uniform current distribution are significant. Figure 4.1 shows a simplified representation of a bridge deck, reduced to a rectangular geometry of repeating units.
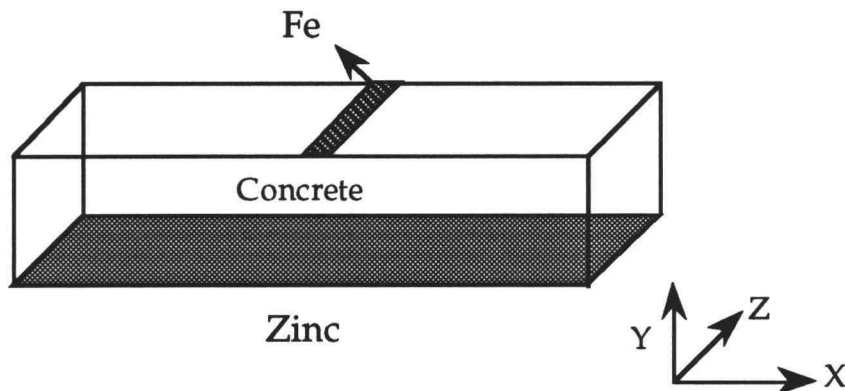
Figure 4.1 Two-dimensional geometry of Fe/concrete/Zn system

A plane of symmetry at the center of the rebar allowed the simulation area to be divided by two, making the computation more efficient. Figure 4.2 shows the geometry used for these simulations. The terms "edge" and "center" of the rebar shown in Figure 4.2 will be used in the following frequently. For a base case, the distance between the zinc and rebar is 25.4 mm (1 inch). The rebar width is 12.7 mm (1/2 inch) and the distance from the center of one reinforcing bar to the next is 304.8 mm (12 inch). Different concrete cover depths are also studied. Dimensions were chosen to represent typical values for the Yaquina Bay Bridge.

A finite difference code (see Appendix A2) was developed to solve Laplace's equation (Equation 3-31) with boundary conditions described by Equation (3-32) at the zinc and Equation (3-33) at the rebar.
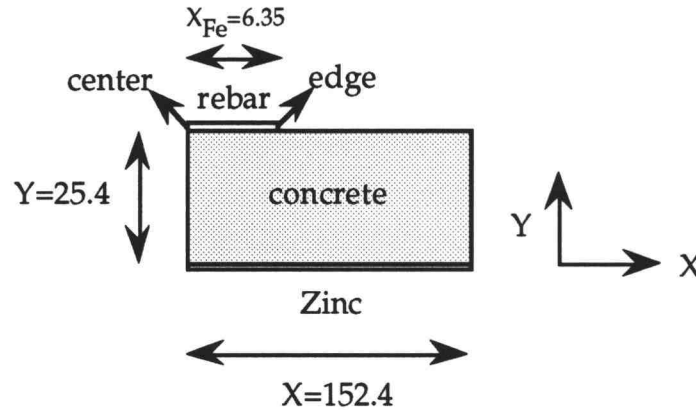
Figure 4.2 Schematic of two-dimensional Fe/Concrete/Zn system, dimensions in [mm] (not to scale)

All other boundaries are considered to be insulating,

$$\nabla\phi\cdot\mathbf{n} = 0 \qquad (4\text{-}1)$$

where $\mathbf{n}$ is the unit vector perpendicular to the insulating surfaces. The equations are solved by means of a Gauss-Siedel iterative method with the help of an over-relaxation factor. An interval halving method is used to solve for the nonlinear boundary condition at the rebar. Iteration concludes when potentials of all points in the domain changed less than a given convergence for two successive iterations. The self-consistency of the solutions is tested as follows: The current density at the rebar surface is calculated independently according to Ohm's law,

$$I = \kappa \frac{\partial \phi}{\partial y}\bigg|_{y=25.4\ \text{mm}} \qquad\qquad (4\text{-}2)$$

and according to the mass transfer/reaction kinetics according to Equation (3-33). These two calculations yield identical values.

4.2 Results and Discussion

The output of the model is presented in five different types of graphs. First, equipotential curves in the concrete are plotted as a function of x and y displacement in the concrete. The potentials are reported versus a $Cu/CuSO_4$ (CSE) electrode with 0 potential at the zinc metal (zinc is grounded). Second, the total current for the cell is reported. This value can be converted to a more general current density using either the surface area of the rebar in the model ($0.635\ cm^2$) or the surface area of the zinc electrode in the model ($15.24\ cm^2$), whichever is appropriate. Third, the "average rebar potential" is plotted. Actually, this value is the arithmetic average of each of the rebar-concrete interfacial potential differences at each of the nodes in the model. The average is plotted (instead of individual space-dependent values) since the size of the reference electrodes in actual experiments (approximately 1.5 cm) is about the size of the rebar, and the "average potential" is an approximation of the value that would actually be determined experimentally. Fourth, the difference between the rebar-concrete interfacial potential differences at the center and edge of the rebar is reported. Finally, the difference between the percentage saturation of oxygen at the center and at the edge of the rebar surface is reported. The saturation value was calculated for water in equilibrium with atmospheric oxygen. These values are used to calculate the depolarization potentials of the rebar-concrete interface.

4.2.1 Equipotential Maps

Figure 4.3 shows equipotential lines as a function of coordinates x and y at an applied potential of -1.0 V for three different cover thicknesses (all other parameters are for the base case as in Table 3.1). These values are reported vs. a $Cu/CuSO_4$ reference electrode. In all cases, the potential in the concrete electrolyte rapidly converges to the zinc potential. For a cover depth of 12.7 mm (1/2 inch) only about 15% of the sprayed zinc contributes to the protection current. Even at a cover of 50.8 mm (2 inch) over half the zinc anode is ineffective. This suggests the effective area of zinc as an anode is considerably less than the entire area of sprayed zinc. The only purpose of the remaining zinc is to maintain electrical continuity. Moreover, the anode will be preferentially consumed directly adjacent to the iron. **Consequently, any calculations of anode life based on current density should use the effective area rather than the total sprayed area.**
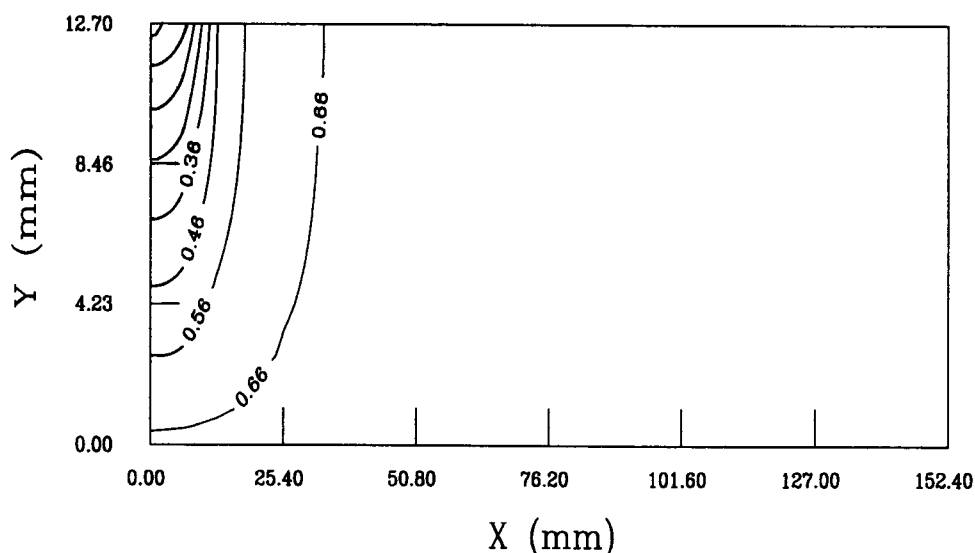

Figure 4.3a Equipotential lines at an applied potential of -1 [V],
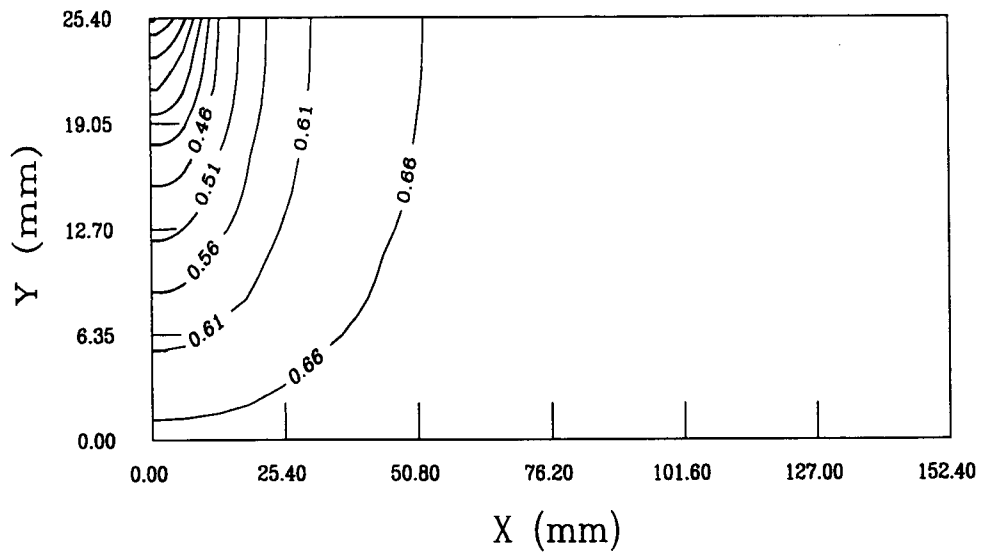cover thickness is 0.5 inch.

Figure 4.3b Equipotential lines at an applied potential of -1 [V],
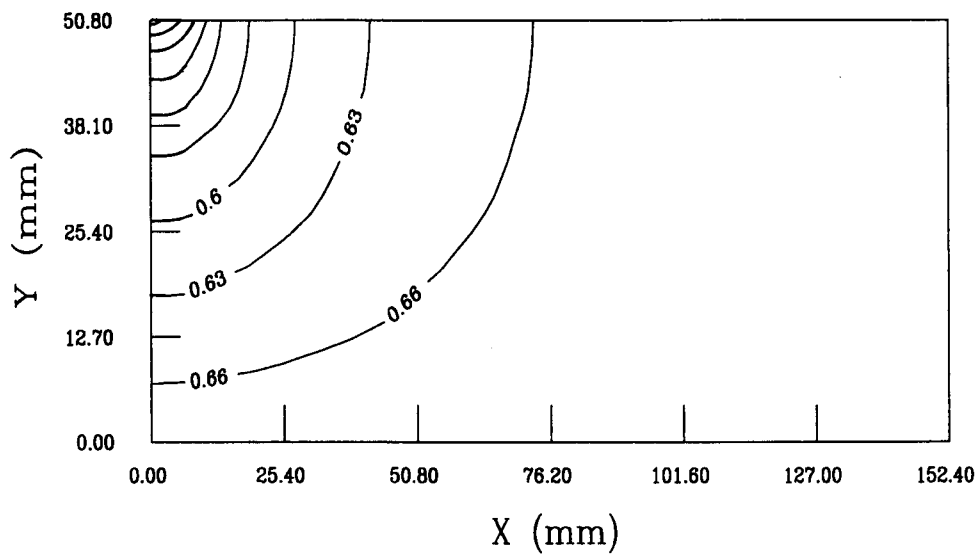cover thickness is 1.0 inch.

Figure 4.3c Equipotential lines at an applied potential of -1 [V],
cover thickness is 2.0 inch.

Figure 4.4 shows a magnified view of the equipotential lines for a cover thickness of 25.4 mm (1 inch) at applied potentials of 0, -1.0, and -2.0 V, respectively. The integrated protection current, the rebar potential and the difference in E_{Fe} between the center and the edge are shown in Table 4.1. As the magnitude of the applied potential increases, the potential on the rebar decreases, as expected. This results in a higher reduction current and better protection. However, decreasing the applied potential below -1.0 V does not change the protection current. At this point, protection is limited by mass transfer of oxygen. At a large enough applied potential (slightly over -2 V[27]), hydrogen evolution will commence, leading to embrittlement of iron and possible cracking of concrete. In the galvanic case, the potential difference between the iron/concrete interface only varies by 7 mV from the center to the edge; however, at the limiting current it varies by 100 mV.

Table 4.1 Calculated values for two-dimensional simulation

Thickness (mm)	E_{appl} (V)	i_{O_2} (mA)	Rebar potential (V vs Cu/CuSO$_4$)	$E_{Fe,center} - E_{Fe,edge}$ (mV)
12.7	0	0.20	-0.65	8
	-1	4.54	-0.95	98
	-2	7.94	-1.39	324
25.4	0	0.18	-0.64	7
	-1	2.24	-1.17	99
	-2	2.27	-2.16	102
50.8	0	0.15	-0.63	7
	-1	0.87	-1.42	41
	-2	0.87	-2.42	41

Figure 4.4a Magnified view of the equipotential lines at an applied potential of 0 [V], cover thickness is 1.0 inch.

Figure 4.4b Magnified view of the equipotential lines at an applied potential of -1 [V], cover thickness is 1.0 inch.
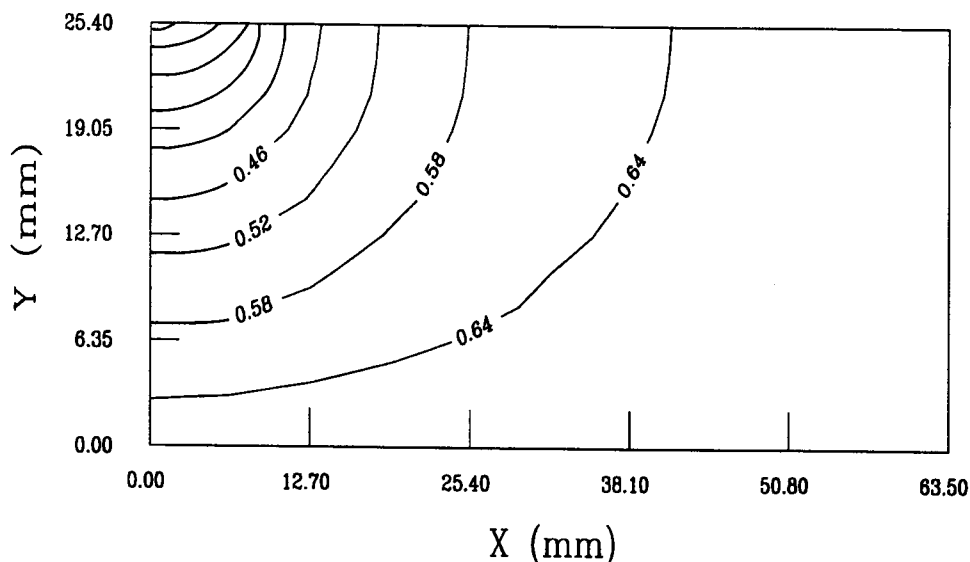
Figure 4.4c Magnified view of the equipotential lines at an applied potential of -2 [V], cover thickness is 1.0 inch.

Figures 4.5 and 4.6 show the magnified views for cover thicknesses of 12.7 mm (1/2 inch) and 50.8 mm (2 inch) respectively. Note the scale of the axis have changed. The integrated protection current, the rebar potential and the difference in E_{Fe} between the center and the edge are also shown in Table 4.1. As the cover thickness decreases to 12.7 mm, there is more oxygen available and the protection current increases. In this case, there is a difference between -2 V and -1 V applied potential. Accordingly, the difference in the potential between the center and the edge exceeds 300 mV. Thicker concrete cover shows the opposite trend.

In all cases, the potential at the edge of the rebar is less (more negative) than that of the center suggesting the center is less protected. When the CP circuit is opened the rebar relaxes to a uniform value, E_{corr}. **Therefore, the reference electrode should be located as close to the center of the rebar as possible.** In extreme cases, protection at the center may coincide with hydrogen evolution at the edge.
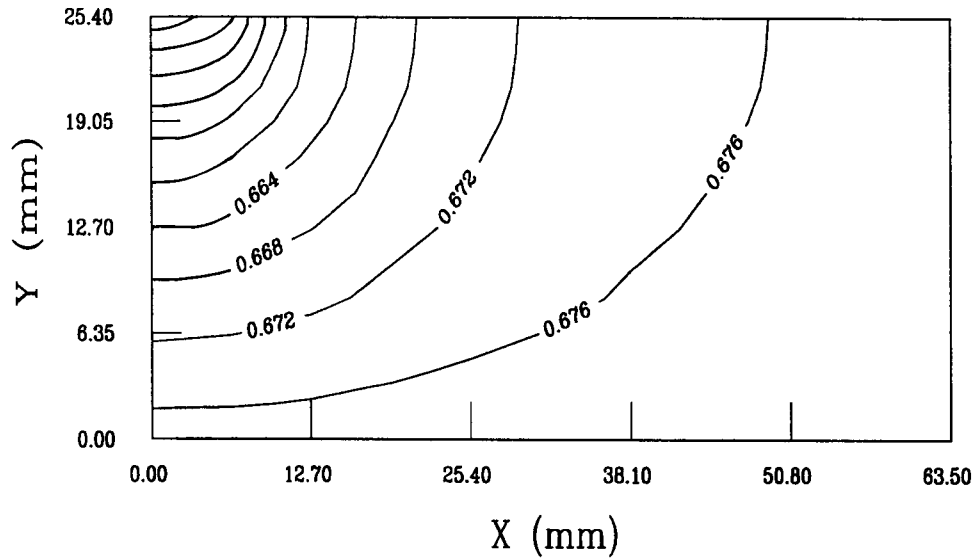
Figure 4.5a Magnified view of the equipotential lines at an applied potential of 0 [V], cover thickness is 0.5 inch.
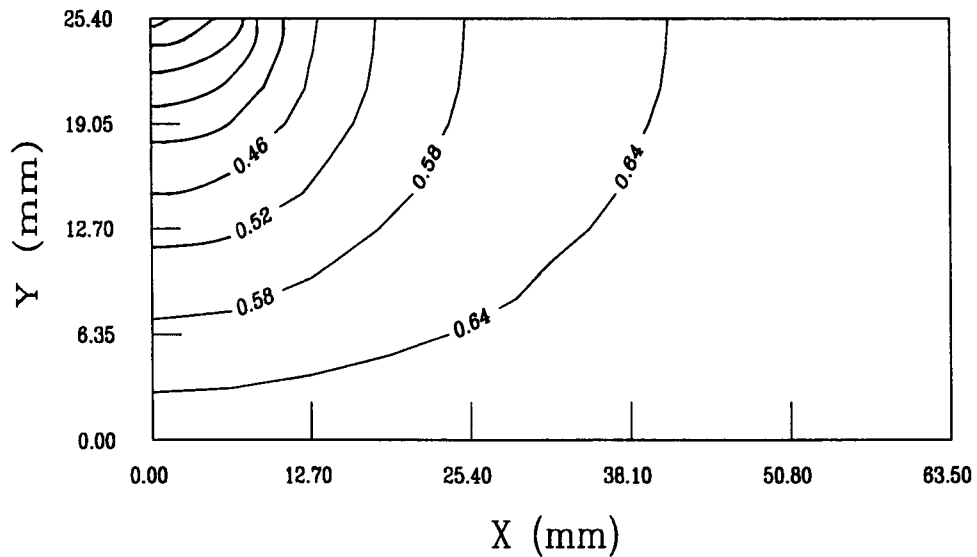

Figure 4.5b Magnified view of the equipotential lines at an applied potential of -2 [V], cover thickness is 0.5 inch.

Figure 4.6a Magnified view of the equipotential lines at an applied potential of 0 [V], cover thickness is 2.0 inch.

Figure 4.6b Magnified view of the equipotential lines at an applied potential of -2 [V], cover thickness is 2.0 inch.
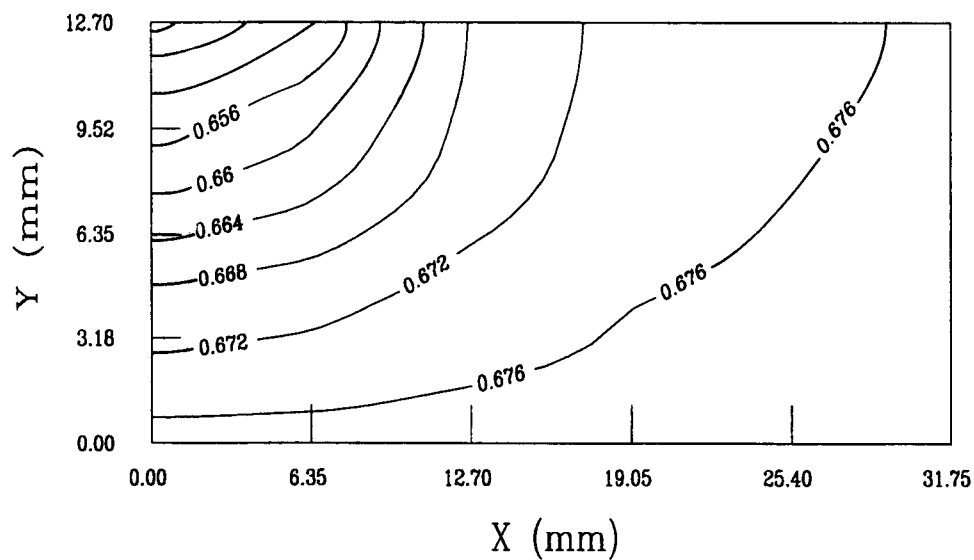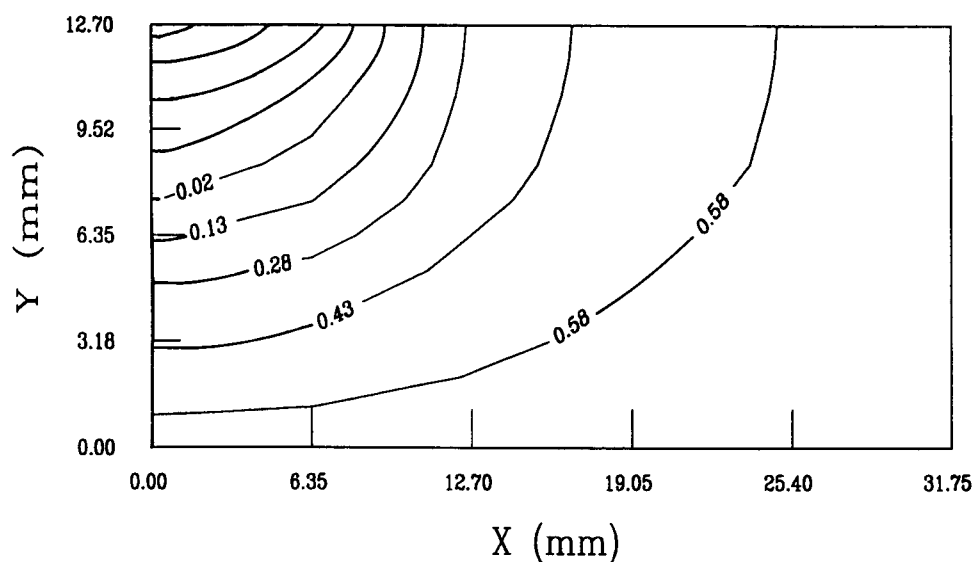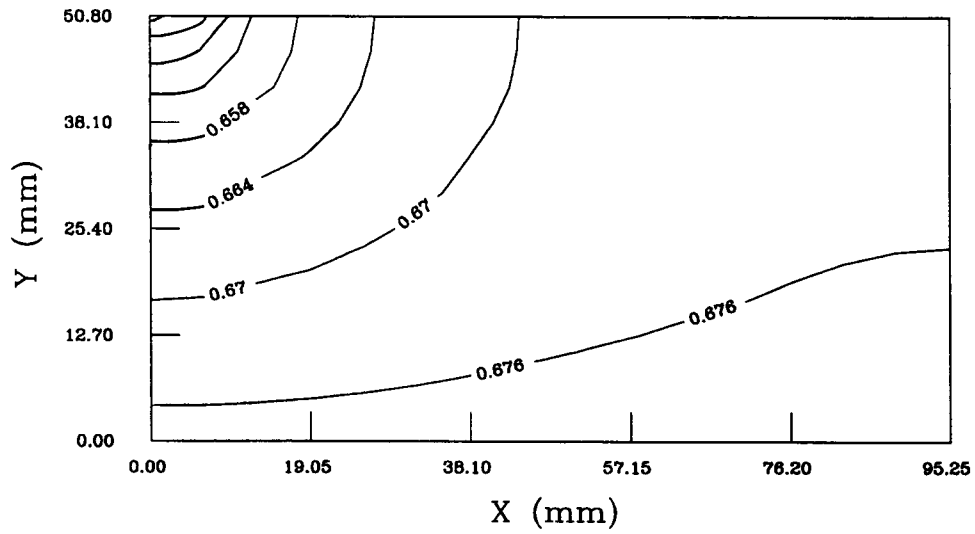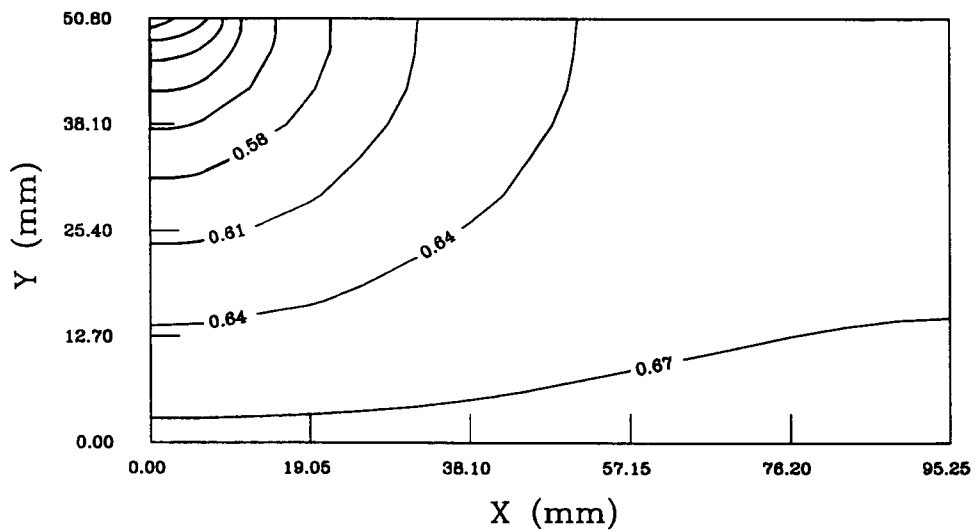
4.2.2 Effect of Pore Saturation

As alluded to in the model development, the degree of pore saturation has a profound effect on the characteristics of the cathodic protection system both in terms of the concrete resistivity and the flux of reacting oxygen to the iron electrode. Since the degree of pore saturation can exhibit large variations, a study on the effect of pore saturation on the system performance is warranted.

Figure 4.7 plots the net current as a function of pore saturation at E_{appl} of 0, -1, and -2 V. In the galvanic case, the current is small and increases with pore saturation. In this case, the current is too small to deplete oxygen at the rebar and the bulk resistivity controls the rate of zinc oxidation. Since the resistivity decreases with increase in pore saturation, the current increases. The two cases of finite applied potential exhibit much larger currents (maximum 4 mA) and go through a maximum with respect to pore saturation. At low pore saturation resistivity controls the current as in the galvanic case. At high pore saturation, the availability of oxygen limits the net current. In fact, above 60% PS, both -1 and -2 V curves fall on top of each other as mass transfer resistance completely dominates reaction kinetics. The protection current peaks when there is an optimum tradeoff between low resistivity and high oxygen availability for a given reaction rate; the reaction rate is fixed by applying a constant potential to the system. This maximum occurs at a lower PS for an applied potential of -2 V, since more oxygen is needed for the faster reaction kinetics.

Figure 4.8 plots rebar potential vs. a $Cu/CuSO_4$ reference electrode as a function of pore saturation at E_{appl} of 0, -1, and -2 V. The sign convention for potential is consistent with the equivalent circuit of Figure 3.4. At high PS, the bulk resistance is small compared to the interface resistance. This can be thought of effectively as a short circuit across the concrete with the rebar potential goes to $E_{appl} + E_{Zn}$ (see equation 3-30). The protection is only limited by how much oxygen is present. At low PS, the bulk resistance is large compared to the interface resistance. This can be thought of effectively as an open circuit across the concrete electrolyte. In this case, the rebar potential goes to E_{corr} (-0.347 V vs. CSE) and the net current goes to zero (refer to Figure 4.7).

Figure 4.9 plots the difference in E_{Fe} between the center and the edge vs. pore saturation at E_{appl} of 0, -1, and -2 V. At an applied potential of -2 V and a PS of 50%, the center of the rebar is 270 mV greater than the edge. This

corresponds to the maximum current discussed above. For most cases with significant protection potentials, the difference in E_{Fe} is greater than 50 mV.
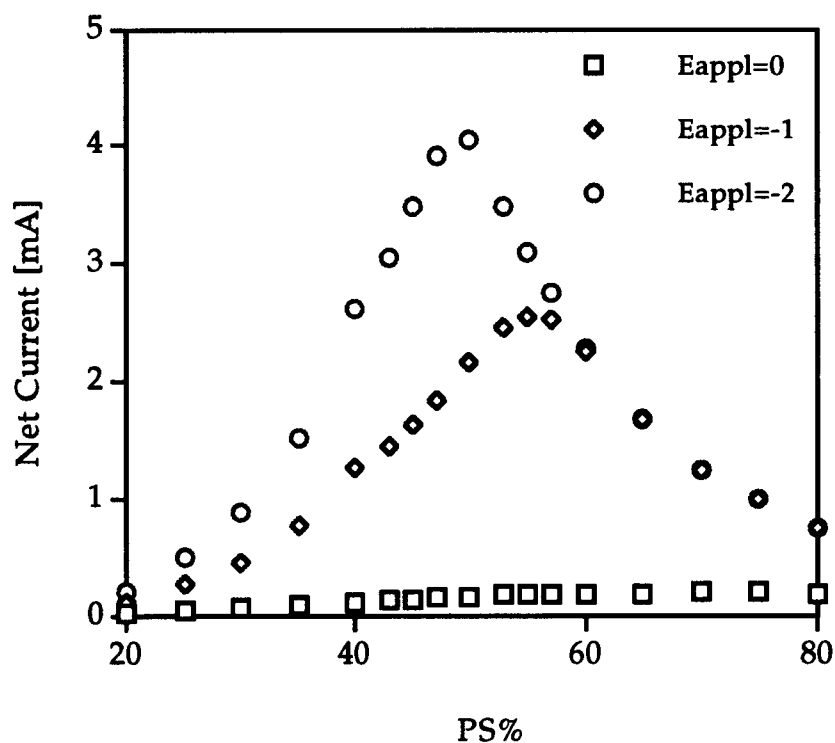
Figure 4.7 Effect of pore saturation on net current
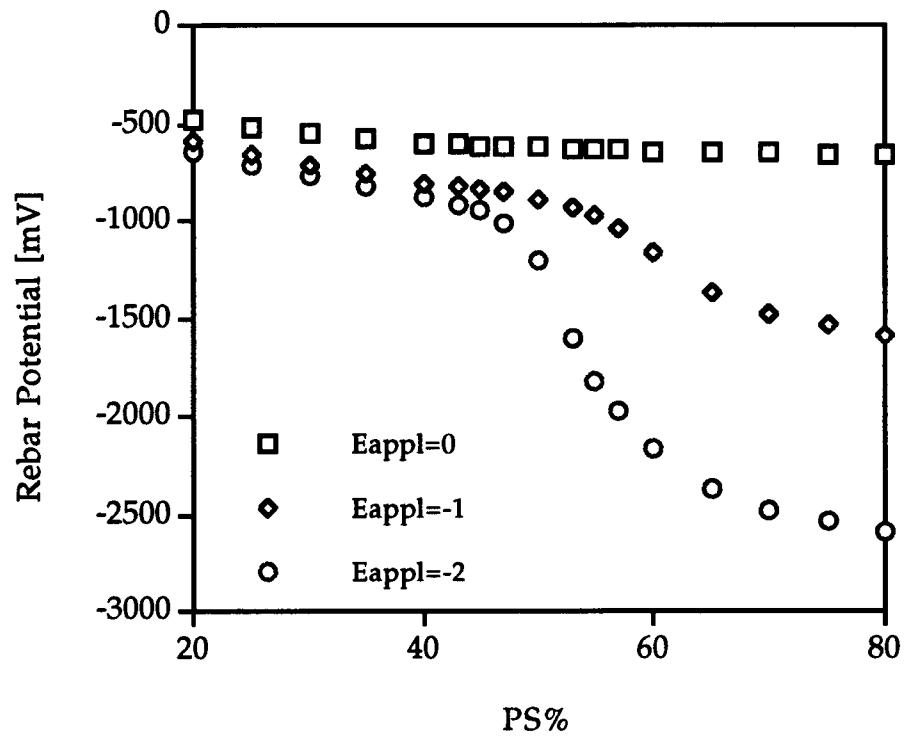
Figure 4.8 Effect of pore saturation on rebar potential
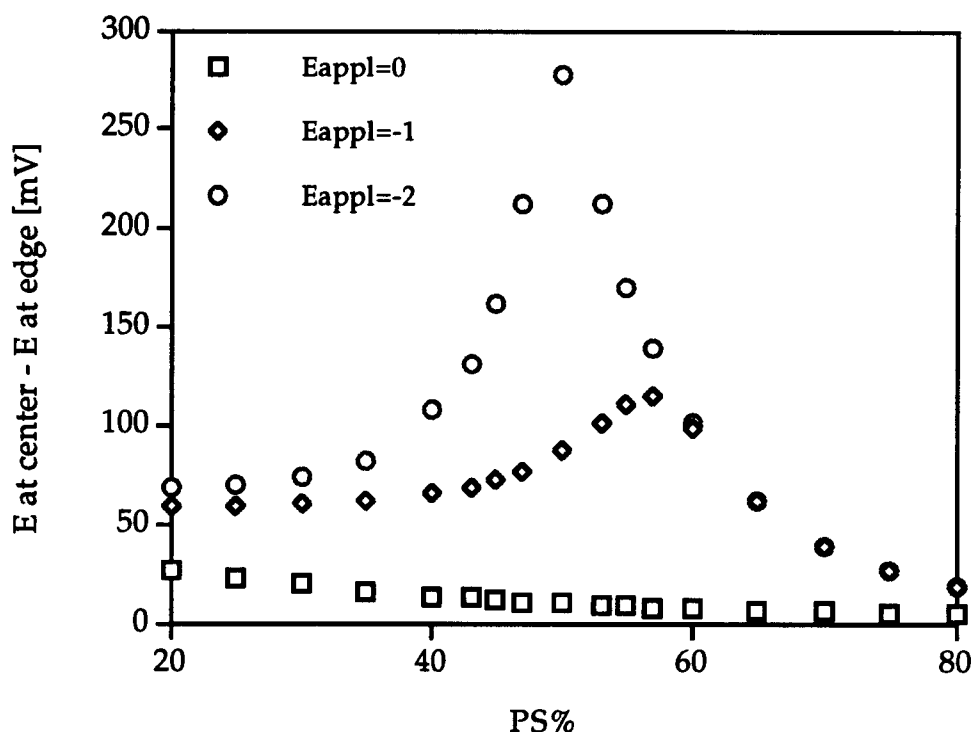
Figure 4.9 Effect of pore saturation on rebar potential difference between center and edge

Figure 4.10 plots the percentage of oxygen concentration at the center of the rebar and at the edge with respect to saturated oxygen concentration vs. pore saturation at E_{appl} of 0 and -2 V. The measure of adequate protection is based on a 100 (or 150) mV depolarization criterion, discussed in section 2 of Chapter 1. A major component of this value can be attributed to the diffusion of oxygen as the system relaxes. From examining the oxygen concentrations at the edge of the rebar vs. the center, the difference in this component of the depolarization potential can be assessed[27]. **Thus at pore saturation above 50% where all the oxygen is consumed (E_{appl}=-2 V) reference cell placement is not critical; however from 30-50% PS, placement of the reference cell can have a large effect on the depolarization measurement.** For example at a PS of 45% a reference electrode placed on the edge would depolarize by 125 mV which would be interpreted as adequate protection while one at the center would only depolarize by 38 mV.
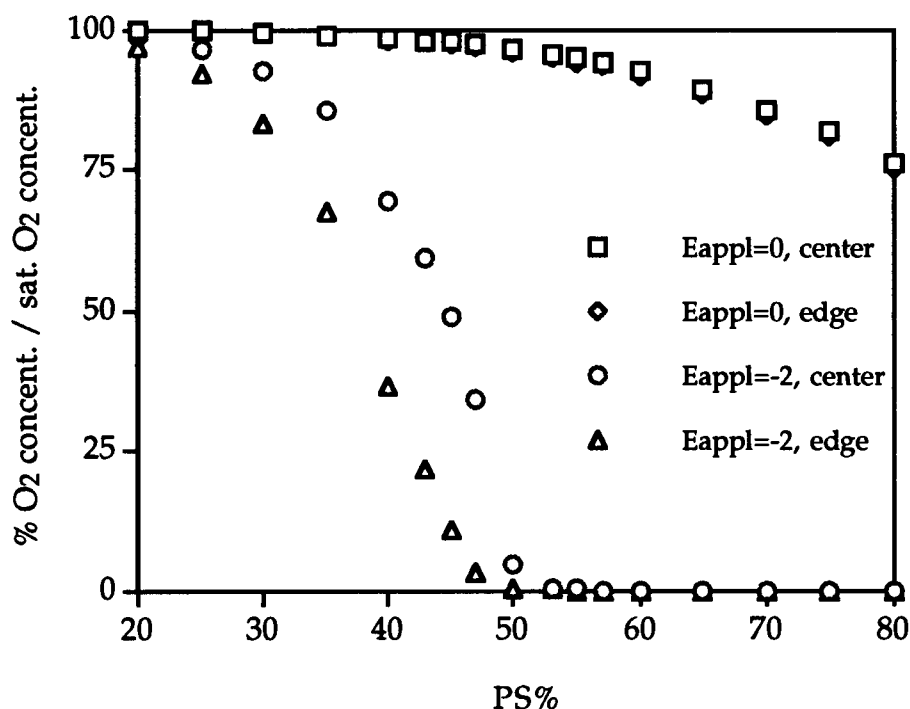
Figure 4.10 Effect of pore saturation on percentage of oxygen concentration

This analysis should not be interpreted as completely describing the depolarization mechanism. In fact in the case just examined part of the potential difference could relax as the instant off potential. Furthermore there are other possible processes some which probably contribute to the depolarization. However, care should be used to place reference electrodes as close as possible to the center of the rebar for dryer concrete decks.

4.2.3 Sensitivity Analysis

Since the input parameters to the model were obtained from available experimental data in the literature (not necessarily at system conditions), there is some uncertainty to their values. In this section, the sensitivity of the output parameters to the input is assessed.

Significant model input parameters to calculation of the potential and current distribution include: (a) the resistivity of the concrete electrolyte, (b) the oxygen reduction equilibrium potential, (c) exchange current density, (d) Tafel slope, (e) the oxygen mass transfer coefficient and (f) the surface oxygen concentration. (The iron kinetics contribute little to the potential distributions discussed above; although they are important in determining corrosion rates.) The first parameter determines the bulk resistance, the next three parameters the charge transfer resistance at the rebar and the final two parameters the mass transfer resistance at the rebar (see Figure 3.4). Since the model combines charge transfer and mass transfer effects into a single boundary condition, Equation (3-33), these five parameters represent the concrete/Fe interfacial resistance. However only three of these five parameters are independent. Examination of Equation (3-20) shows that the equilibrium potential and the exchange current density are related. For the sensitivity analysis, the former was fixed at its base case value and only the exchange current density was varied. Similarly, the relation between the oxygen mass transfer coefficient and the oxygen concentration in the bulk is constrained by the limiting current density, Equation (3-24). Accordingly the value for oxygen concentration was fixed and the mass transfer coefficient was varied in the sensitivity analysis. It is not expected that the bulk oxygen concentration deviates significantly from its base case value.

The sensitivity analysis consists of varying the four independent input parameters from their base case values. These parameters: the conductivity of the concrete electrolyte (Figure 4.12), the oxygen mass transfer coefficient (Figure 4.13), the oxygen reduction exchange current density (Figure 4.14), and the inverse of cathodic Tafel slope, b_{O_2}, (Figure 4.15) are plotted vs. net current, rebar potential, the difference in E_{Fe} between the center and the edge, and the oxygen concentration at the center of the rebar and at the edge.

As Figure 4.11a illustrates when the conductivity is low (resistivity is high), the system approaches as an open circuit and protection is ineffective. At high conductivity all the available oxygen is consumed and the current goes to the limiting current value. The behavior of concrete conductivity on rebar potential (Figure 4.11b), the difference in E_{Fe} between the center and the edge (Figure 4.11c) is similar to the pore saturation as discussed in the last section. The behavior of the percentage of oxygen concentration with respect to concrete conductivity for E_{appl} of 0 and -2 V is shown in Figure 4.11d. Again, for -2 V of

E_{appl} and high values of conductivity, mass transfer resistance of oxygen dominates and the oxygen concentration goes to zero.
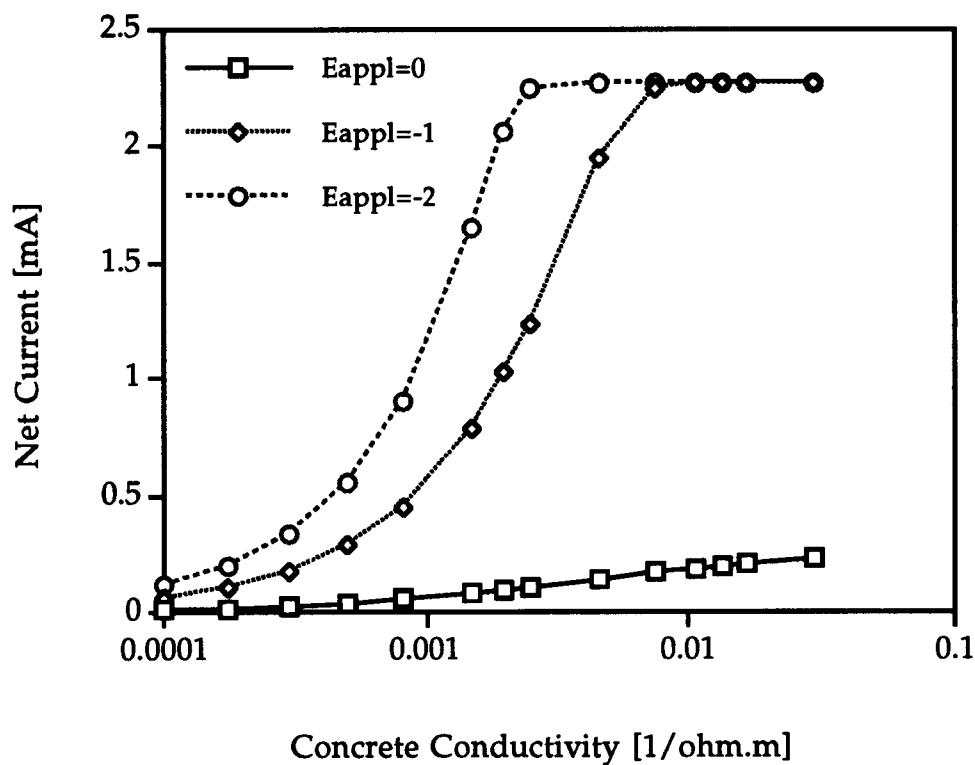
Figure 4.11a Effect of concrete conductivity on net current
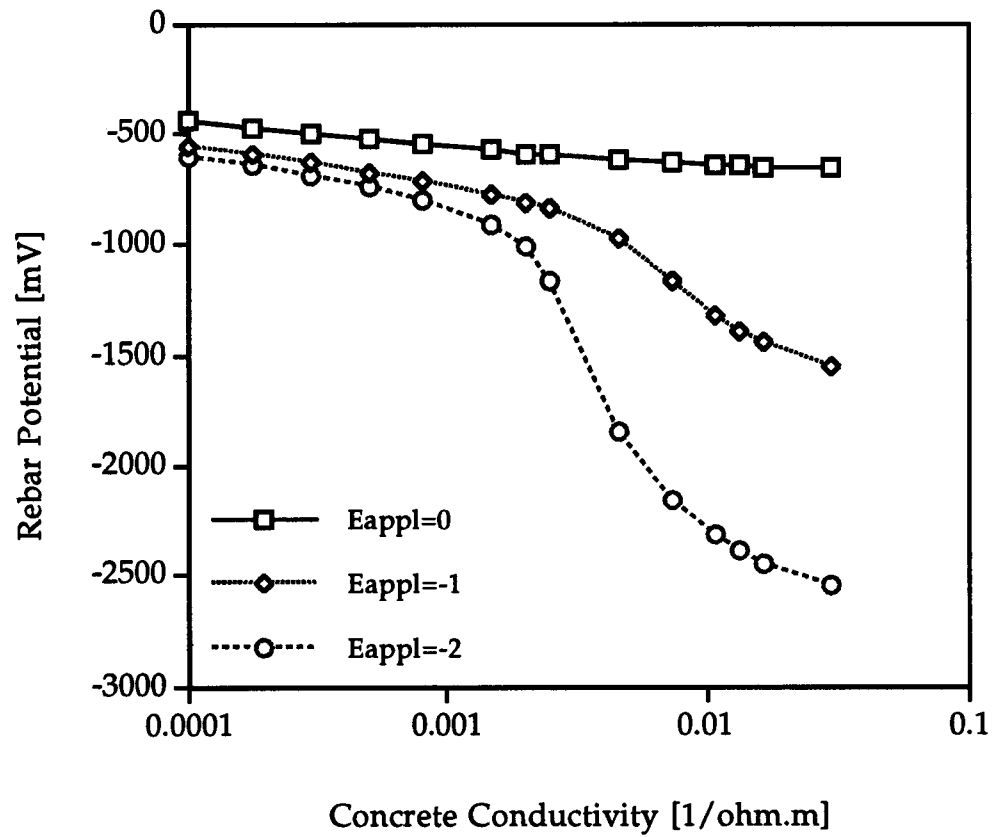
Figure 4.11b Effect of concrete conductivity on rebar potential
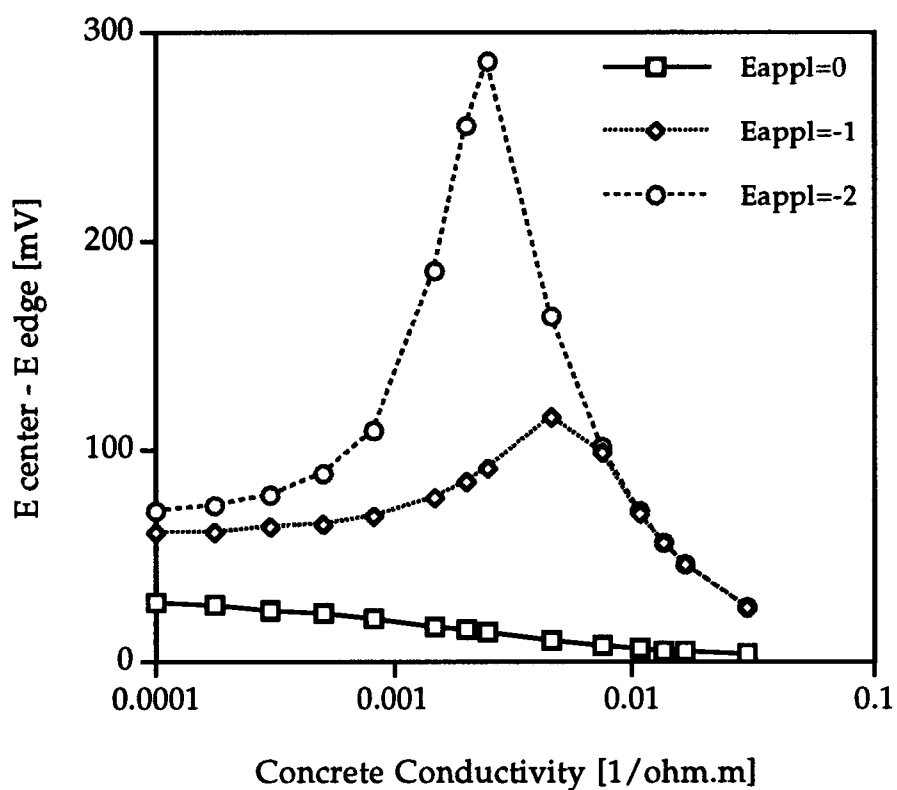
Figure 4.11c Effect of concrete conductivity on rebar potential difference
between center and edge
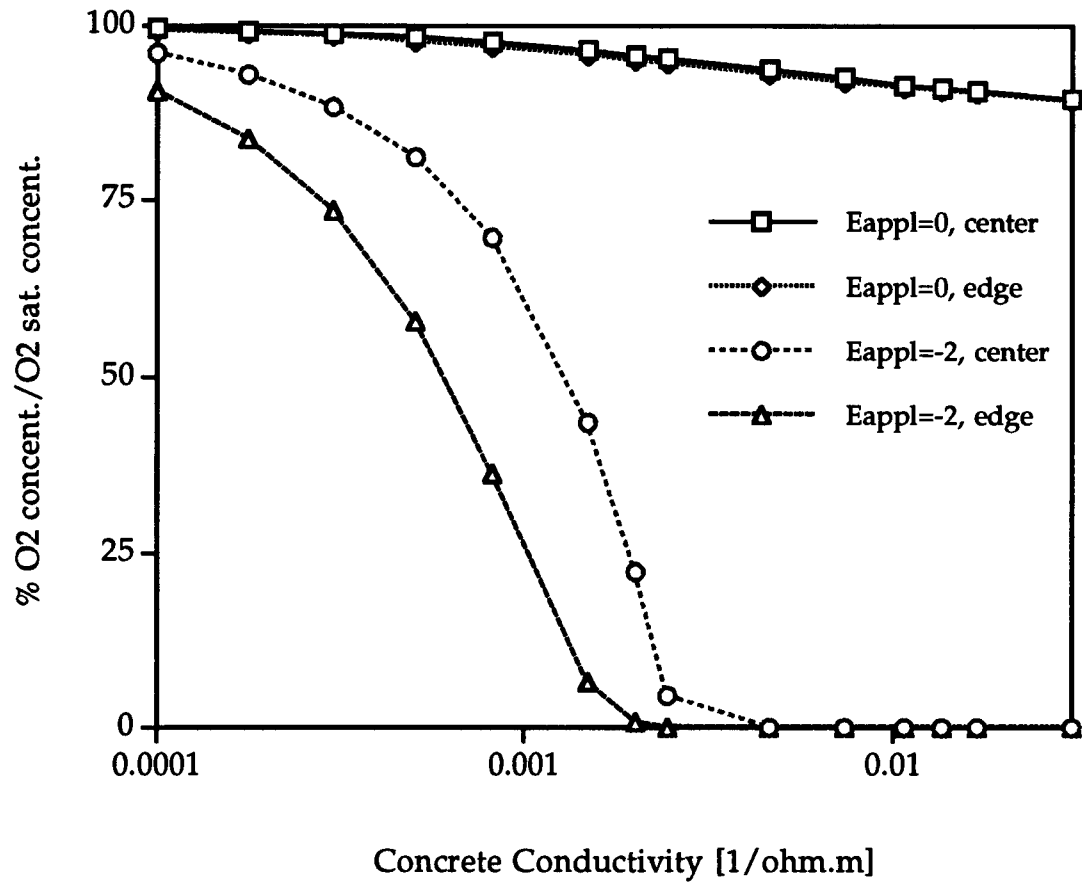
Figure 4.11d Effect of concrete conductivity on percentage of oxygen
concentration

As the oxygen mass transfer coefficient goes to zero, the system approaches open circuit behavior as shown in Figure 4.12a-d. At large oxygen mass transfer coefficients, the concentration of oxygen at the rebar approaches the saturation value. In this case the inherent kinetics of oxygen reduction and the associated iR_B determine the system response. As shown in Figure 4.12d, significant differences in oxygen concentration between the edge and center occur for mass transfer coefficients greater than 3×10^{-7} m/s.
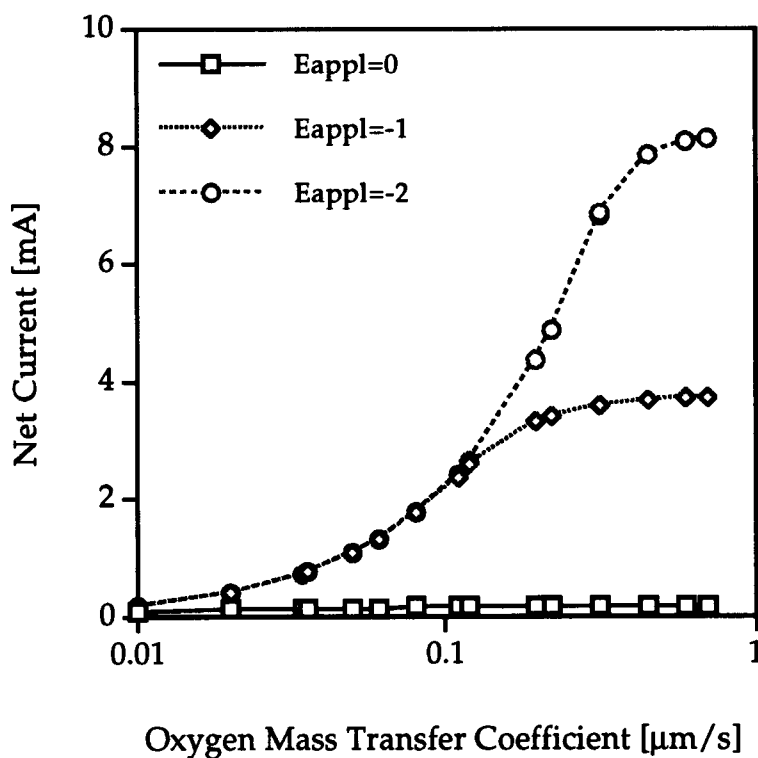
Figure 4.12a Effect of oxygen mass transfer coefficient on net current
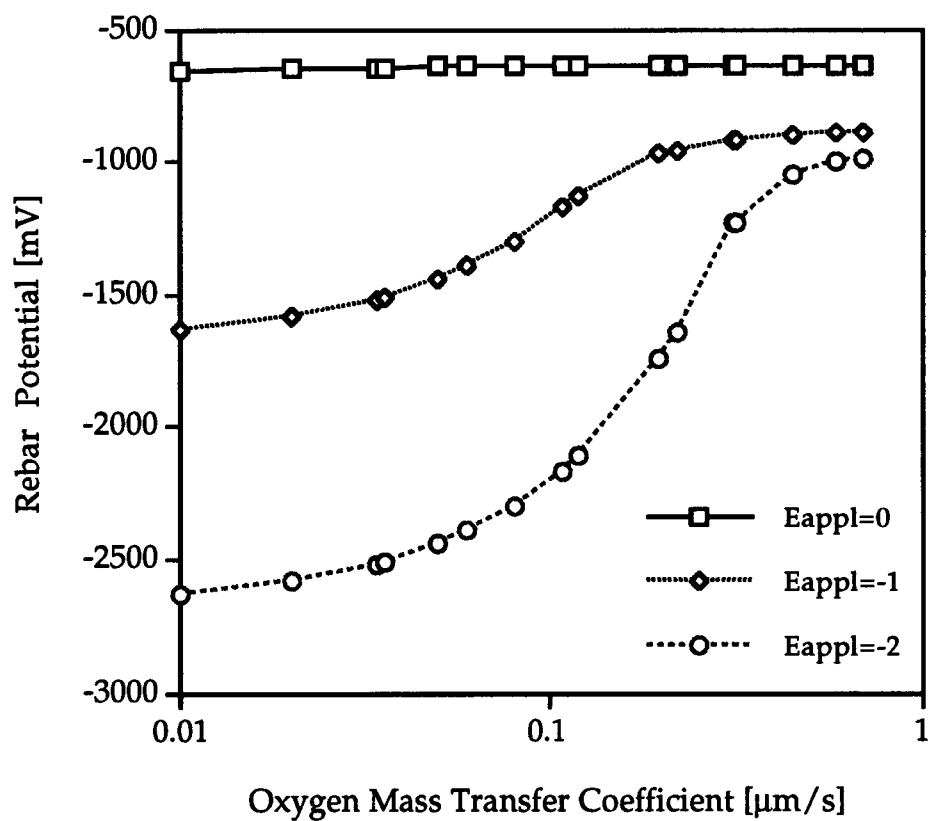
Figure 4.12b Effect of oxygen mass transfer coefficient on rebar potential
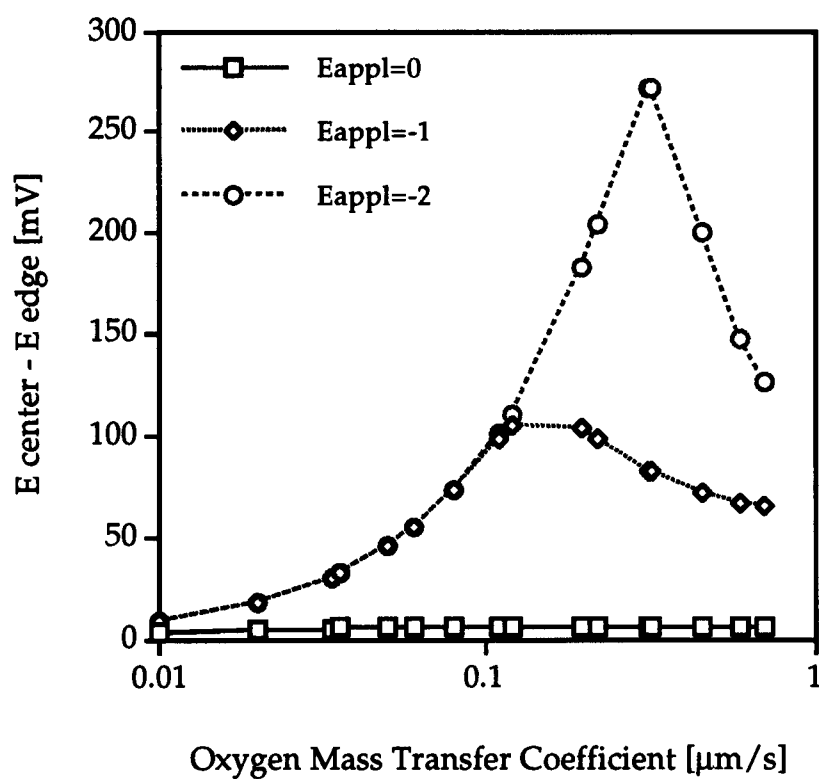
Figure 4.12c Effect of oxygen mass transfer coefficient on rebar potential
difference between center and edge
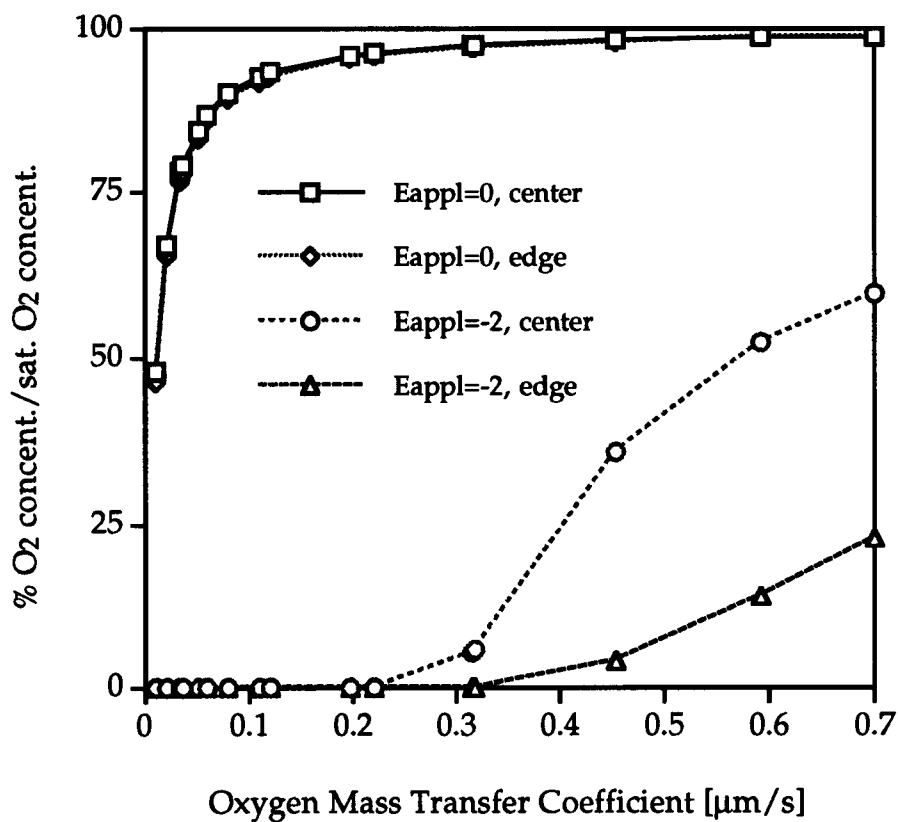
Figure 4.12d Effect of oxygen mass transfer coefficient on oxygen concentration

Figure 4.13a illustrates that there are three regions of behavior for the oxygen exchange current density. At very low values, oxygen reduction is negligible and no protection current flows. Of course, corrosion would also occur at slow rates. At high values, the protection current is limited by oxygen availability. At intermediate values charge transfer resistance controls the protection current. The higher the applied potential the lower the transition to this intermediate region. In fact for E_{appl} of -2 V an exchange current density as low as 10^{-10} μA cm^{-2} still yields limiting current conditions. The behavior for the difference in E_{Fe} between the center and the edge (Figure 4.13c) mirrors the behavior of protection current. The functionality with the inverse of the Tafel slope, b_{O_2}, (Figure 4.14) is opposite the exchange current density.
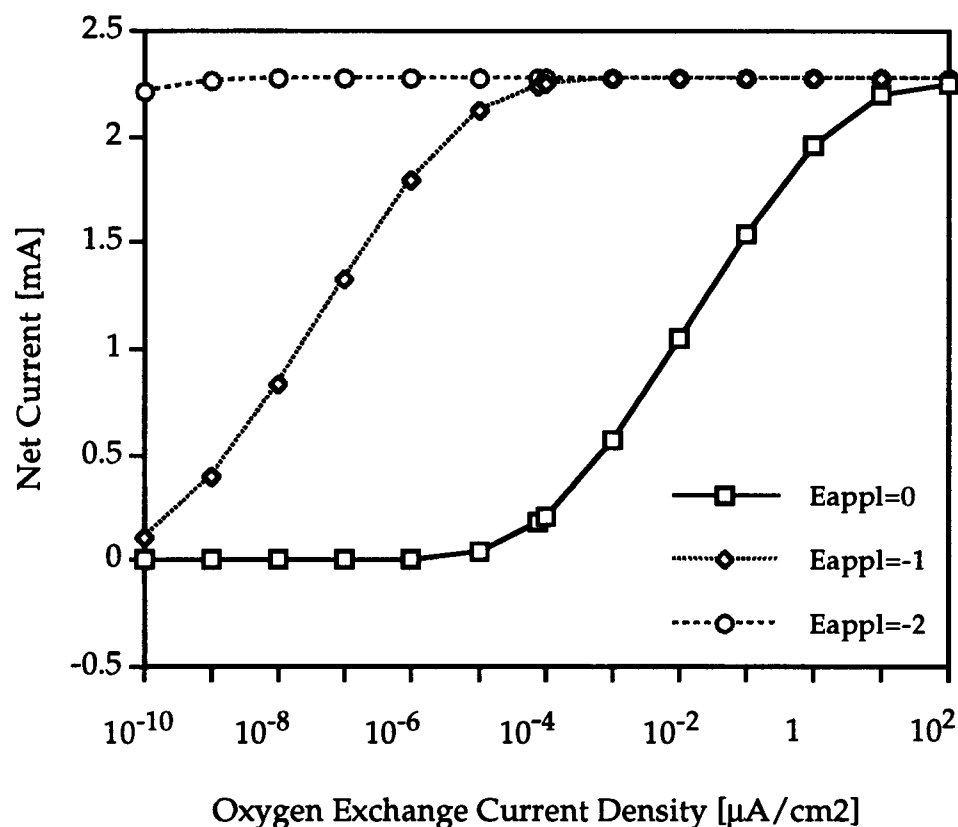
Figure 4.13a Effect of oxygen exchange current density on net current
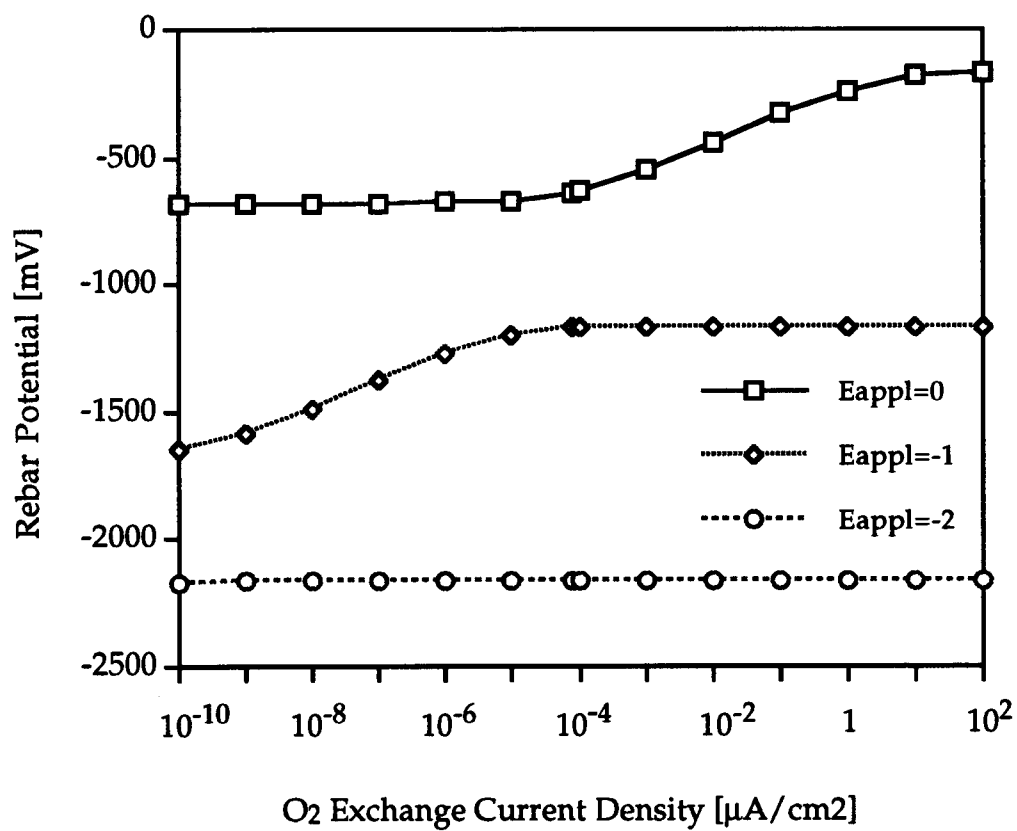
Figure 4.13b Effect of oxygen exchange current density on rebar potential
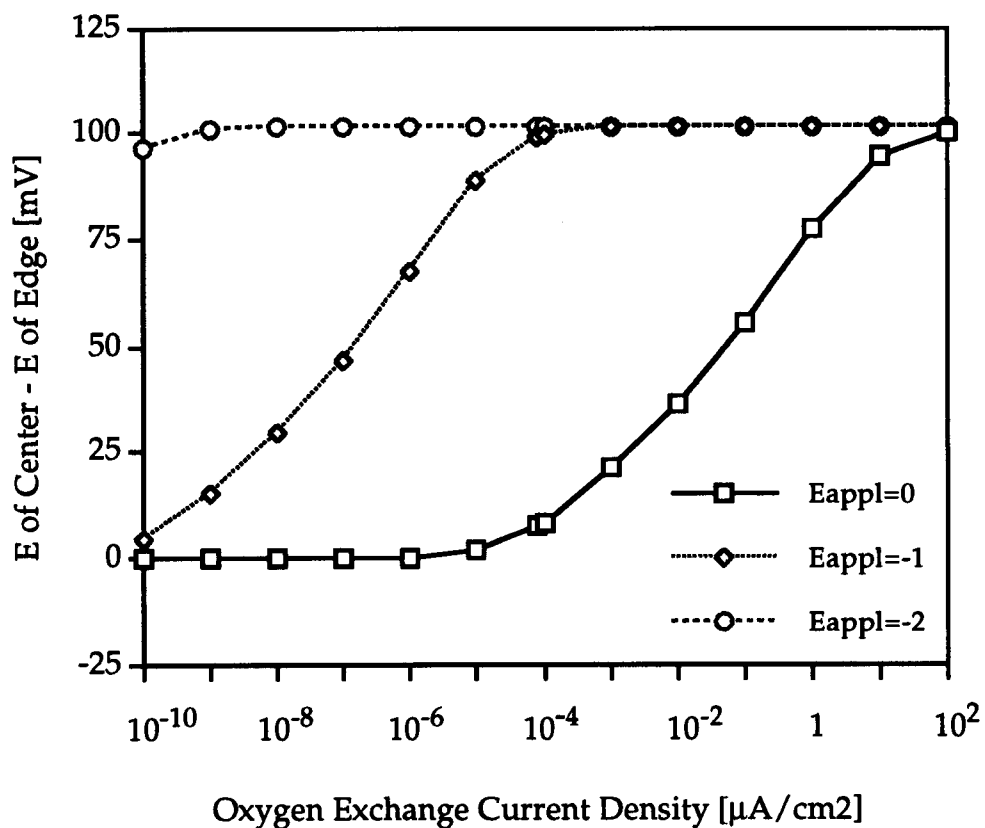
Figure 4.13c Effect of oxygen exchange current density on rebar potential
difference between center and edge
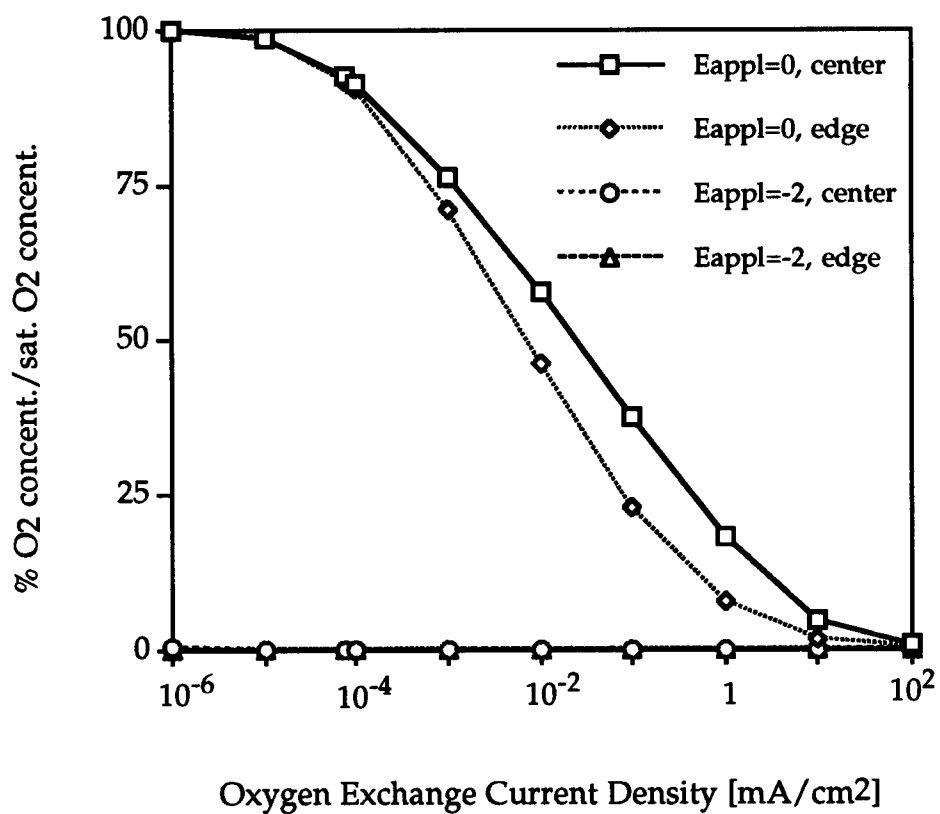
Figure 4.13d Effect of oxygen exchange current density on percentage of oxygen concentration
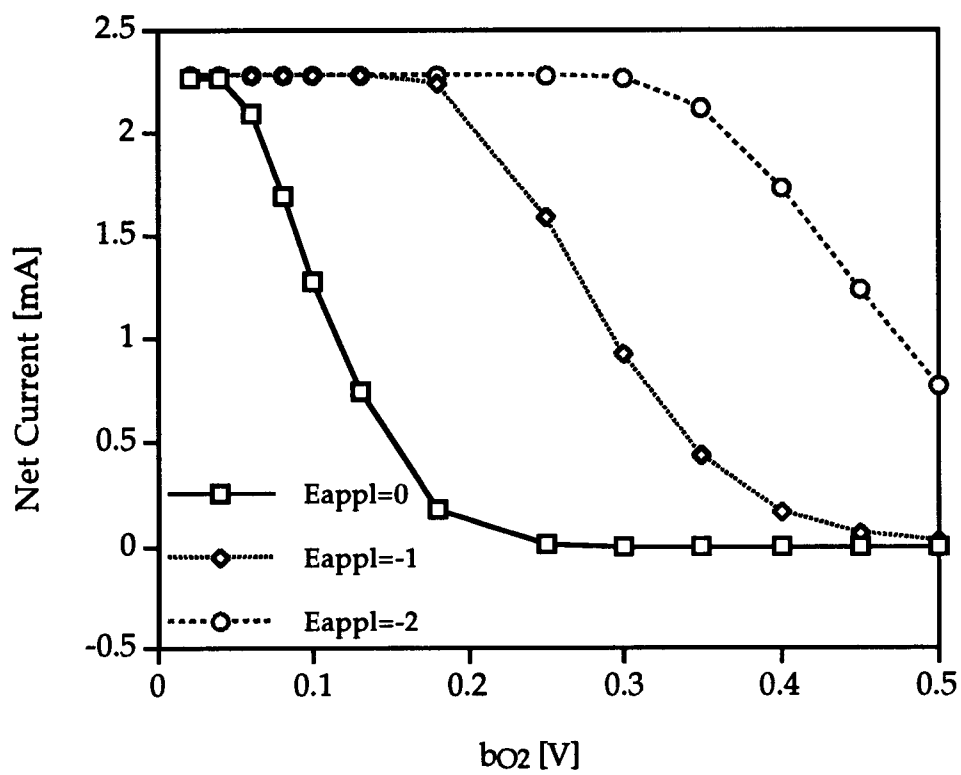
Figure 4.14a Effect of b_{O_2} on net current
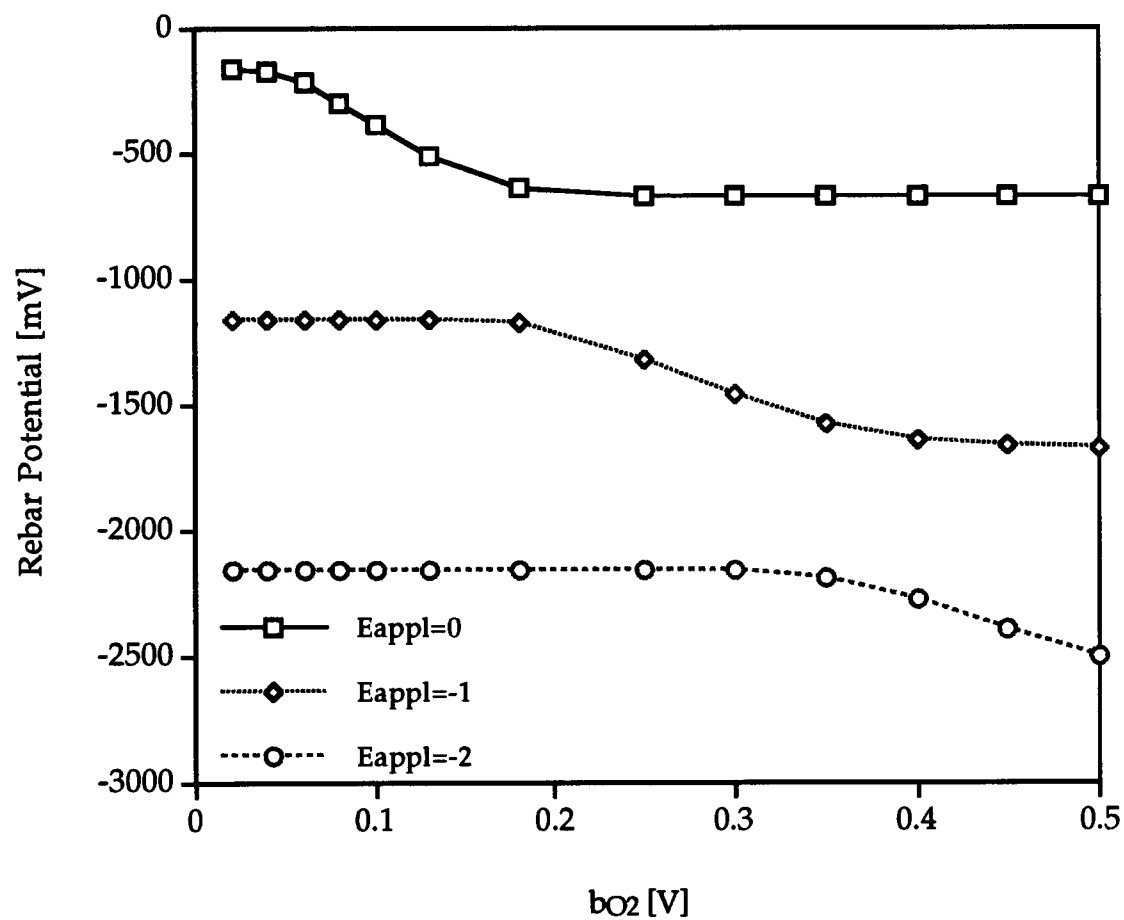
Figure 4.14b Effect of b_{O_2} on rebar potential

125

100

75

E of center - E of edge [mV]

50

25

0

Eappl=0

Eappl=-1

Eappl=-2

-25

0   0.1   0.2   0.3   0.4   0.5

b_{O_2} [V]
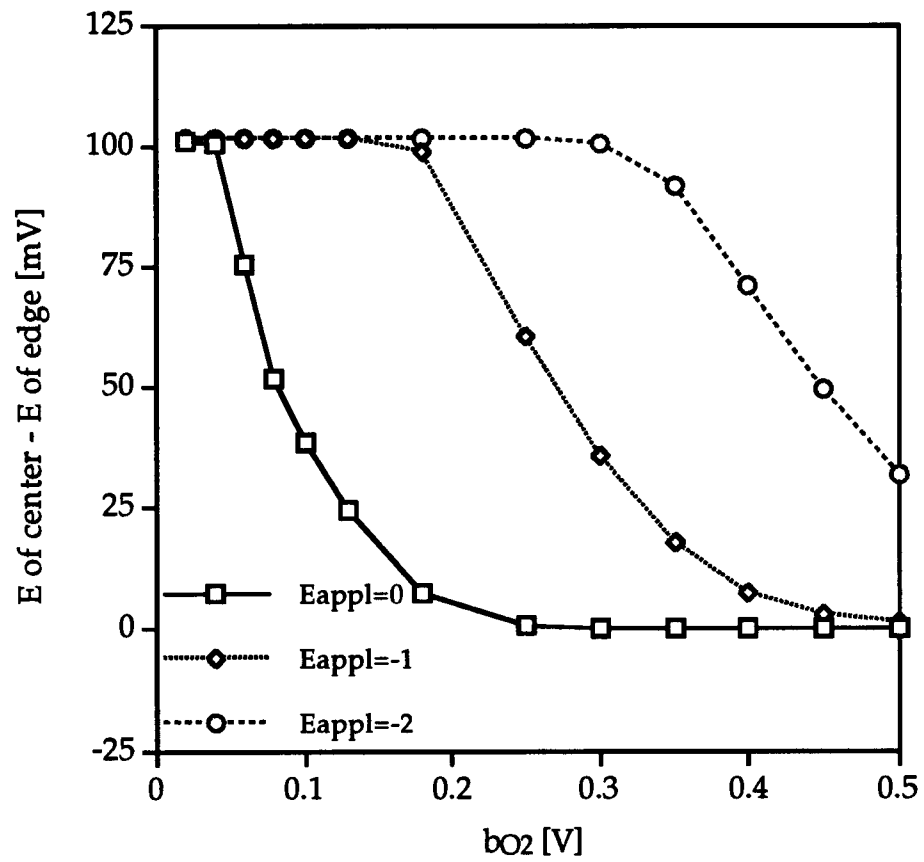
Figure 4.14c Effect of b_{O_2} on rebar potential difference between center and edge
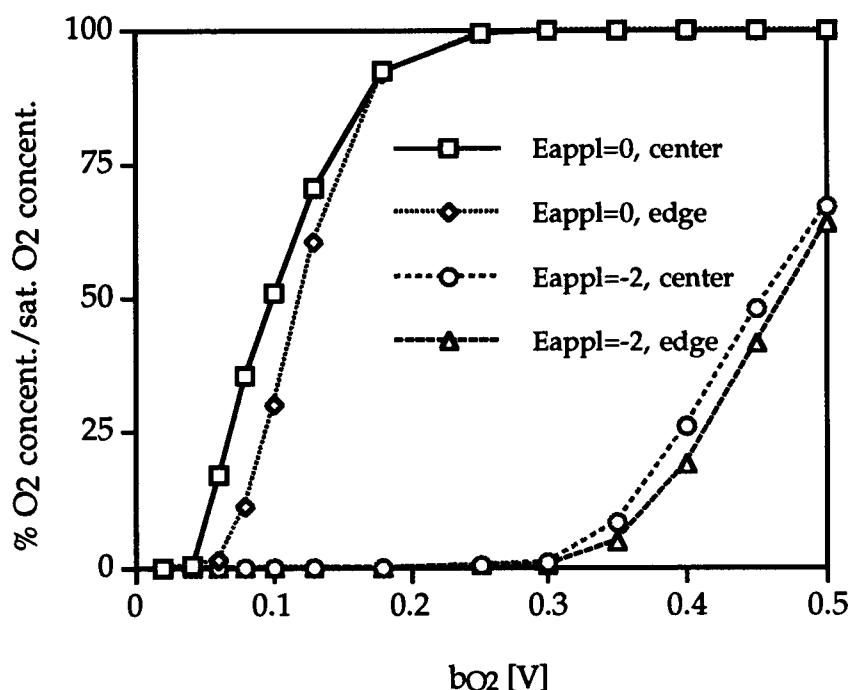
Figure 4.14d Effect of b_{O_2} on percentage of oxygen concentration

4.3 Comments on Three-dimensional Simulation

Two types of rebar exist in reinforced concrete bridges: rebar to which potential is applied, the king rebar, and rebar which is not directly protected, the cross rebar. However, the cross rebar is indirectly protected through contact with the king rebar. Configuration of these rebars at one side of a concrete block with sprayed zinc at the other side, represents a three-dimensional geometry shown in Figure 4.15.

The king and cross rebars may or may not be welded together. The current procedure at Oregon Department of Transportation (ODOT) is measuring the resistance between the two; for values of 1 Ω or greater the bars are welded which makes the bar to bar resistance small.

A three-dimensional model was developed to determine the adequate protection of the cross rebar. The applied potential to the cross bar was obtained

by subtracting the Ohmic potential drop between the bars from the applied potential to the king rebar through an implicit method. It turned out that for bar to bar resistance of 1 Ω or less the potential difference between the bars was only a few milivolts. This potential drop was absolutely negligible compared to potential drop across the rebar (from center to the edge) for the cases studied in two-dimensional geometry. This in turn suggested bar to bar resistance of 1 Ω is not an issue in studying cathodic protection in reinforced concrete such that a two-dimensional model could adequately represent the actual scenario.
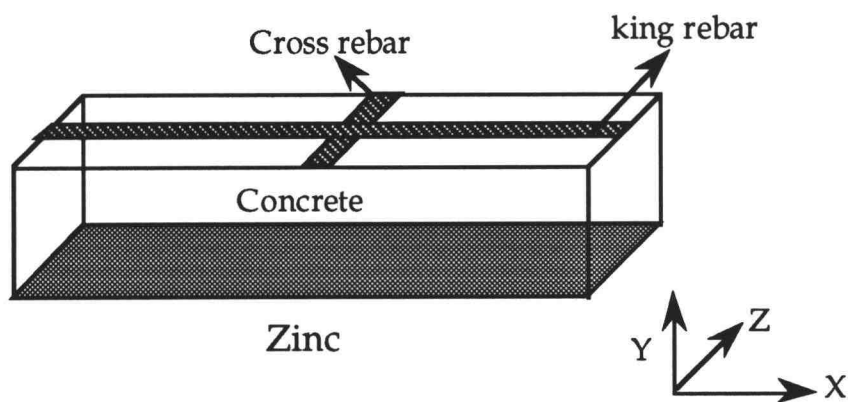
Figure 4.15 Schematic of a three-dimensional geometry

The geometry used for the simulation section was simple. It consisted of sprayed zinc, a piece of flat rebar, and a block of concrete in the middle. This configuration is unable to predict the potential distribution on the back of the rebar which is buried in concrete in actual field systems. Modifying the geometry for a better representation of the actual systems is recommended.

5. CONCLUSIONS AND FUTURE WORK

5.1 Conclusions

In this chapter, first, the conclusions from this research are presented. Second, future work is addressed.

Experimental conclusions:

1.   The concrete block was reasonably homogeneous, the potential differences at the Fe and Zn interfaces were negligible compared to the potential difference across the concrete, and the Ag/AgCl electrodes did behave as would be predicted from first principles. Thus the test cell was indeed a satisfactory system for testing other reference electrodes.

2.   Locating the reference electrode on top of the concrete block could be a major source of error.

3.   Graphite probes behaved as well as the Ag/AgCl reference electrode. Furthermore, the home-made graphite probes behaved the same as the commercial ones and the Ag/AgCl reference electrode. This will allow much greater experimental latitude since the home-made probes are much more economical than the commercial ones.

4.   The conditioned graphite probes showed potential values closer to each other than those of the unconditioned ones. Also the reproducibility of the probes increased after conditioning.

5.   Embedded graphite probe behaved similarly to the Ag/AgCl reference electrode. They both well tracked the applied potential.

Simulation conclusions:

6.   Any calculations of anode life based on current density should use the effective area rather than the total sprayed area.

7.   As the magnitude of the applied potential increases, the potential on the rebar decreases. At a large enough applied potential, hydrogen evolution will commence.

8.   In the galvanic base case, the potential difference between the iron/concrete interface only varies by 7 mV from the center to the edge; however, at the limiting current it varies by 100 mV.

9.   As the cover thickness decreases, there is more oxygen available and the protection current increases at large applied potentials. Accordingly, the difference in the potential between the center and the edge also increases.

10.   The potential at the edge of the rebar is less (more negative) than that of the center suggesting the center is less protected. Therefore, the reference electrode should be located as close to the center of the rebar as possible.

11.   The degree of pore saturation has a profound effect on the characteristics of the cathodic protection system both in terms of the concrete resistivity and the flux of reacting oxygen to the iron electrode. Since the degree of pore saturation can exhibit large variations, a study on the effect of pore saturation on the system performance is warranted.

12.   Current goes through a maximum with respect to pore saturation.

13.   At high PS, protection is limited by availability of oxygen. At low PS, the bulk resistance dominates.

14.   The higher the current the larger the potential difference between the center and the edge.

15.   At pore saturation above 50% all the available oxygen is consumed and reference cell placement is not critical; however from 30-50% PS, placement of the reference cell can have a large effect on the depolarization measurement.

16.   A sensitivity of the output to the input parameters was determined.

5.2 Suggestions for Future Work

1.   The performance of the electrodes under controlled variations in environmental conditions (e.g., temperature 0-30 C, relative humidity 40-100%) is proposed for future work.   Since the response mechanism in concrete is unknown for the graphite electrode, this step is important.

2.   The chemical species that poise the potential of the graphite electrode in concrete are unknown. It would be useful to determine the reactions that are responsible for poising the electrode in order to predict the sensitivity of the electrode to environmental variables.

3.   In order to reproduce the actual field systems, it is recommended that future tests be performed on concrete blocks with embedded iron and zinc plates. Those tests should monitor long-term stability of embedded graphite electrodes under conditions similar to those of the 100-mV depolarization test or the 3-electrode controlled potential protection circuit.

4.   Physical parameters (e.g. concentrations and mass transfer coefficients) of the charge carriers in concrete need to be evaluated so that diffusion and migration effects to the current can be delineated.

5.   In the current model, the potential difference at the zinc/concrete interface was treated as a constant. However, a better understanding of the processes occurring at the zinc electrode is needed.

6.   The geometry used for the simulation section was simple. It consisted of sprayed zinc, a piece of flat rebar, and a block of concrete in the middle. This configuration is unable to predict the potential distribution on the back of the rebar which is buried in concrete in actual field systems. Modifying the geometry for a better representation of the actual systems is recommended.

7.   Transient processes should be included in the simulation.

BIBLIOGRAPHY

1. Dunker, K.F. and B.G. Rabbat, "Why America's Bridges are Crumbling, "Scientific American, March 1993. pg. 66.

2. Strutfull, R.F., "Cathodic Protection of a Bridge Deck," Material Performance **13**, 24 (1974).

3. News, "Florida, Oregon Project Bridge Substructures," Civil Engineering, Oct. 1991. pg. 18.

4. Hime, W. and B. Erlin, "Some Chemical and Physical Aspects of Phenomena Associated with Chloride-Induced Corrosion," in *Corrosion, Concrete, and Chlorides*, ACI SP-102, F. W. Gibson Ed., American Concrete Institute, Detroit, 1987, p. 1.

5. Barthalomew J. et al., "Control Criteria and Materials Performance Studies for Cathodic Protection of Reinforced Concrete," Prepared for the Strategic Highway Research Program, SHRP-S-670 (1993).

6. Funihashi, M. and J.B. Bushman, "Technical Review of 100mV Polarization Shift Criterion for Reinforcing Steel in Concrete," Corrosion **47**, No. 5, NACE 1989.

7. Funihashi, M. and W.T. Young "Investigation of 100mV Polarization Shift Criterion for Reinforcing Steel in Concrete," Paper 193 NACE CORROSION/92, 1992.

8. Bennett, J.E. and T.A. Mitchell "Depolarization Testing of Cathodically Protected Reinforcing Steel in Concrete," Materials Performance, Dec. 1990. pg. 20.

9. Bennett, J.E. and T.A. Mitchell "Depolarization of Cathodically Protected Reinforcing Steel in Concrete," Paper 373 NACE CORROSION/89 1989.

10. Laird, R.C.G. "Performance Evaluation Testing of Conductive Cathodic Protection Systems on Thin Parking Garage Slabs," Paper 553, NACE CORROSION/91 1991.

11. Bard, A.J. and L.R. Faulkner, *Electrochemical Methods, Fundamentals and Applications*, John Wiley & Sons, 1980. pg. 119.

12. Roy, D.M. et al. "Concrete Microstructure Porosity and Permeability," Prepared for the Strategic Highway Research Program, SHRP-S-628 (1993).

13. Papadakis V.G., C.G. Vayenes, and M.N. Fardis, "Physical and Chemical Characteristics Affecting the Durability of Concrete," ACl Materials Journal **8**, 186 (1991).

14. Sandler, S.I., *Chemical and Engineering Thermodynamics*, John Wiley & Sons, 1989. pg. 437.

15. Gjorv, O. and O. Vennesland, "Evaluation and Control of Steel Corrosion in Offshore Concrete Structures," SP 100-79 in *Concrete Durability*, John M Scanlon Ed., American Concrete Institute, 1987. pg. 1575.

16. Gonzalez, J.A., W. Lopez, and P. Rodriguez, "Effects of Moisture Availability on Corrosion Kinetics of Steel Embedded in Concrete, Corrosion **49**, 1004 (1993).

17. Tuuti K., *Corrosion of Steel in Concrete*, Swedish Cement and Concrete Research Institute, 1982.

18. Lawrence, C.D., "Transport of Oxygen through Concrete," British Ceramics Proceedings **35**, 277 (1984).

19. Hurling, H., "Durability of Concrete Structures under Normal Outdoor Exposure," RILEM Seminar (1984).

20. Kobayashi, K. and K. Shuttoh, "Oxygen Diffusivity of Various Cementatous Materials," Cement and Concrete Research **21**, 273 (1991).

21. Locke C.E. and A. Simon, "Electrochemistry of Reinforcing Steel in Salt-Contaminated Concrete," Corrosion of Reinforcing Steel in Concrete ASTM STP 713, pg. 3.

22. Pourbaix M. *Atlas of Electrochemical Equilibria* NACE1974.

23. West, J.M., *Basic Corrosion and Oxidation*, Ellis horwood Limited, 1980. pg. 92.

24. Sagues, A.A. and S.C. Kranc, "On the Determination of Polarization Diagrams of Reinforcing Steel in Concrete," Corrosion **48**, 624 (1992).

25. Naish, C.C., A. Harker and R.F.A. Carney, "Concrete Inspection: Interpretation of Potential and Resistivity Measurements," in *Corrosion of Reinforcement in Concrete*, C. Page, K. Treadway, and P. Bamforth, Eds., Elsevier Applied Science, London-New York, 1990, pg. 314.

26. Sagues, A.A. and R.G. Powers, "Low-Cost Sprayed Zinc Galvanic Anode for Control of Corrosion of Reinforcing Steel in Marine Bridge Substructures,"

Prepared for the Strategic Highway Research Program, SHRP-88-ID024 (1994).

27. Koretsky, M., "Evaluation of Embedded Reference Cell Performance in Reinforced Concrete Bridges," HP & R Study RES 4-1 #5294, 1994, in preparation.

28. Mindess, S. and J.F. Young, *Concrete*, Prentice-Hall, Inc., 1981, pg. 25.

29. Brown, D.S. and J.D. Allison, "MINTEQA1, An Equilibrium Metal Speciation Model," Environmental Research Laboratory, U.S. Environmental Protection Agency, 1987.

APPENDICES

Appendix A
Zinc/Concrete Equilibrium Model

In this appendix, the concentration of zinc ions at the zinc/concrete interface are approximated from a simple local equilibrium model of the concrete. While this model cannot account for experimental values of the zinc potential it does provide insight into the zinc-concrete chemistry.

During the course of cathodic protection, Zn^{2+} is produced at the concrete/zinc interface according to Reaction (2-7). The Zn^{2+} that is produced at the interface will simultaneously react with constituents of the concrete and diffuse away into the bulk of the concrete.

In order to access the interaction of Zn^{2+} with the concrete, an equilibrium model of the zinc interface was developed. For the chemical equilibrium model, the number of moles of each of the chemical components of the concrete per liter of "free" water in the pore space must be calculated. The elemental composition of portland cement is shown in Table A.1[28], and the composition of concrete per unit volume is shown in Table A.2. This composition is in accordance with ODOT mix formulation from a 1953 bridge project.

Table A.1 Composition of portland cement

Oxide	Common Name	Composition (weight %)	Molecular Weight (g/mol)
CaO	lime	63.0	56
SiO_2	silica	22.0	60
Al_2O_3	alumina	6.0	102
Fe_2O_3	ferric oxide	2.5	160
MgO	magnesia	2.6	40
K_2O	alkali	0.6	94
Na_2O	alkali	0.3	62
SO_3	sulfur trioxide	2.0	80
		total=99.0	

Table A.2 Composition of concrete

Component	Composition (lb/yd^3)
cement	564
aggregate	2100
sand	1115
water	270

A porosity of concrete (volume of pore space / total volume) of 0.27 is used. A pore saturation of 48% is used.

Table A.3 Elemental composition of concrete

Oxide	Common Name	Composition[a] (mol/l$_{total}$)[b]	Composition[a] (mol/l$_{pore\ water}$)[c]
CaO	lime	3.7643	29.046
SiO$_2$	silica[d]	12.2519	94.537
Al$_2$O$_3$	alumina	0.1968	1.519
Fe$_2$O$_3$	ferric oxide	0.0523	0.403
MgO	magnesia	0.2175	1.678
K$_2$O	alkali	0.0214	0.165
Na$_2$O	alkali	0.0162	0.125
SO$_3$	sulfur trioxide	0.0837	0.645

[a] The number of figures should not be interpreted as the precision with which the quantity is known. The sand is treated as if it were 100% silica, and the aggregate is treated as though it were inert.

[b] Computed from Columns 3 and 4 of Table A1.1 and Row 1 of Table A1.2.

[c] Computed from Column 3 of Table A1.3 with porosity=0.27 and pore saturation=48%.

[d] The sand is approximated as 100% silica sand.

From these values, the number of moles of each element per liter of water in the pore space is calculated, as shown in Table A.3. The assemblage of mineral phases that would form from these elements and water as well as the resulting

free activities (concentrations) of ions in the water phase at equilibrium are then calculated, using the geochemical equilibrium computer program MINTEQA1[29] for the thermodynamic data.

The result is a hypothetical, well defined matrix with which Zn^{2+} ions react when they are produced. This equilibrium representation of concrete is shown in Table A.4.

Table A.4 Equilibrium model of concrete[a]

A. Solid Phases

Wollastonite	$CaSiO_3$
Ca-nontronite	$CaFe_{12}Al_2(SiO_3)_{22}(H_2O)_6$
Leonhardite	$Ca_2Al_4(SiO_3)_8(H_2O)_7$
Diopside	$CaMg(SiO_3)_2$
Microcline	$KAl(SiO_3)_2SiO_2$
Quartz	SiO_2
Gypsum	$CaSO_4$

B. Solution Chemistry

species	C (mM)	log(C)
H^+		-10.35
Anions		
SO_4^{2-}	70.7	
$NaSO_4^-$	65.4	
KSO_4^-	22.4	
$H_3SiO_4^-$	0.3	
OH^-	0.2	
Total Anionic Charge	-230.0	
Cations		
Na^+	184.6	
K^+	44.8	
Ca^{2+}	0.2	
Total Cationic Charge	+229.8	

Table A.4 (Continued)

C. Zinc Chemistry

Solid Phases

Zinc Silicate	$ZnSiO_3$	
Solution Species	C (pM)	log(C)
Zn^{2+}		-13.763
$Zn(OH)^+$	109	
$Zn(SO_4)_2^{2-}$	307	
Total Soluble Zn(II)	416	

[a] Composition of concrete given in Table A.3, Column 4; thermodynamic data from the MINTEQA1 database[29].

The major features of this model are: pore water solution pH = 10.35 (this low pH represents an **equilibrium** state which, in practice, concrete does not reach); there are 9 chemical components, 7 solid phases, and 1 liquid phase, leaving only one degree of freedom in the solution phase composition. The major soluble ions are Na^+ and SO_4^{2-}, with concentrations in the 0.1 - 0.2 M range. The major approximations in this approach are: (a) temperature = 25 C; (b) the water activity is unity; (c) the activity coefficients of the solution species are unity; (d) concrete can be represented by discrete mineral phases; and (e) other components such as CO_2 and NaCl were neglected. Variations in the first three of these approximations might change the assemblage of mineral phases and the solution-phase concentrations by a small amount, but the basic result is the same: a high-pH, moderate ionic strength solution, with SO_4^{2-} as the dominant anion.

To represent this Zn/concrete interface during cathodic protection, it is approximated that the charge introduced by Zn^{2+} is exactly balanced by the charge introduced by the diffusion of SO_4^{2-} from the bulk of the concrete. (The loss of SO_4^{2-} is ultimately compensated by OH^- generated from Reaction (1-2),

preserving charge balance.) When equal quantities of Zn^{2+} and SO_4^{2-} are added to the matrix described above, the following sequence of reactions takes place:

$$Zn^{2+} + CaSiO_3(s) \rightarrow ZnSiO_3(s) + Ca^{2+} \qquad \text{(A-1)}$$

$$Ca^{2+} + SO_4^{2-} \rightarrow CaSO_4(s) \qquad \text{(A-2)}$$

Thus, the net reaction is:

$$Zn^{2+} + SO_4^{2-} + CaSiO_3(s) \rightarrow ZnSiO_3(s) + CaSO_4(s) \qquad \text{(A-3)}$$
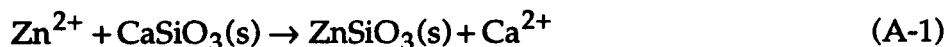
The solubility of $ZnSiO_3(s)$ is very low; thus, based on the local equilibrium model, the formation of $ZnSiO_3(s)$ is expected almost immediately when cathodic protection is begun. (A solution of the diffusion equation for semi-infinite, constant current boundary conditions, with $D_{Zn^{2+}} = 2 \times 10^{-12} \text{ m}^2 \text{ s}^{-1}$, $I = 1 \text{ mA}$ m^{-2}, and corrected electrode area, shows that total Zn(II) concentration at the electrode surface reaches 5×10^{-10} M within 1 s of the current being turned on. As seen in Table A.4, only 4×10^{-10} M Zn(II) is soluble in the concrete matrix).

As cathodic protection proceeds, it is expected to see a region depleted in SO_4^{2-} building from the Zn electrode outwards into the bulk of the concrete, and deposition of $ZnSiO_3(s)$ and $CaSO_4(s)$ near the electrode surface.

Under the initial conditions, after precipitation of $ZnSiO_3(s)$ but before significant depletion of SO_4^{2-}, the concentration of free Zn^{2+} can be calculated from the local equilibrium model of concrete (Table A.4C) and the potential E_{Zn} can be calculated from Equation A-4:

$$E^{eq}_{Zn/Zn^{2+}} = E^o_{Zn/Zn^{2+}} + \frac{RT}{nF} \ln a_{Zn^{2+}} \qquad \text{(A-4)}$$

These values are log $[Zn^{2+}]$ = -13.763 M, and E_{Zn} = -1.49 V vs CSE (in the absence of charge transfer and mass transfer overpotential). The measured value of E_{Zn} is -0.678 V versus CSE. Obviously, the zinc electrode does not appear to be poised by this sequence of reactions.

Appendix B
A Fortran Program for Two-dimensional Model

```
C  The program 'PROTECT' finds potential distribution in 2 dimensional
C  geometry.
C
     IMPLICIT REAL*8 (A-H,O-Z)
     REAL*8 IDOTFE
     Dimension E(0:200,0:200)
     ITMAX=200000
     EMAX=1.0E-15
C
C  EZN:zinc potential (Cu/CuSO4)
     EZN=-0.678
C
C  NX and NY:number of intervals in the X and Y directions respectively
     NX=40
     NY=20
     NPX=NX+1
     NPY=NY+1
C
C  A:conductivity in the bulk of concrete
     A=0.007441
     B=0.00
C
C  XL and YL:lengths in the X and Y directions respectively; FEX:width of
C  the iron in the X direction
     XL=0.0635
     YL=0.0254
     FEX=0.00635
     DELTX=XL/NX
     DELTY=YL/NY
C
C  HENRY:Henry's constant
     HENRY=33.064
C
C  W:overrelaxation factor
     W=1.3
C
C  IDOTFE:oxygen reduction exchange current density; DEFF:oxygen mass
C  transfer
C  coefficient; BULKCONC:oxygen concentration in the bulk; BC:inverse of
C  Tafel
C  slope for oxygen reduction; ENUMBER:equivalent number of electron
C  moles per 1 mole of oxygen; EEQ:equilibrium potential of oxygen
```

```
C  reduction
     IDOTFE=7.7E-7
     DEFF=1.09E-7
     BULKCONC=8.5
     BC=0.18
     ENUMBER=4.0
     EEQ=0.189
C
C  F and FARAD:fundamental constants
     F=38.9
     FARAD=96485.0
     KMAX=100
     EEE=0.001
C
C  CURNTLIM:limiting current density
     CURNTLIM=ENUMBER*FARAD*DEFF*BULKCONC
C
C  XIOX:iron oxidation exchange current density; EOFE:equilibrium potential
C  of iron oxidation; BA:inverse of Tafel slope for iron oxidation
     XIOX=7.1E-5
     EOFE=-0.76
     BA=0.41
C
C  EAPL:applied potential
     EAPL=0.0
C
C  determine the node where the iron edge is located
                 X=0.0
                 DO 211 I=1,NPX
                 IF (ABS(X-FEX).LE.0.00001) THEN
                 IFE=I
                 PRINT*,IFE
                 ENDIF
                 X=X+DELTX
   211           CONTINUE
C
C  potential values are stored in an output file: OUT.DAT
     OPEN   (UNIT=3,FILE='OUT.DAT',STATUS='UNKNOWN')
C
C  zinc potential is constant
     DO 1 I=1,NPX
     E(I,1)=-EZN
   1 CONTINUE
C
C  EE:maximum error; IT:number of iteration
     EE=0.0
```

```
      IT=0
C
C  guess an initial value for the unknown potentials
      DO 4 J=2,NPY
      DO 3 I=1,NPX
      E(I,J)=0.6
  3   CONTINUE
  4   CONTINUE
C start iteration
  9   IF(INT(IT/100).EQ.FLOAT(IT/100.0)) THEN
      PRINT*,EE,IT
      ENDIF
      EE=0.0
      IT=IT+1
      DO 15 J=2,NY
      I=1
      E(I-1,J)=E(I+1,J)
      CALL INTERIOR(E,I,J,A,B,DELTX,DELTY,EE,W)
      I=I+1
  14    IF (I.NE.NPX) THEN
          CALL INTERIOR(E,I,J,A,B,DELTX,DELTY,EE,W)
          I=I+1
          GO TO 14
          ENDIF
      E(I+1,J)=E(I-1,J)
      CALL INTERIOR(E,I,J,A,B,DELTX,DELTY,EE,W)
  15  CONTINUE
C
C  go to the level where rebar is located
      J=NPY
      I=1
  16  IF (I.NE.NPX) THEN
          IF (I.GT.IFE) THEN
          E(I,J+1)=E(I,J-1)
          CALL INTERIOR(E,I,J,A,B,DELTX,DELTY,EE,W)
          ELSE
            IF(I.EQ.1) THEN
            EHOLD=E(I,J)
            E(I-1,J)=E(I+1,J)
            CALL SUCCESS (E,I,J,IDOTFE,DELTX,DELTY,BC,KMAX,EEE,EEQ,
     +                    A,B,CURNTLIM,EAPL,XIOX,EOFE,BA)
            ENEW=E(I,J)
            E(I,J)=EHOLD*(1-W)+W*ENEW
            ERROR=ABS((E(I,J)-EHOLD)/E(I,J))
            IF(EE.LT.ERROR) EE=ERROR
            ELSE
```

```
            EHOLD=E(I,J)
            CALL SUCCESS (E,I,J,IDOTFE,DELTX,DELTY,BC,KMAX,EEE,EEQ,
     +                    A,B,CURNTLIM,EAPL,XIOX,EOFE,BA)
            ENEW=E(I,J)
            E(I,J)=EHOLD*(1-W)+W*ENEW
            ERROR=ABS((E(I,J)-EHOLD)/E(I,J))
            IF(EE.LT.ERROR) EE=ERROR
            ENDIF
          ENDIF
        I=I+1
        GO TO 16
        ELSE
        E(I+1,J)=E(I-1,J)
        E(I,J+1)=E(I,J-1)
        CALL INTERIOR(E,I,J,A,B,DELTX,DELTY,EE,W)
        ENDIF
       IF (EE.LE.EMAX) THEN
       PRINT*,EE,IT
       X=0.0
            DO 21 I=1,NPX
            WRITE(3,*)I,X
            WRITE (3,25) (E(I,J), J=1,NPY)
            X=X+DELTX
            WRITE(3,*)
   21       CONTINUE
       J=NPY
       SUM=0.0
        DO 99 I=1,IFE
        SUM=SUM+E(I,J)
   99 CONTINUE
      AVG=SUM/IFE
      WRITE (3,91) AVG,IFE,J,E(IFE,J)
      WRITE (3,*)
C
C calculate oxygen concentration at the center of iron, OXGCENT
      XNUMCNT=CURNTLIM*IDOTFE*EXP(-2.3*(EAPL-E(1,J)-EEQ)/BC)
      DENMCNT=CURNTLIM+IDOTFE*EXP(-2.3*(EAPL-E(1,J)-EEQ)/BC)
      CURCNT=XNUMCNT/DENMCNT
      OXGCENT=(BULKCONC - CURCNT/(ENUMBER * FARAD*DEFF))/
     +              HENRY
C
C calculate oxygen concentration at the edge of iron, OXGEDG
      XNUMEDG=CURNTLIM*IDOTFE*EXP(-2.3*(EAPL-E(IFE,J)-EEQ)/BC)
      DENMEDG=CURNTLIM+IDOTFE*EXP(-2.3*(EAPL-E(IFE,J)-EEQ)/BC)
      CUREDG=XNUMEDG/DENMEDG
      OXGEDG=(BULKCONC-CUREDG/(ENUMBER*FARAD*DEFF))/HENRY
```

```
      WRITE(3,*)
      WRITE(3,*)'OXGCENT',OXGCENT,' OXGEDG',OXGEDG
C
C determine the net current, CURT, through Ohm's law
      CURT=0.0
       DO 55 J=2,NPY
       I=1
       CURT=(E(I,J)-E(I,J-1))*(DELTX/2.0)
        DO 45 I=2,NX
        CURT=CURT+(E(I,J)-E(I,J-1))*DELTX
   45  CONTINUE
       I=NPX
       CURT=CURT+(E(I,J)-E(I,J-1))*(DELTX/2.0)
       CURT=(-A/DELTY)*CURT
       WRITE(3,*)J,CURT
       CURT=0.0
   55 CONTINUE
      GO TO 100
      ENDIF
       IF (IT.LE.ITMAX) THEN
       GO TO 9
       ENDIF
      PRINT*,'NO CONVERGENCE'
C
C format statements
   25 FORMAT(6(e12.5,1X))
   91 FORMAT(2X,'AVG = ',E12.5,10X,'E(',I2,',',I2,')=',E12.5)
C
  100  END
C
C
C subroutine INTERIOR determines potential values in bulk of concrete
C
      SUBROUTINE INTERIOR(E,I,J,A,B,DELTX,DELTY,EE,W)
      IMPLICIT REAL*8 (A-H,O-Z)
      DIMENSION E(0:200,0:200)
      XKAPPA=A+B*(J-1)*DELTY
      DERKAPPA=B
      DX=DELTX**2.0
      DY=DELTY**2.0
      EHOLD=E(I,J)
      ENEW=(2.0*XKAPPA*DY*(E(I+1,J)+E(I-1,J))
     +      +((2.0*XKAPPA+DERKAPPA*DELTY)*E(I,J+1)+(2.0*XKAPPA
     +      -DERKAPPA*DELTY)*E(I,J-1))*DX)/
     +      (4.0*XKAPPA*(DX+DY))
      E(I,J)=EHOLD*(1-W)+W*ENEW
```

```fortran
      ERROR=ABS((E(I,J)-EHOLD)/E(I,J))
      IF(EE.LT.ERROR) EE=ERROR
      RETURN
      END
C subroutine SUCCESS and function FUNC determine potential values at
C the rebar
C
      SUBROUTINE SUCCESS (E,I,J,IDOTFE,DELTX,DELTY,
     +      BC,KMAX,EEE,EEQ,A,B,CURNTLIM,EAPL,XIOX,EOFE,BA)
      IMPLICIT REAL*8 (A-H,O-Z)
      REAL*8 IDOTFE
      DIMENSION E(0:200,0:200)
      XKAPPA=A+B*(J-1)*DELTY
      DERKAPPA=B
      COEFF1=2.0*XKAPPA+DERKAPPA*DELTY
      DX=DELTX**2.0
      DY=DELTY**2.0
      DENOMIN=4.0*XKAPPA*(DX+DY)
      X1=-5.0
      X2=5.0
      XACC=1.0E-15
      FMID=FUNC(CURNTLIM,IDOTFE,EAPL,X2,EEQ,BC,XKAPPA,DY,E,I,J
     +           ,COEFF1,DELTY,DX,DENOMIN,XIOX,EOFE,BA)
      F=FUNC(CURNTLIM,IDOTFE,EAPL,X1,EEQ,BC,XKAPPA,DY,E,I,J
     +         ,COEFF1,DELTY,DX,DENOMIN,XIOX,EOFE,BA)
      IF(F*FMID.GE.0.) PAUSE 'ROOT MUST BE BRACKETED IN RTBIS'
       IF(F.LT.0.) THEN
       RTBIS=X1
       DDX=X2-X1
       ELSE
       RTBIS=X2
       DDX=X1-X2
       ENDIF
        DO 10 KK=1,KMAX
        DDX=DDX*0.5
        XMID=RTBIS+DDX
        FMID = FUNC (CURNTLIM, IDOTFE, EAPL, XMID, EEQ, BC, XKAPPA,
     +             DY,E,I,J,COEFF1,DELTY,DX,DENOMIN,XIOX,EOFE,BA)
       IF(FMID.LE.0.) RTBIS=XMID
       IF(ABS(DDX).LT.XACC.OR.FMID.EQ.0.) GO TO 11
   10  CONTINUE
      PRINT*,'NO CONVERGENCE IN BISECT'
          GO TO 2
   11 E(I,J)=RTBIS
      FF=FUNC(CURNTLIM,IDOTFE,EAPL,RTBIS,EEQ,BC,XKAPPA,DY,E,I,J
     +          ,COEFF1,DELTY,DX,DENOMIN,XIOX,EOFE,BA)
```

```
      IF(FF.GT.EEE) THEN
      PRINT*,'ASSIMPTOTE'
      ENDIF
 2    RETURN
      END
      FUNCTION FUNC (CURNTLIM , IDOTFE, EAPL, AA, EEQ, BC, XKAPPA,
     +            DY, E,I,J,COEFF1,DELTY,DX,DENOMIN,XIOX,EOFE,BA)
      IMPLICIT REAL*8 (A-H,O-Z)
      REAL*8 IDOTFE
      DIMENSION E(0:200,0:200)
      XNUM=CURNTLIM*IDOTFE*EXP(-2.3*(EAPL-AA-EEQ)/BC)
      DENM=CURNTLIM+IDOTFE*EXP(-2.3*(EAPL-AA-EEQ)/BC)
      ANODE=XIOX*EXP(2.3*(EAPL-AA-EOFE)/BA)
      BOUND=XNUM/DENM-ANODE
      FUNC=AA-(2.0*XKAPPA*DY*(E(I+1,J)+E(I-1,J))+(COEFF1*(-2.0*DELTY/
     +      XKAPPA*BOUND)+4.0*XKAPPA*E(I,J-1))*DX)/DENOMIN
      RETURN
      END
```